NASA CONTRACTOR REPORT

NASA CR-108

/99

NASA CR-108

N64-31204

(ACCESSION NUMBER)

(PAGES)

(NASA CR OR TMX OR AD NUMBER)

FACILITY FORM 602

(THRU)

/

(CODE)

(CATEGORY)

A THEORETICAL AND EXPERIMENTAL STUDY OF A SUPERCONDUCTING MAGNETICALLY-SUPPORTED SPINNING BODY

by Roger D. Bourke

Prepared under Grant No. NsG-133-61 *by*
STANFORD UNIVERSITY
Stanford, Calif.

for

NATIONAL AERONAUTICS AND SPACE ADMINISTRATION • WASHINGTON, D. C. • OCTOBER 1964

NASA CR-108

A THEORETICAL AND EXPERIMENTAL STUDY OF A SUPERCONDUCTING MAGNETICALLY-SUPPORTED SPINNING BODY

By Roger D. Bourke

Prepared under Grant No. NsG-133-61 by
STANFORD UNIVERSITY
Stanford, Calif.

for

NATIONAL AERONAUTICS AND SPACE ADMINISTRATION

For sale by the Office of Technical Services, Department of Commerce,
Washington, D.C. 20230 -- Price $2.75

ABSTRACT

3/204

Various aspects of the design and operation of a magnetically-supported superconducting rotor are studied. The forces on a magnetically-supported body are calculated and compared to experimentally observed values.

A method is presented for calculating the magnetic field and forces on the surface of a diamagnetic body in the field of one or more axi-symmetric coils. The force and field effects of a small deviation from the nominal axial symmetry are derived. The results of the field calculations are used in the equations of motion to predict the behavior of a supported superconducting spinning body.

Experimental apparatus and techniques used in achieving temperatures necessary for superconductivity ($4^{\circ}K$) are described. Details of the rotor, coils, spin up system, and instrumentation are given. A description of the procedure used in operating the system is given.

The experimental results agree quite closely to those which have been calculated and it is therefore concluded that this work presents reliable quantitative tools for designing magnetically-supported, axially-symmetric superconducting bodies to be operated in nominally axially symmetric fields.

Author

TABLE OF CONTENTS

TABLE OF CONTENTS (CONT)

LIST OF TABLES

LIST OF ILLUSTRATIONS

LIST OF ILLUSTRATIONS (CONT)

ACKNOWLEDGMENTS

The work described in this thesis was sponsored by the National Aeronautics and Space Administration under Grant No. 133-61. The author wishes to express his thanks to NASA for their full support and interest in this project.

The author was aided immeasurably by the comments and help of his fellow students, in particular Mr. Robert H. Tuffias, who contributed many hours during the academic year 1963-64. Professor John A. Dempsey of the University of Miami was exceptionally helpful during his visit as an NSF visiting research fellow during the summer of 1963.

Several members of the electronics laboratory tube shop participated in constructing the apparatus. The author is particularly indebted to Mr. Frank Peters for the glass blowing artistry and skill he used in constructing the cryostat.

The author would like to thank his three advisors, Profs. Robert H. Cannon, Jr. and Daniel B. Bershader of Aeronautics and Astronautics and Prof. William M. Fairbank of Physics for their suggestions and comments during the course of the research.

I. INTRODUCTION

A. PURPOSE

The research described in this thesis was undertaken in support of a proposed experiment to test the General Theory of Relativity. As detailed in Chapter II, the original purpose was to construct a magnetically-supported cylindrical body and to study and control its motions while spinning.

During the course of the research it became evident that the details of the phenomena of superconductive support were not sufficiently established to carry out the originally conceived project directly. The purpose evolved to one of studying the properties of superconductive magnetic support, of using these studies to develop a mathematical model for the dynamics of an axially-symmetric spinning body so supported, and of experimentally verifying the theoretically-established static and dynamic behavior.

B. UTILITY

The dominant friction forces acting on a magnetically-supported body are those due to the viscosity of the medium surrounding it. Thus if the region around the body is nearly evacuated the frictional effects should be exceedingly small. Indeed, Harding at JPL has measured the exponential decay constant for a one-inch niobium sphere, spinning in a pressure of less than 10^{-6} mm of Hg, to be about 600 days. This implies that the friction coefficient is in the order of 10^{-6} dyne-cm/(rad/sec)(assuming a linear friction relation).

The applications for such a low-friction device are many. One of the most obvious is a gyroscope and much effort has been put forth to build one (see Chapter II). A second application is a magnetically supported accelerometer. Such a device should have an extremely low threshold and therefore would be well suited for measurement of minute accelerations such as those encountered by a satellite passing through the rarefied upper atmosphere.

Another space vehicle application is suggested by the following: Under certain conditions attitude control can be accomplished most economically using reaction wheels to store angular momentum in various directions. If these reaction wheels were magnetically supported they could operate for a very long time at essentially constant speed without exchanging any of their momentum with the satellite. This would be particularly appropriate if the satellite had a complete cryogenic guidance package using superconducting computer circuitry.

One might think that the problem of maintaining low temperatures would offset the advantages of superconductivity. On the contrary, with proper insulation four to five pounds of solid hydrogen can keep a one-foot sphere cold for a year (see Chapter VII) in a completely passive (and therefore highly reliable) system.

Several laboratory devices would also benefit from the low-friction properties and other advantages of magnetic support.

C. SCOPE

The scope of this thesis encompasses the following: A method is presented for calculating the magnetic field and forces on the surface of a superconducting body in the field of one or more axi-symmetric coils. The force and field effects of a small deviation from the nominal axial symmetry -- i.e., if the axis of the body is displaced and rotated somewhat from the axis of the field -- are derived, and the results are used in the equations of motion to predict the dynamic behavior. These results are experimentally confirmed using an instrumented, magnetically-supported spinning superconducting body.

D. CONTRIBUTION

This thesis presents the quantitative tools for designing a magnetically-supported superconducting body. It draws on an established method of fluid mechanics to calculate the field and force on an axially symmetric body in an axially symmetric field, and it extends this method to arbitrary small deviations from symmetry. It shows that the problem of small deviations is similar to that of a body of revolution at an angle of attack with respect to a fluid, and can be solved by similar methods.

After calculating the various magnetic parameters and using them to develop the equations of motion, this work compares the theoretical results to the observed behavior of an essentially arbitrary axially-symmetric body. It investigates experimentally problems of support, instrumentation, and operation of such a system and reports their favorable solution. It shows very close agreement between the calculated and observed dynamic behavior.

Whereas in the past only theoretical and experimental work on spheres has been reported, this thesis extends the state of the art substantially by establishing the design fundamentals for building very-low-friction cylindrically symmetric bearings.

II. THEORY OF SUPERCONDUCTIVE SUPPORT

A. HISTORY

In 1911 the Danish physicist H. Kamerlingh Onnes discovered that the electrical resistivity of several metals became suddenly immeasurably small as they were cooled to a few degrees above absolute zero [Ref. 1]. This remarkable phenomenon he termed superconductivity. He later found that this superconductive state could be quenched if the specimen was brought into a region of magnetic field whose value was above some temperature dependent critical value.

Professor S. C. Collins of MIT is one of several experimenters who have attempted to determine the true value of the resistivity of the superconducting state. He induced a continuously circulating current in a superconducting lead ring and kept it below the critical field for approximately two and one half years. During that time he was unable to detect any degradation in the current whatsoever. From this he concluded that the resistivity of the lead was no greater than 10^{-21} ohm-cm (compared with the purest copper, a nonsuperconductor, whose low temperature resistivity is about 10^{-9} ohm-cm). Thus a superconductor possesses a conductivity which is at least 10^{12} times that of any ordinary material.

In 1933 Meissner and Ochsenfeld discovered another distinct property of pure superconductors: If a solid superconductor is cooled in a magnetic field, then this field is expelled during the transition from the normal to superconducting states, rather than being frozen in as one would expect from assuming infinite conductivity. This, the Meissner effect, implies that regardless of the state of the superconductor above the transition temperature, below that temperature its interior will be free of magnetic flux.

This apparent reversibility in the transition from the normal to superconducting states lead F. and H. London to apply thermodynamics to superconductivity and to propose their phenomenological theory [Ref. 2]. One of the consequences of this theory is that the magnetic field penetrates only a short distance into the interior of a superconductor and, therefore, if the sample has dimensions of the order of millimeters or larger, it acts like a perfect diamagnet of permeability zero.

In 1952 Ivan Simon of the Arthur D. Little Co. [Ref. 3] noted that a perfect diamagnet such as a superconductor was repelled rather than attracted by magnetic fields and therefore could be supported against the force of gravity by a properly arranged field generator. He calculated the forces on such a body using a hydrodynamic analogy, and experimentally confirmed his results by stably supporting a sphere. Simon generated his magnetic field by various methods: Two concentric but non-coplaner copper coils of different radii were used initially but had the disadvantage of introducing Joule heating to the low temperature environment; similarly shaped lead rings were used carrying persistent current; several types of permanently-magnetized rings were employed. (Evidently the relatively high-field superconductor, niobium, was not available in suitable form for a coil at this time.) The levitated sphere was made of two hollow hemispheres pressed out of lead foil and welded at their equators. His experiments were successful in that he was able to support the body stably and even rotate it at low speeds.

Culver and Davis of the RAND Corporation [Ref. 4] proposed in 1957 that a refinement of Simon's basic experiments might prove useful in constructing a precision gyroscope. They pointed out that a gyroscope capable of withstanding reasonable accelerations was feasible if the rotor was a hollow spherical shell constructed of some high-critical-field material. They proposed that the spin axis orientation of such a gyro could be read out by optically tracking a pattern scored on the equator of the ball. Furthermore, they suggested means for minimizing the residual magnetic flux trapped in the rotor. At the time their proposal was presented it apparently looked quite promising as an inertial guidance device.

Dr. T. A. Buchhold started development of a superconducting gyroscope at General Electric sometime before 1960. In Ref. 5 he discusses the gyro and suggests several other applications of superconductivity. He shows tentative designs for a magnetic thrust bearing and an annular bearing around a shaft; a photo of a working model is included. He also presents a design for a motor using the diamagnetic property of superconductors. In a later article [Ref. 6] Buchhold expands upon the bearing idea, calculating the characteristics and advantages of various configurations.

In 1959 the Jet Propulsion Laboratory undertook development of a spherical cryogenic gyro using the ideas set forth by Culver and Davis. The first effort was toward calculating magnetic fields about a diamagnetic sphere due to several coils. Methods were developed for making these calculations both when the axes of the coils and the axis of the sphere were coincident, and when the two were offset.

Harding and Tuffias at JPL [Ref. 7, 8] checked these analytical results by levitating a sphere with a single coil. Figure 9 of Ref. 7 shows a lead-plated ping-pong ball supported by the field of a single niobium coil. Using the analytical techniques they had developed, they arrived at a near-optimum arrangement for supporting a spherical rotor.

Experiments have continued under the direction of Dr. Harding with one particularly startling result; all superconductors so far tested, although they possess zero DC resistivity, seem to be heated when subjected to a low frequency AC magnetic field. This property seems to drastically curtail the performance of a system which was so optimistically envisioned at its inception [Refs. 9-11].

Work has continued on the cryogenic gyro at the General Electric Co. where investigation of low-frequency losses in superconductors has produced results similar to those of Harding [Ref. 12]. A parallel study of a superconductive gyro has been carried on at Minneapolis-Honeywell; their findings are in agreement with those mentioned above.

The history of the Stanford effort is interesting in its own right. In 1960 Professor L. I. Schiff, chairman of the Stanford Physics Department, noted that one of the consequences of general relativity is that a gyroscope in the gravitational field of the earth does not keep its angular momentum fixed in space as predicted by Newton, but rather undergoes a slow precession [Ref. 13]. The effect is enhanced if the gyro is carried in a satellite which orbits the earth several times per day. Unfortunately, the magnitude of the effect, even in a satellite, is only seven seconds of arc per year, much below the random drift level of any conventional gyroscope [Ref. 14]. On the other hand, operation in a satellite reduces the required support forces by six orders of magnitude or more, and thus contributes substantially to the feasibility of the experiment, [Ref. 15].

Professor W. M. Fairbank suggested that the experiment might best be carried out at cryogenic temperatures possibly using a magnetically-supported superconducting sphere. He also proposed [Ref. 16] that the spin axis orientation readout might be accomplished in the following way: A magnetically-supported cylindrically shaped body would be made to spin synchronously and coaxially with the sphere. A Mössbauer emitter would be placed on the rotor and a corresponding Mössbauer absorber on the cylinder (Fig. 1). If the two bodies were spinning coaxially (Fig. 1A) there would be no relative motion between the Mössbauer pair, so that total absorption would be observed at the counter. When the spin axis of the sphere was inclined to that of the cylinder (Fig. 1B) there would be relative motion between the emitter and absorber and this would be detected at the counter.

Experiments by Fairbank and Bol have shown that at reasonable spin speeds this method will detect angular misalignment of the axes to less than .1 seconds of arc.

Since the Mössbauer readout is applicable over a rather narrow range of relative velocities, it might be best to align the cylinder with the ball and then quantitatively read the orientation of the cylinder with respect to its fixed surroundings by more conventional optical or capacitive means.

The Mössbauer readout method depends heavily on being able to track the cylinder precisely and control its motions accordingly. Consequently, the natural motions of the cylinder need to be known beforehand so that adequate compensation can be applied. The original purpose of the work described herein was to build and test a model of such a cylinder and to study its natural behavior.

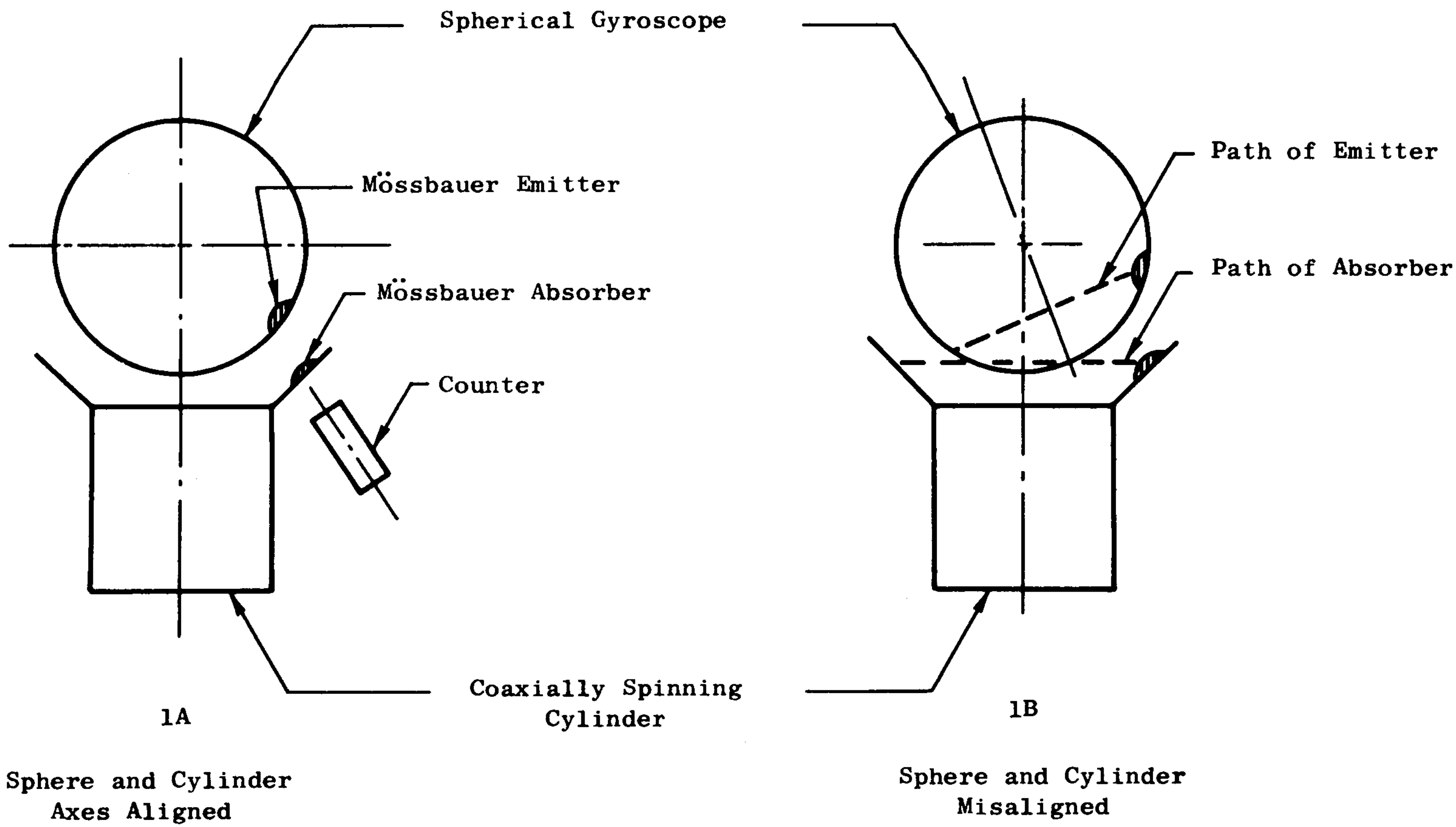

FIG. 1. MÖSSBAUER READOUT METHOD FOR A SUPERCONDUCTING GYRO

B. PHENOMENA OF SUPERCONDUCTIVITY

The most significant characteristic of a superconductor is that it has zero resistance to steady current. If a sample of superconducting material is cooled in the absence of a magnetic field, then at some critical temperature, T_c, the resistivity suddenly drops to zero. (The transition actually takes place over a few hundredths of a degree for pure samples.) The value of the critical temperature depends on the material of the sample; e.g., for tin $T_c = 3.72^{o}K$, and for lead $T_c = 7.18^{o}K$. If a sample is at a temperature $T < T_c$ and is then subjected to a magnetic field H on its surface, it will remain superconducting as long as H is less than some critical value H_c. For $H > H_c$ the material reverts to its normally resistive state. This critical field, H_c, is dependent on temperature in such a way that H_c decreases as T increases. Thus there is a region in the H-T plane inside of which the body is superconducting and outside of which it is normal (see Fig. 2A).

The critical field versus temperature curves for several materials are shown in Fig. 2B. Note that the critical field at zero degrees is also a function of the material and is denoted by H_o; e.g., for tin H_o = 306 örsted and for lead H_o = 803 örsted.

A second distinct characteristic of a superconductor is that it expells magnetic field and therefore acts as a perfect diamagnet. This property does not follow from the first, for if infinite conductivity were assumed, then a superconductor cooled in a magnetic field would trap this field and hold it constant regardless of any variations in the external field. On the contrary, however, it was found experimentally that if a superconductor is cooled in the presence of a magnetic field it then rejects this field during the transition, after which its interior is free of flux. Thus the magnetization of a superconductor is independent of the path by which it arrives at this state.

This flux expulsion property, or Meissner effect, is only valid for the superconducting material itself. A ring of superconducting material, for instance, does not expell the flux from its center, but only from its body. Figures 3A and 3B show such a ring in the normal and superconducting states.

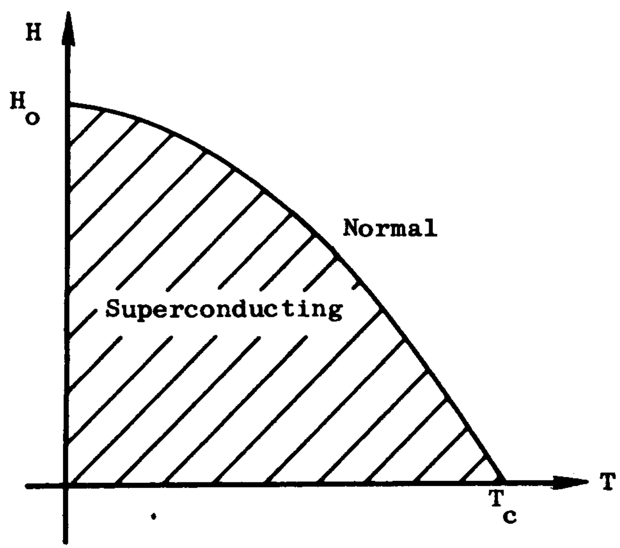

2A

Regions in the H-T Plane

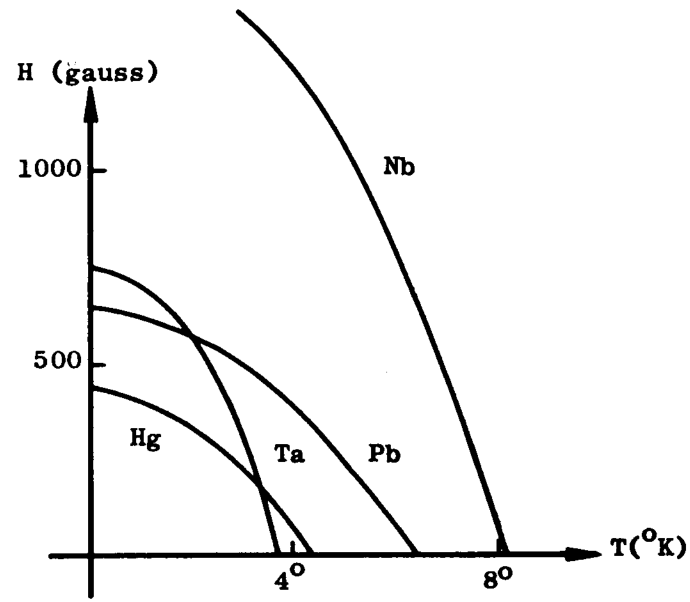

2B

Transitions for Various Metals

FIG. 2. CRITICAL FIELD VERSUS TEMPERATURE

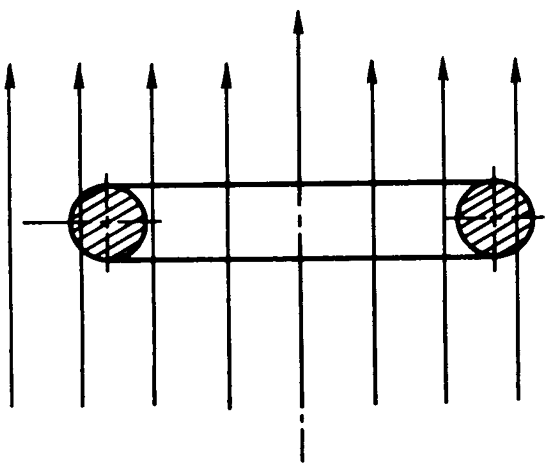

3A

Ring in the Normal State

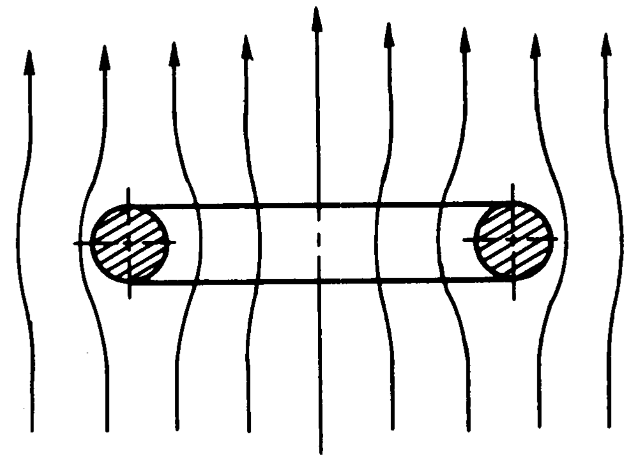

3B

Ring in the Superconducting State

FIG. 3. SUPERCONDUCTING RING IN A MAGNETIC FIELD

The energy which drives out the magnetic field during the transition is a latent energy associated with the mass of material and analogous to the latent heats of condensation or solidification. Therefore, if we expect a certain region to be free of magnetic flux by virtue of the Meissner effect, that region must necessarily contain superconducting material. A hollow superconducting shell, for example, will not free its interior of flux as a result of the Meissner effect. Any flux captured within the shell must, however, somewhere penetrate the surface as seen by the following argument: Consider a shell containing no magnetic material but some flux entirely within its interior (Fig. 4A). Since lines of flux are solenoidal (close on themselves) we may integrate $\vec{H}\cdot\vec{ds}$ along a continuous flux line within the interior. For this integral to be non-zero there must necessarily be some current enclosed, which is clearly impossible; thus H must be everywhere zero in this case. It may be concluded that a superconducting shell either has flux passing through its wall or no flux within its interior.

Figure 4B shows a possible state of flux which penetrates the shell at its poles. The penetrating flux is held in place by a persistent current flowing in a surrounding superconducting loop. Note that once the state of flux has been established and the shell is superconducting, no changes can be imposed unless the critical field is exceeded, for any changes will be opposed by the persistent currents. Thus if such a shell is cooled in truly zero field it will have no flux passing through its surface and no flux in its interior.

It should be noted that although the Meissner effect is a property of the pure superconducting state, many materials, the so called Type II superconductors, exhibit less than complete flux expulsion or none whatsoever. Niobium-tin for instance, a metal which has the asset of remaining superconducting in very high magnetic fields, demonstrates a very incomplete Meissner effect. Associated with this incomplete Meissner effect is less-than-ideal behavior under AC magnetic fields [Ref. 9]. Regardless of their Meissner properties, all superconductors seem to have zero DC resistivity.

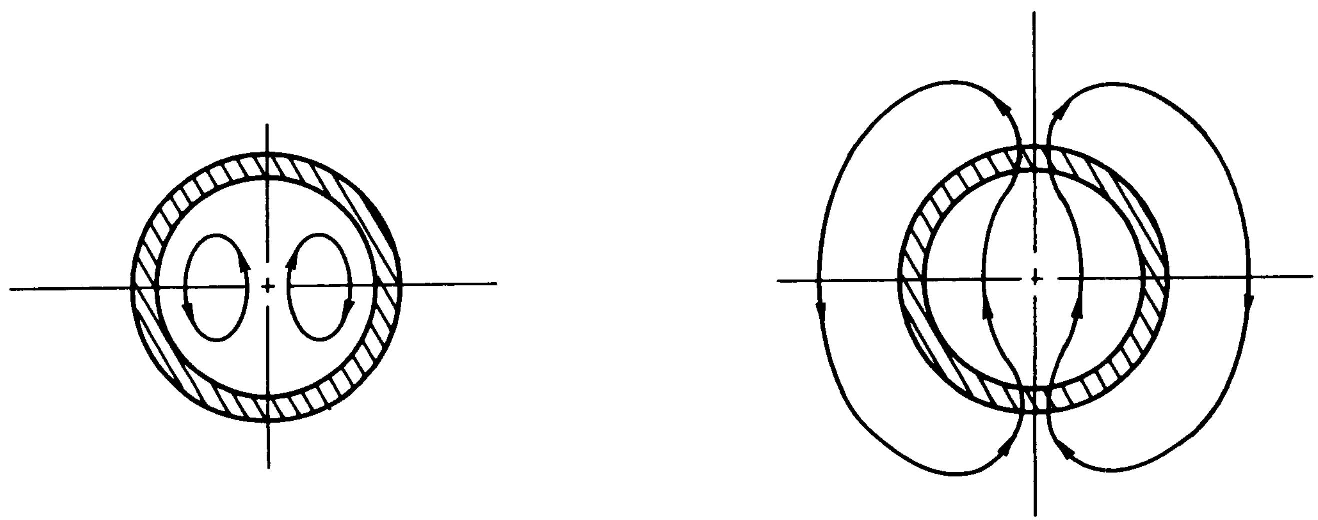

Trapped Flux Within Shell

4A

Trapped Flux Penetrating Shell

4B

FIG. 4. SUPERCONDUCTING SHELL WITH TRAPPED FLUX

F. London [Ref. 2] has shown that Maxwell's equations cannot be used to describe superconductive phenomena either by letting the resistivity go to zero or by letting the permeability go to zero, or both. Rather, London asserts that the current in a superconductor is shared by the normal electrons and the super (zero resistance) electrons, and each has a different current density,

$$\vec{j} = \vec{j}_n + \vec{j}_s \quad . \tag{1}$$

The normal current follows Ohm's Law with resistivity of the normal state

$$\vec{j}_n = \sigma \vec{E} \quad . \tag{2}$$

The supercurrent, on the other hand, obeys a new set of relations, the London Equations:

$$\text{curl } \vec{j}_s = - \vec{H}/c \quad , \tag{3}$$

$$\frac{\partial}{\partial t} \Lambda \vec{j}_s = \vec{E} \quad , \tag{4}$$

where Λ is a constant of the material and of order 10^{-31} sec^2. The total current obeys Maxwell's equations using the normal value of the permeability:

$$\text{curl } \vec{H} = 4\pi \vec{j}/c + \dot{\vec{D}}/c \tag{5}$$

$$\text{curl } \vec{E} = - \dot{\vec{H}}/c \tag{6}$$

$$\text{div } \vec{H} = 0 \tag{7}$$

$$\text{div } \vec{E} = 4\pi p \tag{8}$$

in gaussian units.

Neglecting the normal and displacement currents, we may combine Eqs. (5) and (3) to obtain:

$$\text{curl curl } \vec{H} = - \frac{4\pi}{\Lambda c^2} \vec{H} .$$

But curl curl = grad div $- \nabla^2$ and since div $\vec{H} = 0$ we have:

$$\nabla^2 \vec{H} = \frac{4\pi}{\Lambda c^2} \vec{H} = \frac{1}{\lambda^2} \vec{H} ,$$

where λ is known as the penetration depth, and is of order 10^{-5} cm. Thus, for quasi-stationary conditions under which the normal and displacement currents can be neglected, the magnetic field within a superconductor obeys the equation:

$$\nabla^2 \vec{H} - \frac{1}{\lambda^2} \vec{H} = 0 . \tag{9}$$

The consequence of Eq. (9) may be illustrated by considering a semi-infinite slab of superconducting material $z > 0$ with a uniform magnetic field $\vec{H} = H_o \hat{y}$ on its surface (Fig. 5). For $z > 0$ London's equations hold so that Eq. (9) may be employed. The problem is effectively one dimensional, i.e., variations only in the z direction can take place so that the equation reduces to:

$$\frac{d^2 H_y}{d z^2} = \frac{1}{\lambda^2} H_y .$$

Therefore H_y decreases exponentially with z, with a characteristic length λ. Since $\vec{H}$ falls off so rapidly with z, the interior of the body, except for a thin "boundary layer," is shielded from the external field. In other words, the body acts like a diamagnet.

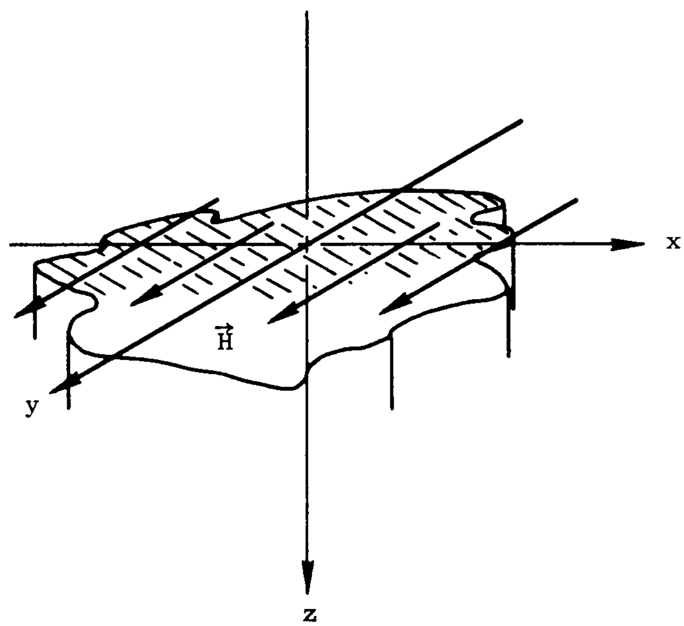

FIG. 5. SUPERCONDUCTING SLAB WITH UNIFORM FIELD

London [Ref. 2, §4] has solved for the magnetic field in and around a superconducting sphere in a uniform field. The result is as follows: For spheres of radius $R \gg \lambda$, the external field is distorted exactly as if the body were a perfect diamagnet of radius $R - \lambda$. Thus a body whose dimensions are on the order of millimeters or larger, acts, for all practical purposes, as a perfect diamagnet.

C. MAGNETIC SUPPORT

The diamagnetic property of superconductors causes repulsive forces to act on their surfaces and makes magnetic support possible. The necessary components are an appropriate field generator and a superconducting surface on the body to be supported.

The flux exclusion phenomenon is a consequence of zero resistivity and is not dependent on the Meissner effect if the body is cooled in zero field. Consider the wire-superconductor system of Fig. 6 and let the wire have initially no current flowing in it. As the current is increased from zero to some value flux lines are created which begin to penetrate the metal surface. These changing flux lines induce currents which, by Lenz's law, oppose the changing flux. In an ordinary conductor at low frequencies the eddy currents diminish due to the resistance, and the field eventually penetrates as if the material were not there (assuming non-magnetic material). In a superconductor the eddy currents persist indefinitely due to the zero resistivity and the flux therefore does not enter beyond a negligibly thin layer.*

---

* Note that an ordinary conductor at high frequencies exhibits this same flux expulsion property and its associated repulsive force because of the finite relaxation time of the eddy currents. The electromagnetic forces due to this anomalous skin effect have been suggested as a possible means of low-friction support.

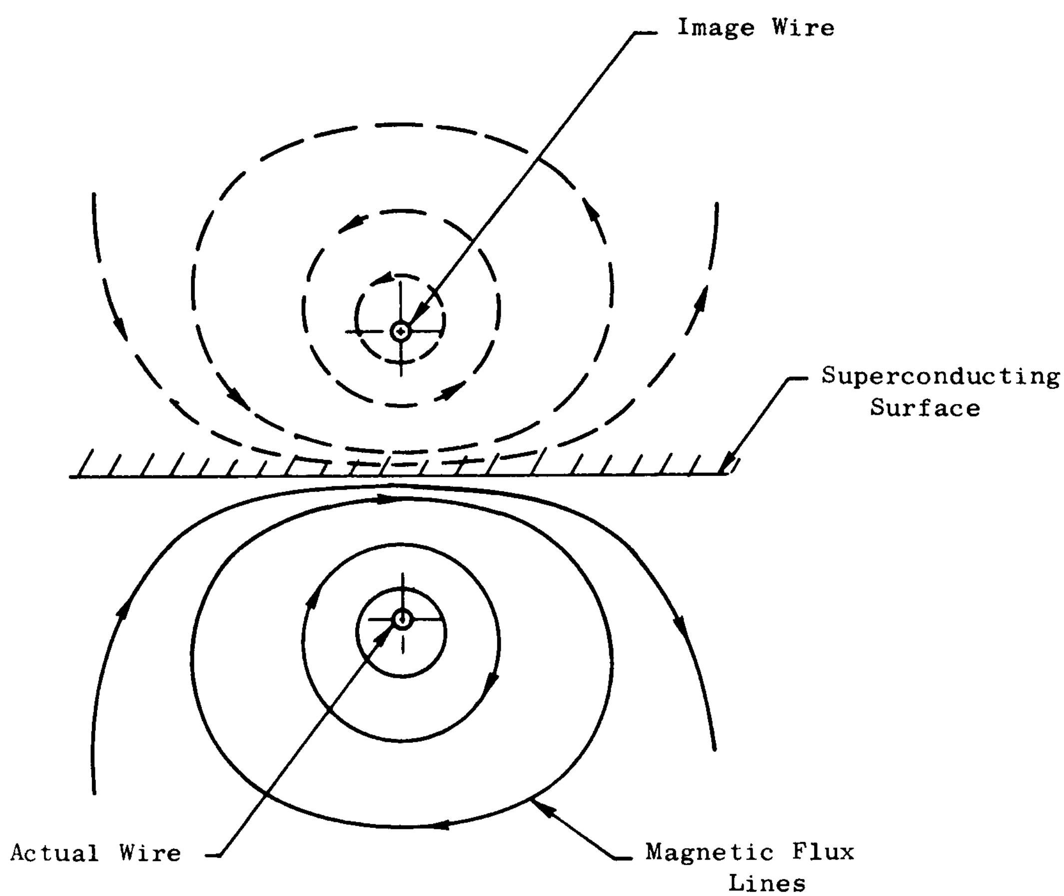

FIG. 6. CURRENT CARRYING WIRE AND SUPERCONDUCTING SURFACE

One of the greatest attributes of this system is that it is inherently stable. This can be seen by considering a diamagnetic plane surface and a nearby current-carrying wire (Fig. 6). The field of this system can be obtained by superposing an image wire inside the body and carrying current in the opposite direction. Note that the actual and image wires repel each other with a force inversely proportional to the distance between them. Thus if the body is being forced down by gravity, it will come into some stable equilibrium position where the gravity force and magnetic force are equal.

III. DESIGN OF ROTOR-SUPPORT SYSTEM

A. CONFIGURATION

The configuration of the actual integrated rotor-support system used in the present research was selected on the basis of the following design criteria:

1. The support should be kept as simple as possible.
2. The supported rotor must be statically and dynamically stable.
3. The weight of the rotor should be kept at a minimum to avoid the need for high magnetic pressures and therefore high fields.
4. The external diamagnetic surface should be shaped so as to give the body the minimum possible demagnetiziation coefficient; i.e., it should locally distort the applied field as little as possible so that field concentration points and the resulting high local fields are minimized.

The simplest possible, easily-obtainable field is that due to a single coil. This has the advantage of being easy to construct in almost any size, deviating very little from predicted value at reasonable distances from the wire, and having the field configuration readily available analytically and in closed form (see Chapter IV, Section C). Furthermore, since work is to be done at superconducting temperatures, zero resistance wire can be used to carry high current through relatively few turns to give almost any necessary field strength. The current can be varied to change the magnetic field, a feature lacking in any permanently-magnetized field generator. When the desired field strength has been established, the current can be trapped, thus minimizing the power fed to the low temperature environment. (Chapter VII, Section C discusses the flux trapping circuit.)

Static stability studies for a sphere supported by a single coil have been carried out by Simon [Ref. 3] and Harding [Ref. 7, 8]. They come to rather diverse conclusions, the former stating that no possible stable configuration exists and the latter showing the opposite with experimental verification.

Roughly speaking, the criterion for static stability is that the forces generated when the body is displaced from equilibrium be such that they tend to restore the body to the equilibrium position. Stability in the vertical direction can be achieved by the principle outlined in Fig. 6, i.e., arranging things so that the body moves away from the field generator as it goes up.

Buchhold [Ref. 5] suggests that lateral stability can be achieved with a coil surrounding a cylinder. A quantitative analysis (Chapter IV) shows that this is only true for certain relations of coil and cylinder radius. Stability for rotations about a horizontal axis is not a clear function of any of the shape parameters, but a few shapes can be predicted by inspection. A thin disk surrounded by a coil would probably be unstable when rotated about an axis in its plane whereas a long cylinder probably would not.

In Chapter IV methods are presented to calculate the forces and moments generated when an arbitrary cylindrically symmetric body is translated or rotated.

Dynamic stability at various spin speeds, on the other hand, does not lend itself to any intuitive approach. In Chapter VI the equations of motion for a spinning body are written, and the stability for small displacements is discussed.

Because of the shallow penetration depth the composition of the interior of the body is arbitrary; in particular, it can be hollow. Furthermore the main structure of the body can be made of some low-density, high-strength material such as aluminum, and the superconductor can then be affixed to the surface by suitable means (e.g., electroplating). The thickness of the coating need only be very large compared to the penetration depth (10^{-5} cm).

The quantity known as the demagnetization coefficient can be illustrated by the equation:

$$H_e = (1 - n) H_c ,$$

where H_e is a uniform parallel field applied to the specimen which just causes the critical field, H_c, to be reached at some point on its surface, and n is the demagnetization coefficient. The value of n gives a measure of the amount of distortion the specimen imparts to the applied field and is only a function of the body shape, as can be seen from the following examples.

For an infinitly long cylinder whose axis is parallel to the applied field, $n = 0$, for in this case the cylinder does not distort the field at all and the entire surface of the cylinder reaches the critical field at once when the applied field reaches H_c.

For a long cylinder whose axis is perpendicular to the applied field, $n = 1/2$, for in this case the specimen starts becoming normal when the applied field becomes $H_c/2$. The critical field is reached at a location on the body which corresponds to the point of maximum velocity in the analogous hydrodynamics problem (see Fig. 7).

For a sphere $n = 1/3$, as can be seen by similar considerations.

For an infinitly thin disk whose axis is parallel to the applied field, $n = 1$, for in this case the strength at the edges is at the critical value for any applied field whatsoever. If the body were perfectly diamagnetic for any field then the value at the edge would be infinity, but long before this happens superconductivity is destroyed and the rather complicated intermediate state prevails.

It may be inferred from the above examples that in order to reduce the field distortion and the factor n, the body must be more or less streamlined and sharp edges should be avoided. The actual value of the demagnetization coefficient is difficult and unnecessary to calculate, but a computer program used to calculate the field distribution indicates that rounding the corners smoothes the field fairly well over the surface of a rotor (see Chapter IV).

It might be mentioned in passing that the problem of avoiding too high a magnetic field at some points on the specimen is almost exactly analogous to the hydrodynamic problem of avoiding cavitation. Cavitation occurs when at some point in the flow field the pressure falls below the vapor pressure of the liquid so that it spontaneously begins

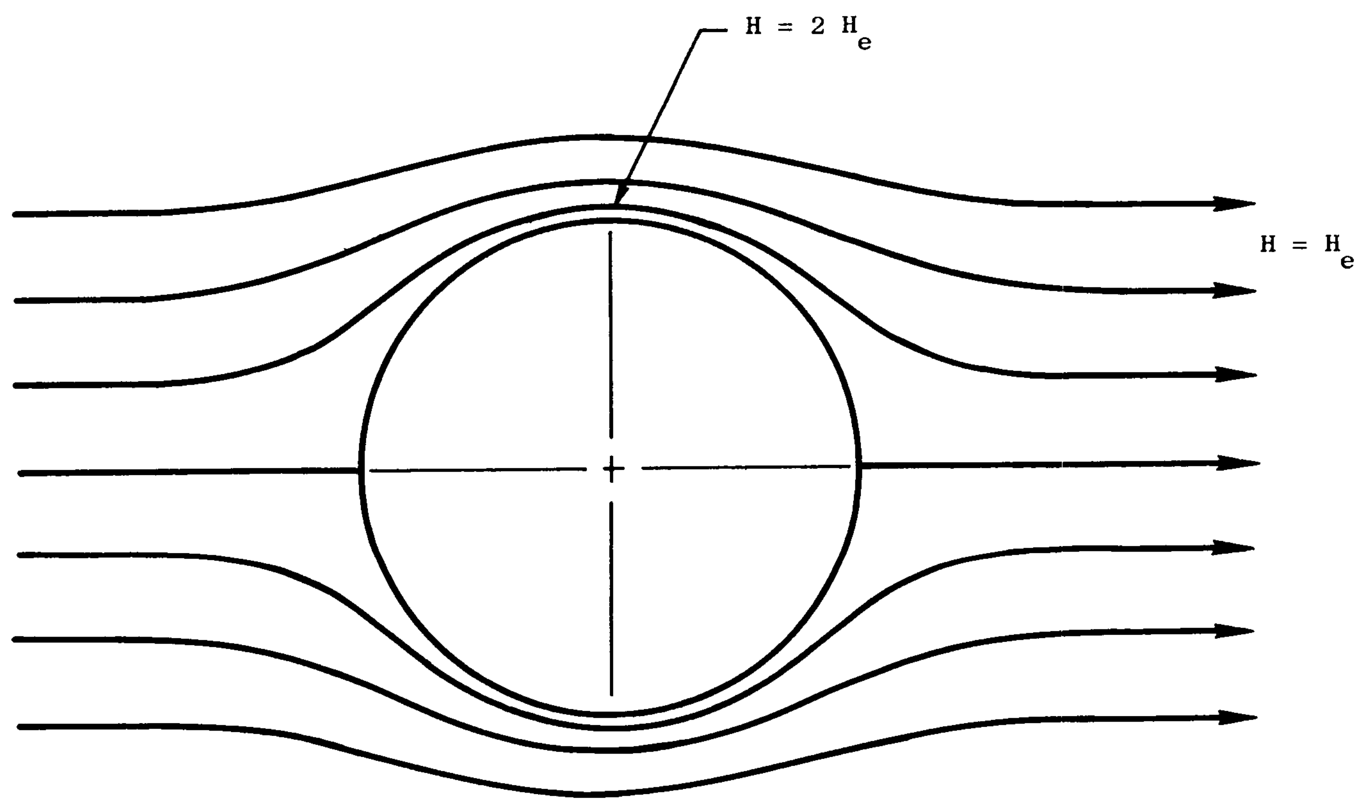

FIG. 7. CYLINDER WITH ITS AXIS PERPENDICULAR TO AN APPLIED FIELD

to boil. Although the actual problem in this case is one of the pressure falling below some critical value, it is completely equivalent, by Bernoulli's equation, to the velocity exceeding some critical value. Since the velocity of an inviscid liquid around a solid body is completely analogous to the magnetic flux density around a similarly-shaped diamagnetic body, the problem in the two cases is to keep the local magnitude of $\vec{B}$, or $\vec{v}$, below some critical level. Also, in both cases, when this requirement is not adhered to catastrophic changes occur so that the problem is no longer described by the simple potential equations. Furthermore, the techniques which have been developed to avoid cavitation (e.g., in hydrofoil design, [Ref. 17]) could well be applied to the design of superconducting bodies.

B. MATERIAL

The primary consideration in selecting the superconducting surface metal is that it must have a critical field which is considerably higher than the fields which will be applied to support it. Were this the sole consideration, one would select niobium or one of its compounds which have tremendously high critical fields at 4°K. Unfortunately niobium, even when prepared in the most careful manner, deviates substantially from the "ideal" behavior of superconductors. This is not to say that its DC resistance is non-zero, but rather that it displays almost no Meissner effect and traps flux prodigiously. Furthermore its AC losses seem to be unusually high [Ref. 9]. At fields much less than critical, niobium still might be the best material, but this would involve using some light substructure and affixing the niobium to its surface. Harding [Refs. 18-20] has investigated niobium coatings on Lucalox and quartz balls by the process of pyrolitic decomposition of niobium-pentachloride with little success. Sputtered films seem to be equally unpromising [Ref. 18]. To date, no one seems to have reported the successful electroplating of niobium by standard methods and although much work has gone into vacuum deposition techniques, it is quite difficult to get films over a few hundred Ångstroms thick. Furthermore, niobium does not lend itself to evaporation because of its high gettering action.

From the standpoint of ideal behavior, the best possible material would be tin. Unfortunately tin is not even superconducting at $4^{\circ}K$ and at $2^{\circ}K$ its critical field is only 210 gauss. Tin can only be used as a superconducting surface if the device to be supported is extremely light (or equivalently, if the gravity force is extremely small, as in a satellite).

Lead seems to be a good compromise between niobium and tin. It displays a fairly complete Meissner effect when prepared carefully and its critical field at $4^{\circ}K$ is 570 gauss, which is relatively high. It also has the advantage of being inexpensive, easily plated and easily electropolished. Chapter VII discusses a method for electroplating lead.

IV. MAGNETIC FIELD CALCULATIONS

A. INTRODUCTION

The fundamental problem in the design or analysis of a magnetically-supported body is the calculation of the magnetic forces acting on its surface. This chapter presents a method for calculating the magnetic field in the vicinity of any axially-symmetric body due to a coaxial field generator. The method was developed to calculate potential fluid flow rather than any electromagnetic quantity, but its application to electromagnetics is completely valid.

The net magnetic forces acting on the body may be found by integrating the square of the derived field strength over its surface. Such things as the maximum field strength, total lifting force and various stability regimes can then be obtained. Furthermore, the body shape or field generator configuration can then be optimized for the criterion that the net force divided by the maximum field should be a maximum.

In this chapter and those following the equations are written in mks units with $\mu_o = 4\pi \times 10^{-7}$ webers/amp-m. It is often more convenient, however, to consider the quantities in electromagnetic cgs units since centimeters, dynes and gauss are more representative of the magnitudes encountered. This will give current in abamps (tens of amperes) and $\mu_o = 4\pi$ gauss-cm/abamp = 4π dyne-cm/abamp^2.

B. MATHEMATICAL FORMULATION

The magnetic force $\vec{dF}$ due to a field $\vec{B}$ on a surface $\vec{dS}$ is given by:

$$\vec{dF} = \frac{\vec{B}}{\mu_o} (\vec{B} \cdot \vec{dS}) - \frac{B^2}{2\mu_o} \vec{dS} .$$

In Chapter II it was noted that the magnetic field penetrates a negligibly small distance into the surface of a superconductor so that the normal component of $\vec{B}$ at the surface can be considered zero to a very high approximation. The force equation then reduces to

$$\vec{dF} = -\frac{B^2}{2\mu_o}\vec{dS} ,$$

where dF/dS is now a pressure on the surface. The problem is to find B^2 at every point.

We shall first consider a region exterior to the superconductor and not including any field generators (i.e., current carrying conductors). Maxwell's equations state:

$$\text{curl } \vec{H} = \vec{j} + \dot{\vec{D}} ,$$

$$\text{div } \vec{B} = 0 .$$

We shall restrict ourselves to the steady-state case so that $\dot{\vec{D}} = 0$ and our exclusion of field generators gives $\vec{j} = 0$. Furthermore we assume the region to contain no magnetic material so that $\vec{H} = \vec{B}$ (in cgs units) and we have:

$$\text{curl } \vec{B} = 0 ,$$

$$\text{div } \vec{B} = 0 .$$

The first equation implies that $\vec{B}$ can be expressed as the gradient of a scalar Φ:

$$\vec{B} = -\text{ grad } \Phi . \tag{10}$$

The second implies that Φ satisfies Laplace's equation for:

$$\text{div } \vec{B} = 0 = \text{div grad } \Phi = \nabla^2\Phi .$$

The boundary conditions follow from the fact that at the surface $B_{normal} = -\partial\Phi/\partial n = 0$ where n is the direction of the normal.

Thus the magnetic field may be found by solving Laplace's equation with the appropriate boundary conditions,

$$\nabla^2\Phi = 0 , \tag{11}$$

$$\left.\frac{\partial\Phi}{\partial n}\right]_S = 0 , \tag{12}$$

where S is the superconducting surface.

Equations (11) and (12) are exactly the same as those that govern the flow of an irrotational inviscid fluid about a solid body S. In the fluid case one would derive the velocity rather than the magnetic field from the potential function Φ.

We shall now consider the problem at hand, i.e., an axially-symmetric superconducting body in the field of one or more current-carrying coils. This is analogous in fluid mechanics to a body surrounded by one or more vortex rings. Figure 8 shows such a body with a single surrounding coil. The region of interest is that exterior to the body but excluding the coil. Note that the presence of the coil creates a subsidiary or source condition on Φ, for the line integral law for $\vec{H}$ gives:

$$\oint_\Gamma \vec{H}\cdot\vec{ds} = \oint_\Gamma \frac{\vec{B}}{\mu}\cdot\vec{ds} = -\oint_\Gamma \frac{\nabla\Phi\cdot\vec{ds}}{\mu} = i ,$$

where Γ is any path surrounding the coil wire (Fig. 8) and i is the current enclosed. This subsidiary integral condition indicates that Φ must have a singularity at the location of the coil. (Recall that one property of regular potential functions is that $\oint \nabla V\cdot\vec{ds} = 0$ around any path as long as V is harmonic.) We are therefore led to introduce the function Φ_c which is the potential of the coil in free space. Excluding the line of the coil, $\nabla^2\Phi_c = 0$ everywhere, and furthermore

$$\oint_\Gamma \vec{\nabla}\,\Phi_c\cdot\vec{ds} = -\mu i ,$$

if Γ surrounds the wire.

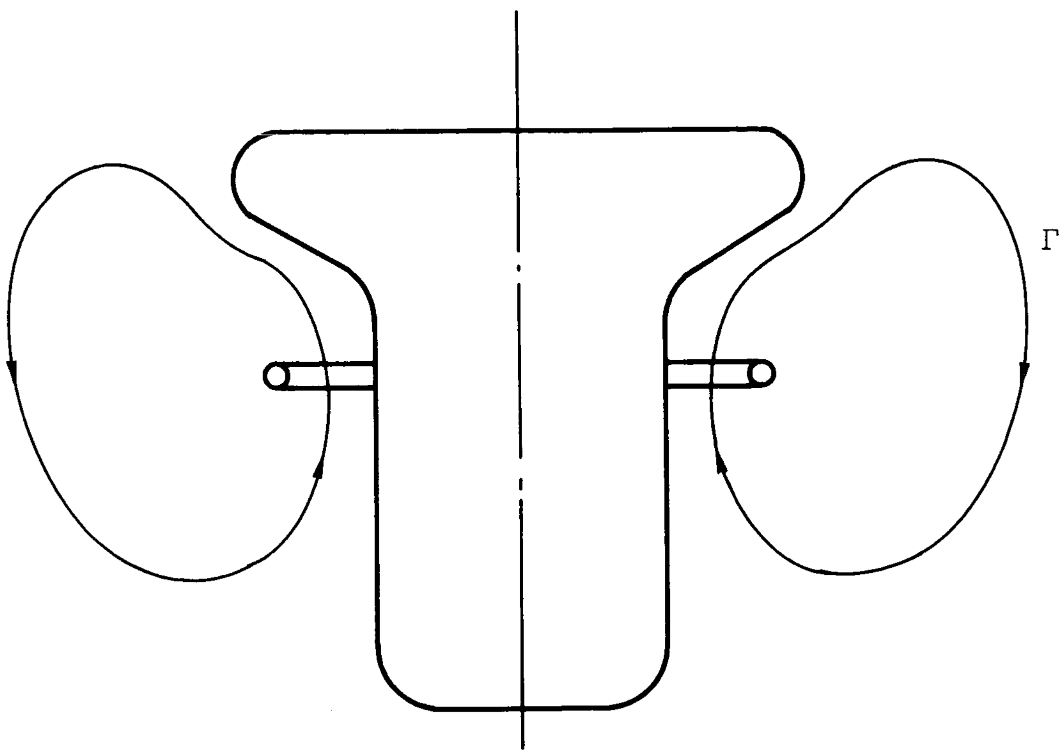

FIG. 8. AXIALLY SYMMETRIC BODY SURROUNDED BY A SINGLE COIL

Because of the linearity of Laplace's equation, we may let Φ be the sum of two functions, the coil potential Φ_c and the body potential φ

$$\Phi = \Phi_c + \varphi \ . \tag{13}$$

The last function, φ, is harmonic and regular at all points exterior to the body. Note that Φ_c provides for satisfaction of the subsidiary condition:

$$\oint_\Gamma \vec{\nabla}\Phi \cdot \vec{ds} = \oint_\Gamma \vec{\nabla}\Phi_c \cdot \vec{ds} = - \mu i \ ,$$

since

$$\oint \vec{\nabla}\varphi \cdot \vec{ds} = 0 \ .$$

The coil potential Φ_c is available analytically (Section D), so the problem is to find φ such that:

$$\nabla^2 \varphi = 0 \tag{14}$$

$$\left.\frac{\partial\Phi}{\partial n}\right]_S = \left.\frac{\partial\Phi_c}{\partial n}\right]_S + \left.\frac{\partial\varphi}{\partial n}\right]_S = 0 \ ,$$

or

$$- \left.\frac{\partial\varphi}{\partial n}\right]_S = \left.\frac{\partial\Phi_c}{\partial n}\right]_S = B_n^o \ . \tag{15}$$

Note that the boundary value, B_n^o, can be interpreted as the normal field at the body surface due to the coil if the body had no effect on the field.

At this point we shall construct the function φ by transforming the differential equation-boundary condition system to a Fredholm Integral Equation of the second kind. The method is one outlined by Kellogg [Ref. 21] and later used by Smith and Pierce [Ref. 22] to solve the analogous fluid mechanics problem. The solution employs an artifice: it assumes that there is an imaginary material spread on the surface which is a source of magnetic lines of flux. It adjusts the distribution of this material so that it will just cancel the externally produced normal field, B_n^o.

Consider an element of surface dS at a point Q on which there is an amount of source material σ dS (Fig. 9). Let this material be such that it produces a field at P

$$d\vec{B} = \frac{\sigma\, dS}{r_{QP}^2} \hat{r}_{QP} .$$

The potential at P is

$$d\varphi(P) = \frac{\sigma(Q) dS(Q)}{r_{QP}} .$$

If the whole body is covered with this distribution σ, then the total potential is

$$\varphi(P) = \oint\!\!\oint \frac{\sigma(Q) dS(Q)}{r_{QP}} . \tag{16}$$

The field at any exterior point P is found by differentiation:

$$\vec{B}(P) = - \text{grad } \varphi(P) = - \oint\!\!\oint \sigma(Q) \text{ grad} \left(\frac{1}{r_{QP}}\right) dS(Q) .$$

At a point on the body surface p, the differentiation is not so straightforward since the integrand becomes singular. Kellogg [Ref. 21] shows that the field at the surface in the normal direction due to the sources is given by:

$$B_n(p) = + 2\pi\sigma(p) - \oint\!\!\oint \sigma(Q) \frac{\partial}{\partial n} \left(\frac{1}{r_{QP}}\right) dS(Q) .$$

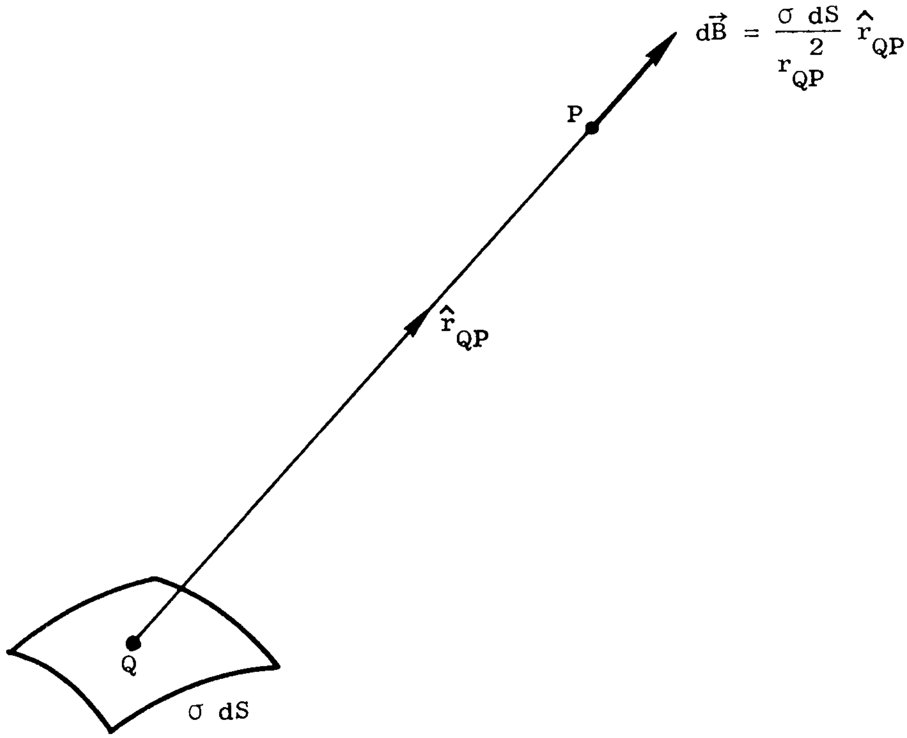

FIG. 9. ELEMENT OF SURFACE SOURCE

If these sources σ are to be arranged in such a way that they just cancel the external normal field, as Eq. (15) suggests, then $B_n(p)$ should be replaced by the known function $-B_n^o(p)$. We then have the integral equation for σ:

$$B_n^o(p) = -2\pi\sigma(p) + \oiint \sigma(Q) \frac{\partial}{\partial n} \left(\frac{1}{r_{QP}}\right) dS(Q) \quad . \tag{17}$$

Once the function σ has been found then the potential due to the sources is obtainable from Eq. (16), and the entire magnetic field from Eqs. (10) and (13).

Although this method was developed to solve problems of fluid mechanics, it bears little physical resemblance to them for there is no surface material analogous to σ. On the other hand, it bears a distinct resemblance to superconductivity wherein eddy currents on the surface arrange themselves in such a way as to cancel the external field. It seems likely that the source strength σ has some relation to the actual current density of the microscopic eddys, although the relation is not immediately clear.

To this point the analysis has been very general: the shape of the body is arbitrary and the external normal field is arbitrary but known. Solving the integral Eq. (17) under these conditions would be quite a chore; for certain specializations, however, great simplifications occur.

Let the body and the external normal field be axially symmetric so that any surface point p or Q can be specified by the arc length from the pole s and the azimuthal angle θ (Fig. 10). Then $dS = r(s)\, d\theta\, dr(s)$ where $r(s)$ is the local radius of the body at s. Also the external normal field, being axially symmetric, is independent of θ so that $B_n^o(p) = B_n^o(s)$. Since there is no angular variation of the boundary value, it follows from Eq. (17) that σ is also independent of θ.* Therefore Eq. (17) reduces to

---

* A proof of this is given in Ref. 21.

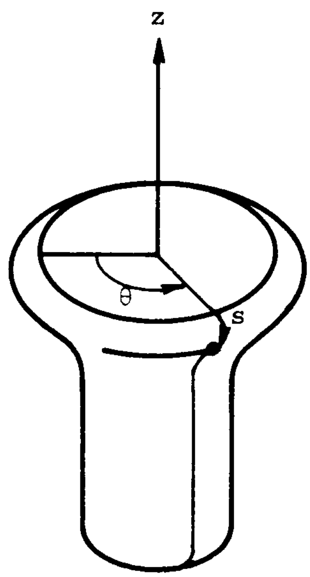

FIG. 10. BODY POLAR COORDINATE SYSTEM

$$B_n^o(s) = 2\pi\sigma(s) - \int_o^L \sigma(s')r(s')\left[\int_o^{2\pi} \frac{\partial}{\partial n}\left(\frac{1}{r_{QP}(s,s';\theta')}\right) d\theta'\right] dr(s'),$$

where the dummy integration variables are now identified by primes. Note that the integral in the square brackets is only a function of the body shape and not of the external field B_n^o. Thus if a body shape is specified, this first integral may be evaluated immediately to give the influence function:

$$F(s,s') = r(s') \int_o^{2\pi} \frac{\partial}{\partial n} \frac{1}{r_{QP}} d\theta' ,$$

and

$$B_n^o(s) = 2\pi\sigma(s) - \int_o^L \sigma(s') F(s,s') dr(s').$$

This one-dimensional integral equation can now be evaluated using the standard technique of assuming that σ is step-wise constant over n intervals of L. Then

$$\int_o^L \sigma(s') F(s,s') dr(s') \cong \sum_{j=1}^{N} \sigma_j \int_{s_{j-1}}^{s_j} F(s,s') dr(s') ,$$

and this integral again can be evaluated to give the influence coefficients:

$$\alpha_{ij} = \int_{s_{j-1}}^{s_j} F(s_i,s') dr(s') .$$

And

$$B_{n_i}^o \cong 2\pi\sigma_i + \sum_{j=1}^{N} \alpha_{ij} \sigma_j$$

$$\cong \sum_{j=1}^{N} (\alpha_{ij} + 2\pi \delta_{ij})\sigma_j .$$

Or in matrix form

$$\{B_n^o\} = [A] \{\sigma\} . \tag{18}$$

Thus the problem of finding the σ's has been reduced to one of solving a set of simultaneous linear algebraic equations with the only inexactness stemming from the fact that the continuous variable σ has been replaced by a step-wise constant function. The solution by this algebraic method may be made as accurate as desired simply by taking N to be sufficiently large. Note that the number N is effectively the number of points at which the boundary conditions are exactly met.

At this point it might be valuable to comment on this particular method of solution and compare it to other methods. First it would seem more straightforward to solve this axially-symmetric problem by putting a line of singularities along the body axis and adjusting their strengths to meet the boundary conditions. This would lead to a one-dimensional integral equation directly (since the integration would only be along the symmetry axis) and would therefore be more conveniently reduced to linear algebra. It seems that for a body with flat ends the method breaks down, apparently because it involves solving a Fredholm integral equation of the first kind for which a solution does not necessarily exist.

A purely analytical solution might be possible for certain types of axially-symmetric bodies, but such methods are usually practical only if the boundary conditions are described along a line on which one of the coordinates is constant. For example, Harding [Refs. 10, 11] has solved the problem of a diamagnetic sphere in the field of a coaxial coil. The resulting solution is in closed form and consists of a single image coil inside the sphere. A similar method can be applied to a cylinder in the field of a coaxial coil, but the solution can only be expressed as an integral and does not appear to describe an image.

The integral equation method presented here has a wide range of applicability. The formulation, Eq. (17), is very general; it refers to any body in any known external normal field B_n^o. It will be shown in the following chapters that this formulation leads to a linear algebra problem for bodies in some non-axisymmetric external fields. The restrictions which reduce the problem to Eq. (18) are not overly severe; they specify that the body and field must be axially symmetric. This encompasses a wide class of problems including a radially-symmetric body in the field of several coaxial coils.

A distinct advantage of the method is that it gives the field on the surface directly without solving for the entire field as one does in the analytic solution. This occurs because at the time the influence coefficient matrix $[A]$ is obtained, a similar matrix $[C]$ is calculated, a typical element of which, c_{ij}, is the tangential field at the surface point i due to a unit source at j. Similarly when calculating B_n^o another column matrix B_t^o is obtained, the elements of which are the tangential field at each describing point due to the external field generator. Thus the total (tangential) field on the body is just given by

$$
\begin{aligned}
\{B\} &= [C]\ \{\sigma\} + B_t^o \\
&= [C]\ [A]^{-1}\ \{B_n^o\} + \{B_t^o\}
\end{aligned}
\tag{19}
$$

A second distinct advantage is now apparent. Once the body shape has been specified the two square matrices $[C]$ and $[A]^{-1}$ may be calculated and stored. The form of the field generator affects only the column matrices $\{B_n^o\}$ and $\{B_t^o\}$, so that for each new coil shape only these need be changed. This greatly facilitates the computation.

C. EXTENSION TO NONSYMMETRIC CASE

A magnetically-supported body, such as the one described here, will, when subjected to disturbances, deviate from its nominally axially symmetric situation. In order to determine the forces which act on the body when it undergoes such a deviation, it is necessary to calculate the magnetic field distribution on the surface. The following section purports to show that such a calculation is possible in two distinct cases:

1. The axis of the body is translated through a small distance (compared to the size of the body) while remaining parallel to the axis of the coil, and
2. the axis of the body is rotated through a small angle about an axis lying in the plane of the coil. Note that combining the two above it is possible to rotate the body about any axis parallel to the plane of the coil.

The method again uses the integral equation formulation (17) and reduces it to a set of simultaneous linear equations as in Eq. (18). The fundamental difference between this and the previous problems is that because of the asymmetries in the external field B_n^o is no longer a function of only one variable. In both of the above cases we shall determine the functions B_n^o in terms of the natural coordinates of the body and then show that the function, and consequently the integral equation, can be separated into symmetric and asymmetric parts. The asymmetric equation will then be solved by techniques similar to those used on the symmetric equation of the previous chapter.

1. Translation

We shall first consider an axially-symmetric body whose axis is parallel to, but offset a distance ϵ from the axis of a coil (Fig. 11A). Let the natural cylindrical coordinates of the body be r, θ, z and those of the coil be ρ, φ, ζ. Let the plane of the coil coincide with $z = 0$ so that its center lies at $r, \theta, z = \epsilon, 0, 0$ (Fig. 11B). The transformation between the two coordinate systems, using the angle δ, is given by

$$\rho \sin\varphi = r \sin \theta$$

$$\delta = \varphi - \theta$$

$$= \arctan \frac{\frac{\epsilon}{r} \sin \theta}{1 - \frac{\epsilon}{r} \cos \theta}$$

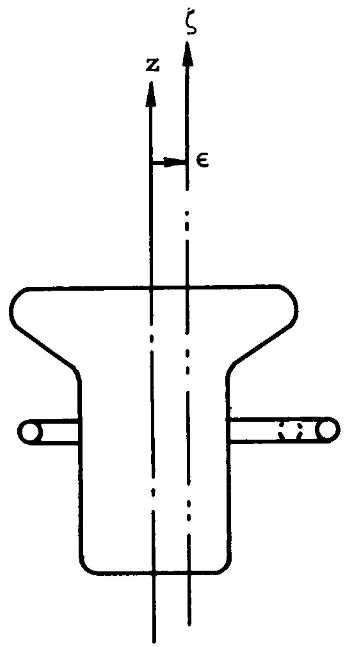

11A

Body and Coil

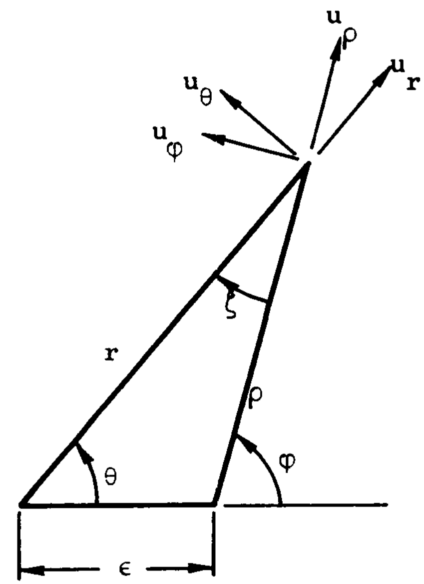

11B

Coordinate Systems

FIG. 11. BODY TRANSLATED THROUGH A DISTANCE ϵ

For small offsets, i.e., $\epsilon/r \ll 1$, the transformation is

$$\rho \cong r - \epsilon \cos \theta$$

$$\sin\varphi \cong (1 + \frac{\epsilon}{r} \cos \theta) \sin \theta$$

$$z = \zeta$$

$$\delta \cong \frac{\epsilon}{r} \sin \theta ,$$

the unit vectors (see Fig. 11B) undergo the transformation

$$u_r = u_\rho \cos\delta - u_\varphi \sin\delta$$

$$u_\theta = u_\rho \sin\delta + u_\varphi \cos\delta$$

$$u_z = u_\zeta \ .$$

For small offsets we have

$$u_r \cong u_\rho - u_\varphi \frac{\epsilon}{r} \sin \theta$$

$$u_\theta = u_\rho \frac{\epsilon}{r} \sin \theta + u_\varphi$$

$$u_z = u_\zeta \ .$$

The field of the undisturbed coil is symmetric in the ρ, φ, ζ system so that if its components are B_ρ, B_φ, B_ζ then $B_\varphi \equiv 0$. We now have the components of the coil field in the body coordinates:

$$B_r = B_\rho\,[(r - \epsilon\cos\theta),\ z]$$

$$B_\theta = B_\rho\,[(r - \epsilon\cos\theta),\ z]\ \frac{\epsilon}{r}\sin\theta$$

$$B_z = B_\zeta\,[(r - \epsilon\cos\theta),\ z].$$

The form of the above vector transformation suggests a method for expressing the field of the coil alone in terms of the body coordinates: B_ρ and B_ζ can be expanded in first-order Taylor Series in ϵ/r

$$\begin{aligned} B_r &= B_\rho(r,z) - \epsilon\cos\theta\ \frac{\partial}{\partial r}\ B_\rho\ (r,z) \\ B_\theta &= B_\rho(r,z)\ \ \frac{\epsilon}{r}\sin\theta \\ B_z &= B_\zeta(r,z) - \epsilon\cos\theta\ \frac{\partial}{\partial r}\ B_\zeta\ (r,z)\ . \end{aligned} \tag{20}$$

The normal component can now be found at each point on the body surface. Let β equal the angle between the tangent to a point of the body profile and the axis of symmetry (Fig. 11A)

$$\begin{aligned} B_n &= \cos\beta\ B_r + \sin\beta\ B_z \\ &= \cos\beta\ (r,z)\ B_\rho(r,z) + \sin\beta\ (r,z)\ B_\zeta(r,z) \\ &\quad - \epsilon\cos\theta\,[\cos\beta\ (r,z)\ \frac{\partial}{\partial r}\,B_\rho(r,z) + \sin\beta\ (r,z)\ \frac{\partial}{\partial r}\,B_\zeta(r,z)]. \end{aligned}$$

Thus we have succeeded in expressing the external normal field in terms of the natural coordinates of the body. The B_n so expressed can now be inserted into the integral equation (17). Before doing this, however, one very important feature of the function B_n should be noted:

the only effect of the asymmetry is the single factor $\cos\theta$ modifying the second bracket. This suggests a separation of the function:

$$B_n(r,\theta,z) = B_{n_{sym}}(r,z) - \epsilon\cos\theta\, B_{n_{asym}}(r,z) \ . \tag{21}$$

Furthermore, it suggests a similar separation of the integral equation variable σ:

$$\sigma(r,\theta,z) = \sigma_{sym}(r,z) + \sigma_{asym}(r,\theta,z).$$

Because of the linearity of the integral equation it can be split into two equations one involving the symmetric quantities and the other the asymmetric,

$$\cos\beta\,(r,z)B_\rho(r,z) + \sin\beta\,(r,z)B_\zeta(r,z) = -\,2\pi\,\sigma_{sym} + \oint\!\!\oint \sigma_{sym}\frac{\partial}{\partial n}\left(\frac{1}{r}\right)dS$$

$$-\epsilon\cos\theta\left[\cos\beta(r,z)\ \frac{\partial B_\rho(r,z)}{\partial r} + \sin\beta(r,z)\ \frac{\partial B_\zeta(r,z)}{\partial r}\right] = -\,2\pi\sigma_{asym} + \oint\!\!\oint\sigma_{asym}\frac{\partial}{\partial n}\left(\frac{1}{r}\right)dS. \tag{22}$$

Note that in the first of these two equations the inhomogeneous part is a function of (r,z) only and therefore may be solved immediately by the method of Smith and Pierce. The second of these two equations has as its inhomogeneity a function of (r,z) multiplied by $\cos\theta$. Lotz [Ref. 23] and Hess [Ref. 24] have both shown that for such an equation the only dependence of σ_{asy} on θ is a factor $\cos\theta$. Similarly, the associated potential function φ_{asym} is proportional to $\cos\theta$. Although Hess assumes in his proof that the inhomogeneity is a specific function dependent on the body shape, it is essentially arbitrary because of the generality of the body. Thus, the second equation can be solved by Hess's method for cross flow on bodies of revolution which is simply a reduction of the integral equation to linear algebra when the σ has a factor $\cos\theta$.

According to Hess, the results of solving the asymmetric problem are as follows: The resultant tangential field has a component along the meridian and proportional to $\cos\theta$, and another component around the circumference (in the θ direction) and proportional to $\sin\theta$. This second component must be added to that of Eq. (20) to obtain the total field in the θ direction; for the B_θ in Eq. (20) did not contribute to the external normal field and has therefore not been accounted for.

The total tangential field on the body is the sum of that due to the symmetric source distribution (the same as when everything is axi-symmetric) and that due to the asymmetric sources. In the direction of the meridian we have

$$B(s,\theta) = B_{sym}(s) + \epsilon\cos\theta\, B_{asym}(s) \ , \tag{23}$$

and in the circumferential direction we have

$$B_\theta(s) = \epsilon\sin\theta\, B'_{asym}(s), \tag{24}$$

where s is again the arc length.

The field having been determined, we are now in a position to calculate the forces on this slightly perturbed body. The body will be considered to be made up of a series of frustra of cones, a typical one of which is shown in Fig. 12. Note that the numerical solution [Refs. 22-24] assumes the body to be made up of such frustra. The tangential field at the surface from Eqs. (23) and (24) is

$$\vec{B} = \vec{B}_m + \vec{B}_\theta$$

$$= (B_{sym} + \epsilon\cos\theta\, B_{asym})\,\hat{m} + \epsilon\sin\theta\, B'_{asym}\,\hat{\theta} \ ,$$

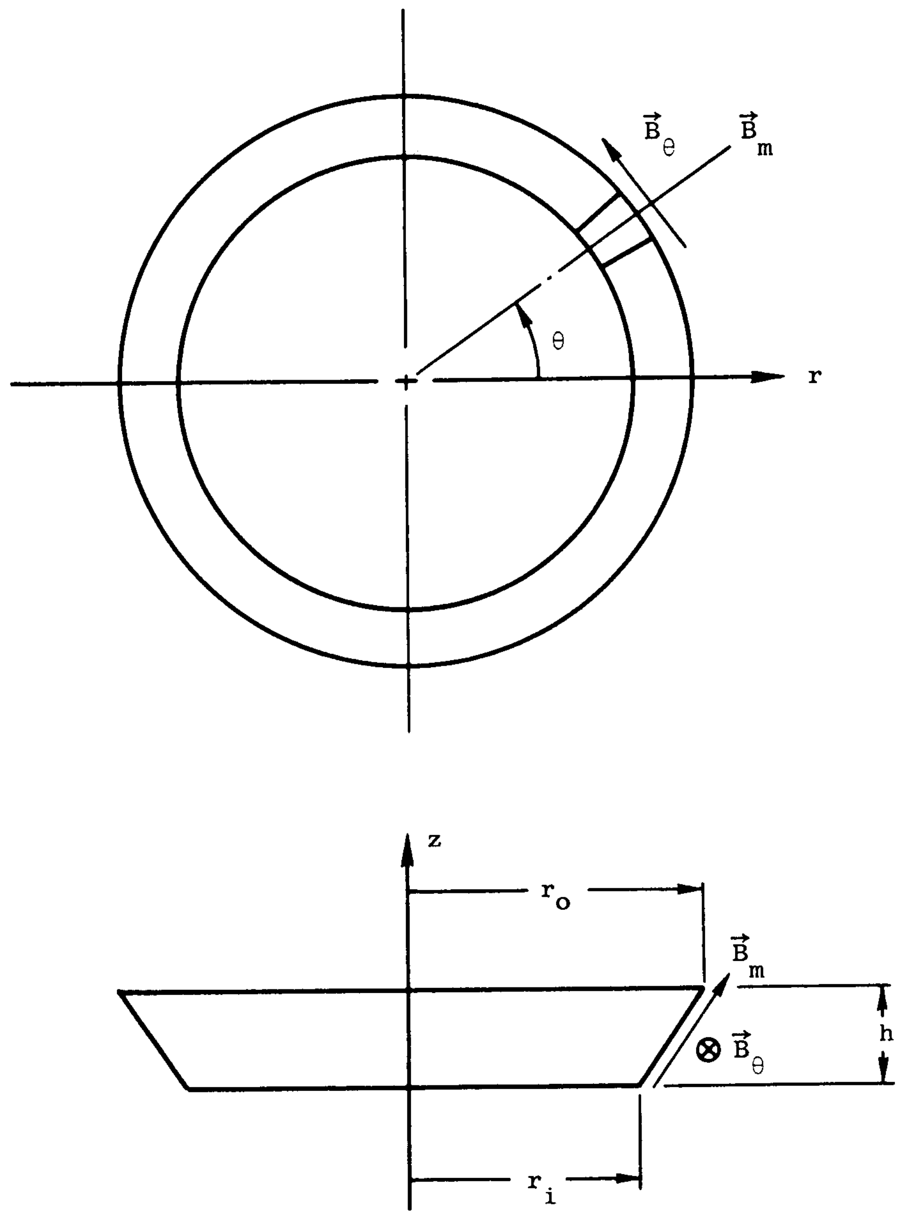

FIG. 12. ELEMENT OF BODY SURFACE AND MAGNETIC FIELD

where $\hat{m}$ is a unit vector in the meridian direction. In the vertical direction the force on the segment bounded by θ and $\theta + d\theta$ is $dF_v = B^2/2\mu_o \; dA_v$ where

$$dA_v = \frac{r_o^2 - r_i^2}{2} \, d\theta$$

$$B^2 = (B_{sym} + \epsilon\cos\theta \, B_{asym})^2 + \epsilon^2 \sin^2\theta \, B'^2_{asym}$$

$$\cong B_{sym}^2 + 2\,\epsilon\cos\theta \, B_{sym} ,$$

to first order in ϵ.

$$F_v \cong \frac{1}{2\mu_o} \int_o^{2\pi} (B_{sym}^2 + 2\,\epsilon\cos\theta \, B_{sym} \, B_{asym}) \, \frac{r_o^2 - r_i^2}{2} \, d\theta$$

$$= \frac{\pi}{2\mu_o} (r_o^2 - r_i^2) \, B_{sym}^2 .$$

Thus, to first order in ϵ, the vertical force is unchanged by the horizontal offset. The net horizontal force can now be found. Note that B^2 is symmetrical about the $\theta = 0, \pi$ line so that there can be no force in the $\theta = \pi/2$ direction. In the $\theta = \pi$ direction however the force on an element is $dF_h = B^2/2\mu_o \cos\theta \; dA_h$ where $dA_h = h \, d\theta \, (r_o + r_i)/2$. Therefore

$$F_h \cong \frac{1}{2\mu_o} \int_o^{2\pi} (B_{sym}^2 + 2\,\epsilon\cos\theta \, B_{sym} \, B_{asym}) \cos\theta \, \frac{r_o + r_i}{2} \, h \, d\theta$$

$$\cong \frac{\epsilon}{2\mu_o} \, B_{sym} \, B_{asym} \; \pi(r_o + r_i) \, h . \qquad (25)$$

Thus the horizontal force is proportional to ϵ and involves only the component of the asymmetric field in the meridian direction.

If one is only interested in the forces on the deflected body and not the field distribution then the column matrix B'_{asym} need not be calculated. It might be noted that although the change in vertical force is second order, the variation in its distribution across the element causes a resultant moment to be applied in the $\theta = \pi/2$ direction

$$dM = \frac{r_o + r_i}{2} \cos\theta \, dF_v$$

$$M = \int_o^{2\pi} \frac{r_o + r_i}{2} \frac{B^2}{2\mu_o} \frac{r_o^2 - r_i^2}{2} \cos\theta \, d\theta$$

$$M = \frac{(r_o + r_i)^2 (r_o - r_i)\pi}{2} \frac{\epsilon}{2\mu_o} B_{sym} B_{asym}. \tag{26}$$

The total horizontal force on the body may be found by summing those which act on each of the elements, Eq. (25), and the location of the resultant may be determined by additionally considering the translation-dependent moments given by Eq. (26). Thus the magnitude and position of the forces acting on an axially-symmetric body when displaced from the axis of several surrounding coils have been completely determined.

2. Rotation

The problem of a body rotated through a small angle about an axis lying in the plane of the coil shall now be attacked. Again it will be found that the asymmetries in the normal field contribute only an additive term with a factor $\cos\theta$, as in Eq. (21), so that the integral equation can be split into a symmetric and an asymmetric part and the latter can be solved by Hess's method.

Consider an axially-symmetric body whose natural coordinates are r, θ, z or x, y, z, and a coil whose natural coordinates are ρ, φ, ζ or ξ, η, ζ. Let the origins and the y and η axes coincide and let the z and ζ axes be inclined an angle δ (Fig. 13). The relationships between the cartesian and cylindrical coordinates in the two systems are

$$r = \sqrt{x^2 + y^2} \; ; \quad \theta = \tan^{-1} \frac{y}{x} \; ; \quad x = r \cos \theta \; ; \quad y = r \sin \theta$$
$$\rho = \sqrt{\xi^2 + \eta^2} \; ; \quad \varphi = \tan^{-1} \frac{\eta}{\xi} \; ; \quad \xi = \rho \cos \varphi \; ; \quad \eta = \rho \sin \varphi \; . \tag{27}$$

The transformation between the body and coil systems is given by a rotation about the y axis

$$\begin{Bmatrix} x \\ y \\ z \end{Bmatrix} = \begin{bmatrix} \cos \delta & 0 & -\sin \delta \\ 0 & 1 & 0 \\ \sin \delta & 0 & \cos \delta \end{bmatrix} \begin{Bmatrix} \xi \\ \eta \\ \zeta \end{Bmatrix} \tag{28}$$

The relations for the unit vectors are

$$\begin{Bmatrix} \hat{x} \\ \hat{y} \\ \hat{z} \end{Bmatrix} = \begin{bmatrix} \cos \delta & 0 & -\sin \delta \\ 0 & 1 & 0 \\ \sin \delta & 0 & \cos \delta \end{bmatrix} \begin{Bmatrix} \hat{\xi} \\ \hat{\eta} \\ \hat{\zeta} \end{Bmatrix} = \begin{Bmatrix} \cos \delta \, \hat{\xi} - \sin \delta \, \hat{\zeta} \\ \hat{\zeta} \\ \sin \delta \, \hat{\xi} + \cos \delta \, \hat{\zeta} \end{Bmatrix} \tag{29}$$

Also

$$\begin{Bmatrix} \hat{r} \\ \hat{\theta} \end{Bmatrix} = \begin{bmatrix} \cos \theta & \sin \theta \\ -\sin \theta & \cos \theta \end{bmatrix} \begin{Bmatrix} \hat{x} \\ \hat{y} \end{Bmatrix} \tag{30}$$

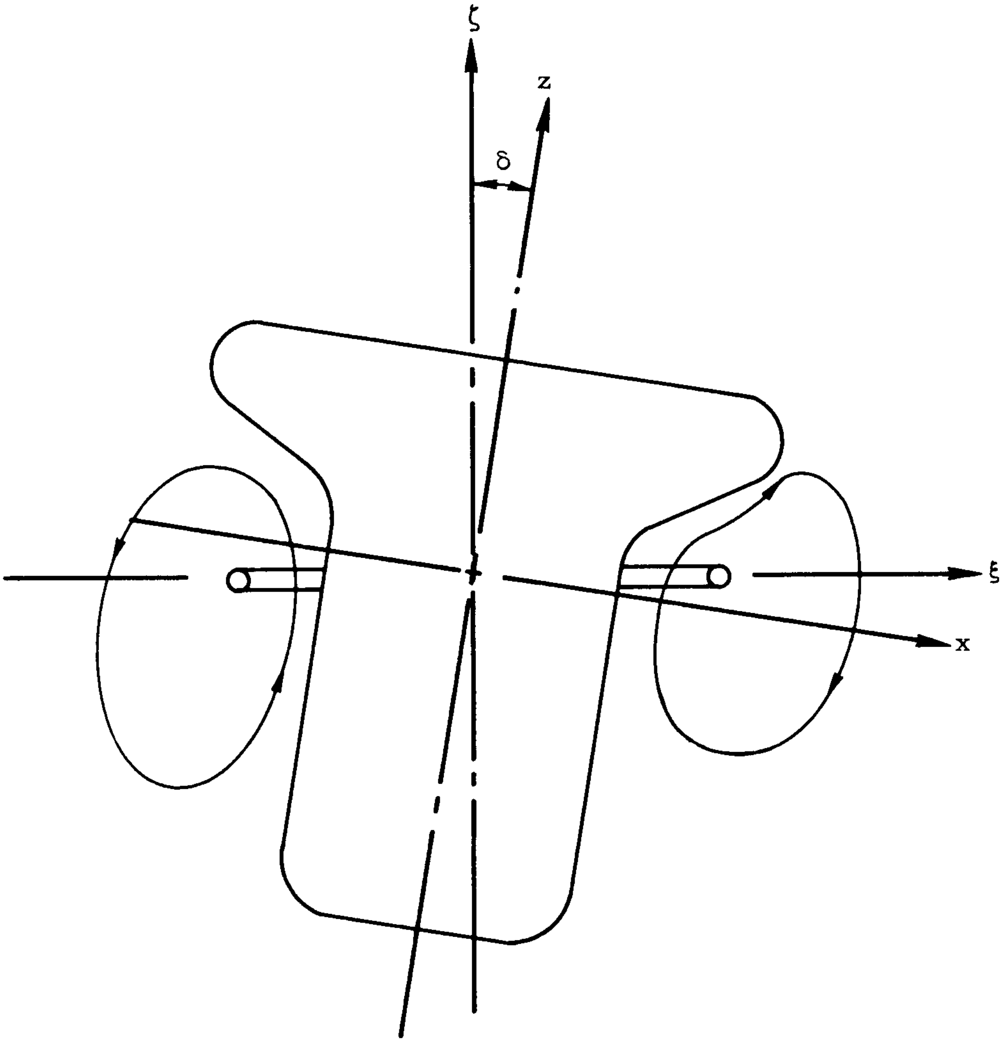

FIG. 13. BODY AND COIL AXES INCLINED AN ANGLE δ

$$\begin{Bmatrix} \hat{\xi} \\ \hat{\eta} \end{Bmatrix} = \begin{bmatrix} \cos\varphi & -\sin\varphi \\ \sin\varphi & \cos\varphi \end{bmatrix} \begin{Bmatrix} \hat{\rho} \\ \hat{\varphi} \end{Bmatrix} \tag{31}$$

From Eqs. (29) and (31) we have

$$\begin{aligned} \hat{x} &= \cos\delta\,(\cos\varphi\,\hat{\rho} - \sin\varphi\,\hat{\varphi}) - \sin\delta\,\hat{\zeta} \\ \hat{y} &= \sin\varphi\,\hat{\rho} + \cos\varphi\,\hat{\varphi} \\ \hat{z} &= \sin\delta\,(\cos\varphi\,\hat{\rho} - \sin\varphi\,\hat{\varphi}) + \cos\delta\,\hat{\zeta}\ . \end{aligned} \tag{32}$$

The cartesian components of the coil field $\vec{B}$ in the body system are found by the transformation of Eq. (32). Note that because of the axial symmetry in the coil system, the component $B_\varphi \equiv 0$.

$$\begin{aligned} B_x &= \cos\delta\,\cos\varphi\,B_\rho - \sin\delta\,B_\zeta \\ B_y &= \sin\varphi\,B_\rho \\ B_z &= \sin\delta\,\cos\varphi\,B_\rho + \cos\delta\,B_\zeta\ . \end{aligned} \tag{32}$$

The cylindrical components may now be found using Eq. (30)

$$\begin{aligned} B_r &= \cos\theta\,B_x + \sin\theta\,B_y \\ &= (\cos\theta\,\cos\delta\,\cos\varphi + \sin\theta\,\sin\varphi)\,B_\rho - \cos\theta\,\sin\delta\,B_\zeta \\ B_\theta &= -\sin\theta\,B_x + \cos\theta\,B_y \\ &= (-\sin\theta\,\cos\delta\,\cos\varphi + \cos\theta\,\sin\varphi)\,B_\rho + \sin\theta\,\sin\delta\,B_\zeta \\ B_z &= \sin\delta\,\cos\varphi\,B_\rho + \cos\delta\,B_\zeta\ . \end{aligned} \tag{33}$$

In order to express $\vec{B}$ properly in body coordinates the coefficients in the above terms must be explicit functions of r, θ, and z. Therefore it is necessary to find ρ, φ, ζ in terms of r, θ, z. From Eqs. (27) and (28) we have

$$\rho = \sqrt{\xi^2 + \eta^2} = \sqrt{\cos^2\delta\ x^2 + 2 \sin\delta \cos\delta\ xz + \sin^2\delta\ z^2 + y^2}$$

$$\varphi = \arcsin \frac{\eta}{\rho} = \arccos \frac{\xi}{\rho}$$

$$\zeta = - \sin\delta\ x + \cos\delta\ z\ .$$

Using Eq. (27) again gives

$$\rho = \sqrt{\cos^2\delta\ r^2 \cos^2\theta + 2 \sin\delta \cos\delta\ r \cos\theta\ z + \sin^2\delta\ z^2 + r^2 \sin^2\theta}$$

$$= r\sqrt{\cos^2\delta \cos^2\theta + \sin^2\theta + 2 \sin\delta \cos\delta \cos\theta\ \frac{z}{r} + \frac{z^2}{r^2} \sin^2\delta}$$

$$\cos\varphi = \frac{\xi}{\rho} = \frac{\cos\delta\ x + \sin\delta\ z}{\rho}$$

$$= \frac{r}{\rho} \left(\cos\delta \cos\theta + \sin\delta\ \frac{z}{r}\right)$$

$$\sin\varphi = \frac{\eta}{\rho} = \frac{y}{\rho}$$

$$= \frac{r}{\rho} \sin\theta$$

$$\zeta = - \sin\delta\ x + \cos\delta\ z\ .$$

Assume now that δ is small so that $\sin\delta = \delta$ and $\cos\delta = 1$, and further than $z/r\ \delta \ll 1$. Using these approximations the above transformations become

$$\rho \cong r\sqrt{1 + 2\,\delta\,\frac{z}{r}\cos\theta}$$

$$\cong r\,(1 + \delta\,\frac{z}{r}\cos\theta)$$

$$\cos\varphi \cong \cos\theta\,(1 + \delta\,\frac{z}{r}\,\frac{\sin^2\theta}{\cos\theta})$$

$$\cong \cos\theta + \delta\,\frac{z}{r}\sin^2\theta$$

$$\sin\varphi \cong \sin\theta\,(1 - \delta\,\frac{z}{r}\cos\theta)$$

$$\zeta \cong z - \delta r\cos\theta\ .$$

The coefficients on the right side of Eq. (33) become

$$\cos\theta\cos\delta\cos\varphi + \sin\theta\sin\varphi \cong$$

$$\cos^2\theta + \sin^2\theta + \delta\,\frac{z}{r}\,(\sin^2\theta\cos\theta - \sin^2\theta\cos\theta) \cong 1,$$

$$\cos\theta\sin\delta = \delta\cos\varphi,$$

$$-\sin\theta\cos\delta\cos\varphi + \cos\theta\sin\varphi \cong$$

$$-\sin\theta\cos\theta + \cos\theta\sin\theta - \delta\,\frac{z}{r}\,(\sin^3\theta + \cos^2\theta\sin\theta)$$

$$= -\,\delta\,\frac{z}{r}\sin\theta\ ,$$

$$\sin\theta\sin\delta \cong \delta\sin\theta,$$

$$\sin\delta\cos\varphi \cong \delta\cos\theta\ .$$

Equation (33) may now be stated as

$$B_r = B_\rho - \delta \cos\theta\, B_\zeta$$

$$B_\theta = \delta \sin\theta\, (B_\zeta - \frac{z}{r} B_\rho)$$

$$B_z \cong B_\zeta + \delta \cos\theta\, B_\rho\ .$$

The field is still not an explicit function of the body coordinates since B_ρ and B_ζ are in terms of ρ and ζ, i.e., $B_\rho = B_\rho(\rho,\zeta)$ and $B_\zeta = B_\zeta(\rho,\zeta)$. The coil coordinates are, however, available in terms of r, θ, z, and B_ρ and B_ζ can be expanded in a first-order two-dimensional Taylor Series to give

$$\begin{aligned} B_\rho &\cong B_\rho(r + \delta z \cos\theta,\ z - \delta r \cos\theta) \\ &\cong B_\rho(r,z) + \delta \cos\theta \left[z \frac{\partial B_\rho(r,z)}{\partial r} - r \frac{\partial B_\rho(r,z)}{\partial z} \right] \\ B_\zeta &\cong B_\zeta(r,z) + \delta \cos\theta \left[z \frac{\partial B_\zeta(r,z)}{\partial r} - r \frac{\partial B_\zeta(r,z)}{\partial z} \right]. \end{aligned}$$

And

$$B_r \cong B_\rho(r,z) - \delta \cos\theta \left[B_\zeta(r,z) - z \frac{\partial B_\rho(r,z)}{\partial r} + r \frac{\partial B_\rho(r,z)}{\partial z} \right]$$

$$B_\theta \cong \delta \sin\theta \left[B_\zeta(r,z) - \frac{z}{r} B_\rho(r,z) \right]$$

$$B_z \cong B_\zeta(r,z) + \delta \cos\theta \left[B_\rho(r,z) + z \frac{\partial B_\zeta(r,z)}{\partial r} - r \frac{\partial B_\zeta(r,z)}{\partial z} \right].$$

Thus the external normal field, $B_n(r,\theta,z)$, takes a form similar to the offset case as shown in Eq. (21) of the previous chapter. The integral equation can then be split into a symmetric and an asymmetric part and the latter solved by Hess's method for bodies of revolution in cross flow. The horizontal forces and the moment about any point can then be calculated by Eqs. (25) and (26).

If the body had been first translated the field of the coil would not simply be B_ρ and B_ζ as used in Eq. (32) but rather would have additive terms of order ϵ. If products of $\epsilon\delta$ are neglected then the effect of the first translation is merely to add the ϵ dependent term of Eq. (21) to the normal field as calculated above. Thus a rotation of the body about any horizontal axis may be considered as a translation followed by a rotation about the plane of the coil, and the result will be correct to first order in δ.

The method used to calculate the normal field in the translation case assumes that $\epsilon/r \ll 1$, and in the rotation case it assumes that $\delta \ll 1$ and $z\delta/r \ll 1$. Note that both of these assumptions fail near where the body intersects its axis because r goes to zero. The second also fails when $z \gg r$, as on an infinite cylinder. A body on which none of the assumptions ever fails must be finite and must not intersect its axis (as a torous would, for example). For most other shapes of interest the situation can be partially corrected by keeping ϵ and $z\delta$ small compared to the radius of the first describing point off the axis, since the external field is actually cancelled at a point midway between the axis and the first describing point.

D. COMPUTER PROGRAMS

The first step in calculating the magnetic fields and forces by the above method is to calculate the normal and tangential influence coefficient matrices [A] and [C] used in Eq. (19). In Ref. 22 integral formulas are given for the elements of these matrices in terms of the coordinates of the i^{th} and j^{th} describing points. The reference suggests that Simpson's rule be used to carry out the integration and gives a guide for selecting the number of intervals.

At the same time it is convenient to form the matrices $[A_{asym}]$ and $[C_{asym}]$ to be used in reduction of the asymmetric integral equation, Eq. (22), and in evaluating the term B_{asym} in Eq. (23). Similar formulas are given in Ref. 24 for elements of these matrices. A program called Influence Coefficient Integration (ICI) has been written to evaluate these four matrices and is listed in Appendix A with its subroutines. The x and y coordinates of the body are first read in, assuming that the x axis is the axis of symmetry (negative z in Figs. 10, 11, and 13). The integrands are evaluated along each of the integration strips by the subroutine INTEGR and the actual integration is performed by the subroutine SIMP. When the matrices are completely filled, those dealing with the influence in the normal direction, $[A]$ and $[A_{asym}]$, are inverted by INVERT. All four matrices are written on the blank magnetic tape 12.

Having the influence coefficient matrices, calculations can be made for the body in an axially-symmetric external field. This is done by the Axially-Symmetric Body (AXBOD) program of Appendix B. The body coordinates and $[A]$ and $[C]$ are read in from the tape generated by ICI. The coil coordinates and strength are read in from cards. The external field is calculated by the subroutine COILFD using the following formulas from §7 of Ref. 25

$$B_r = \frac{\mu I}{2\pi} \frac{z}{r\sqrt{(a+r)^2+z^2}} \left[-K(k^2) + \frac{a^2+r^2+z^2}{(a-r)^2+z^2} E(k^2) \right]$$

$$B_z = \frac{\mu I}{2\pi} \frac{1}{\sqrt{(a+r)^2+z^2}} \left[K(k^2) + \frac{a^2-r^2-z^2}{(a-r)^2+z^2} E(k^2) \right] \tag{34}$$

$$k^2 = \frac{4ar}{(a+r)^2+z^2} ,$$

where K and E are complete elliptic integrals of the first and second kind respectively; a is the coil radius; r, z are polar coordinates of a system whose origin is at the center of the coil. Once the field has been calculated it is integrated over the surface to give the net force in the minus x direction (lift).

The field distribution may be printed by adjusting the control variable LO, and the maximum field and its location are printed separately. The subroutine DERIVE provides for printing out the lift force and maximum field for various currents. The variable KOILN allows the field to be generated by more than one coil. Note that the forces due to several coils cannot be added directly since each is proportional to the field squared. Rather the field of the collection is first summed and when the square of the sum integrated to give the force. The program continues to read cards defining coil geometry until they are exhausted.

The program OFFSET listed in Appendix C solves the problem of a body whose axis is parallel to but offset from the axes of the coils, Eqs. (22) and (23). It first calculates the field for the on-axis body exactly as in AXBOD with the control variable LOFST set equal to one. It then goes back and reads the asymmetric influence coefficient matrices and proceeds to solve this problem with LOFST = 2. The derivatives of the field components are evaluated by the subroutine FLDDER from the formulas below which are obtained by straightforward but laborious differentiation of Eqs. (34)

$$a\,\frac{\partial B_r}{\partial r} = -B_r\left\{\frac{1}{r^*} + \frac{r^*(r^{*2} - 1 + z^{*2})}{[(1+r^*)^2 + z^{*2}][(1-r^*)^2 + z^{*2}]}\right\} + \frac{\mu I}{2\pi a}\,\frac{6z^*(1-r^{*2}+z^{*2})}{[(1+r^*)^2+z^{*2}]^{3/2}}$$

$$\cdot\,\frac{E(k^2)}{[(1-r^*)^2 + z^{*2}]^2}$$

$$a \frac{\partial B_z}{\partial r} = \frac{-(1+r^*)B_z}{(1+r^*)^2 + z^{*2}} + \frac{(1-r^*)(1-r^{*2} + z^{*2})B_r}{z^*[(1-r^*)^2 + z^{*2}][(1+r^*)^2 + z^{*2}]} + \frac{\mu I}{2\pi a} \frac{2E(k^2)}{r^*[(1-r^*)^2 + z^{*2}]}$$

$$\frac{1}{(1+r^*)^2 + z^{*2}} \left\{ -1 + \frac{(1-r^{*2} + z^{*2})[(1+r^*)^2 + z^{*2} - r^*(3r^*+1)]}{[(1+r^*)^2 + z^{*2}][(1-r^*)^2 + z^{*2}]} \right\}$$

$$k^2 = \frac{4r^*}{(1+r^*)^2 + z^{*2}} , \tag{35}$$

where r^*, z^* are the natural coordinates of the coil normalized by (divided by) the coil radius. Since these expressions are relatively complicated they were checked against the finite difference

$$\frac{B(r + h/2, z) - B(r - h/2, z)}{h} ,$$

for various values of r and z with $h = 10^{-1}$ through 10^{-7}.

The program matrix multiplies to obtain B_{asym} of Eq. (23) and then calculates the horizontal force from Eq. (25). The location of the resultant force is found considering the translation-dependent moment of Eq. (26). The restoring force constant, location of the resultant, and increase in maximum field per unit offset are printed.

The program listed in Appendix D calculates the field in a body rotated through an angle DELTA about an axis located at XT. The program is identified as TILT and operates exactly as OFFSET, that is it evaluates the symmetric field and then the asymmetric field. In evaluating the asymmetric external normal field the program first translates the body through a distance such that when the body is rotated through the specified angle the body and field axes intersect at the location given by XT. The derivatives of the field components with respect to z must be obtained as well as those in Eqs. (35).

No additional differentiation is necessary, however, as the following argument shows. Recall that the coil field is derivable from some scalar potential Φ_c introduced in Eq. (13). The components are then given by

$$B_r = -\frac{\partial \Phi_c}{\partial r} \quad ; \quad B_z = -\frac{\partial \Phi_c}{\partial z}$$

$$\frac{\partial B_z}{\partial r} = -\frac{\partial^2 \Phi_c}{\partial r \partial z} \quad ; \quad \frac{\partial B_r}{\partial z} = -\frac{\partial^2 \Phi_c}{\partial z \partial r} = \frac{\partial B_z}{\partial r}$$

$$\frac{\partial B_r}{\partial r} = -\frac{\partial^2 \Phi_c}{\partial r^2} \quad ; \quad \frac{\partial B_z}{\partial z} = -\frac{\partial^2 \Phi_c}{\partial z^2} .$$

In cylindrical coordinates

$$\nabla^2 \Phi_c = \frac{\partial^2 \Phi_c}{\partial r^2} + \frac{1}{r} \frac{\partial \Phi_c}{\partial r} + \frac{\partial^2 \Phi_c}{\partial z^2} = 0 .$$

Therefore

$$\frac{\partial B_z}{\partial z} = -\frac{\partial^2 \Phi_c}{\partial z^2} = \frac{\partial^2 \Phi_c}{\partial r^2} + \frac{1}{r} \frac{\partial \Phi_c}{\partial r}$$

$$= -\frac{\partial B_r}{\partial r} - \frac{1}{r} B_r .$$

Thus the z derivatives are obtainable from the r derivative of Eqs. (35); this is done by the subroutine BDERIV. Having obtained the field, the program calculates the torque about the axis of rotation using Eqs. (25) and (26). It prints out this result as well as the restoring moment per unit rotation, the net horizontal force if any, and the maximum increase in field per unit rotation.

E. COMPUTER RESULTS

1. Sphere

In evaluating the results of the various computer programs it is desirable to compare them to some known standard. This is possible if one chooses as the body of interest a sphere. As stated earlier, Harding has solved the problem of a diamagnetic sphere in the field of one or more coils and, for the case that the axes of the two coincide, the solution is obtained by an image coil within the sphere (Appendix A of Ref. 7). The mutual repulsion of the image and actual coils gives the net lift force. Figure 14 shows two distinct coil-sphere geometries. A single coil support is shown in Fig. 14A with a .635 cm radius sphere and a 1.147 cm radius coil. The JPL results are given in Table 1A along with those of the present method for various elevations z. Note that the present method was used to meet the boundary conditions at 50 and 100 points. Figure 14B shows a sphere with two coaxial coils of specified relative geometry. The lift forces for this arrangement are compared in Table 1B.

It should be noted that the results compared were obtained by two distinctly different methods. Harding determined the coefficients in an infinite series of Legendre Polynomials to meet the boundary conditions exactly. Inexactness in his method stems from representing the series by a finite number of terms, whereas in the present method it stems from meeting the boundary conditions at a finite number of points.

An analytic solution for an ellipsoid in the field of a coil is also available [Ref. 26] but the results have not been compared to the present method.

2. Cylinder

The design criteria for a cylindrically-symmetric body have been discussed in Chapter III and drawings of the actual rotor are included in Chapter VII. A IOX tracing of the actual fabricated and plated rotor was made using an optical comparitor, and from this 110 describing points were selected for the computer solution. The tracing

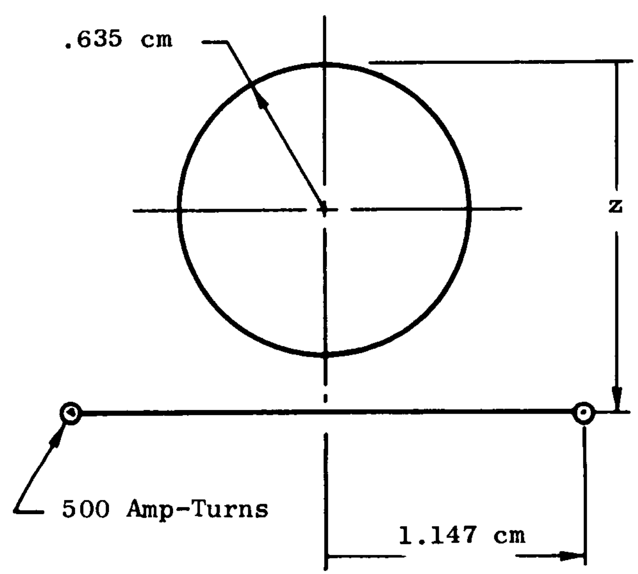

14A

Single Coil

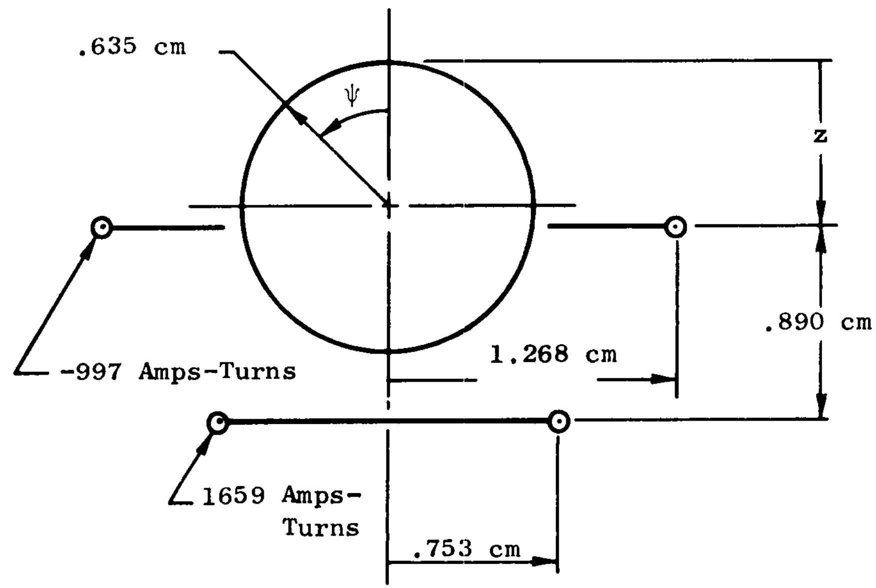

14B

Two Coils

FIG. 14. SPHERE-COIL SYSTEM

TABLE 1A

COMPARISON OF CALCULATED LIFT FORCES BY HARDING'S AND PRESENT METHODS

Geometry of Fig. 14A; Constant Coil Strength

z(cm)	Lift Force (Kilodynes)		
	Harding's Method	Present Method	
		50 pts	100 pts
1.135	5.443	5.358	5.400
1.435	4.124	4.054	4.088
1.635	2.802	2.753	2.777

TABLE 1B

Geometry of Fig. 14B; Constant Coil Strength

z(cm)	ψ for Max Field (^{o})			Lift Force (Kilodynes)		
	Harding	50 pts	100 pts	Harding	50 pts	100 pts
1.0234				3.234	3.146	3.234
.635				27.12	25.74	26.26
.4292	138.5	135.	134.	81.26	77.63	78.77
-.1816	95.8	95.4	96.3	91.88	86.77	88.39
.0016	113.5	102.6	104.3	219.2	170.4	173.6

is presented in Fig. 15 along with the locations and strengths of five ideal (infinite current density) coils which are used to represent the finite-sized actual coil, an outline of which is shown on the tracing. The strength of the tangential field is plotted in the normal direction along the rotor surface to the scale shown. Note that in contrast to the usual sort of plot, the spacing of the lines has nothing to do with the field strength. Each line simply starts at a point where the boundary conditions are met.

By moving all the coils up or down an equal amount it is possible to determine the coil current necessary to support a given weight at various elevations. Figure 16A shows such a relationship for a slightly different rotor, with experimental points obtained by a capacitive bridge method discussed in Chapters V and VII. Figure 16B shows the current and maximum field versus height for the body traced in Fig. 15. Note that the elevation and current for the minimum of the maximum field can be read directly from the plot.

The program OFFSET which calculates the restoring forces on the translated body can also be checked against results for a sphere obtained by Harding at JPL. The solution for a sphere whose axis does not coincide with that of the coils is not as simple as the on-axis case. Harding [Ref. 27] has solved the problem by expanding the body potential in a series of Legendre Polynomials about the sphere's center. This method is not limited to small offsets but rather can find the forces for any sphere-coil system. Table 2 compares the results obtained by the JPL and present methods for the cases shown in Fig. 14. The present method states that the resultant horizontal force passes through the sphere's center, as one knows it must because no torques can act on the body.

For the body of interest shown in Fig. 15 the OFFSET program states that the line of action of the horizontal force intersects the axis at a point 2.796 cm below the upper pole. The variation of the horizontal force location and restoring constant is plotted as a function of elevation in Fig. 17.

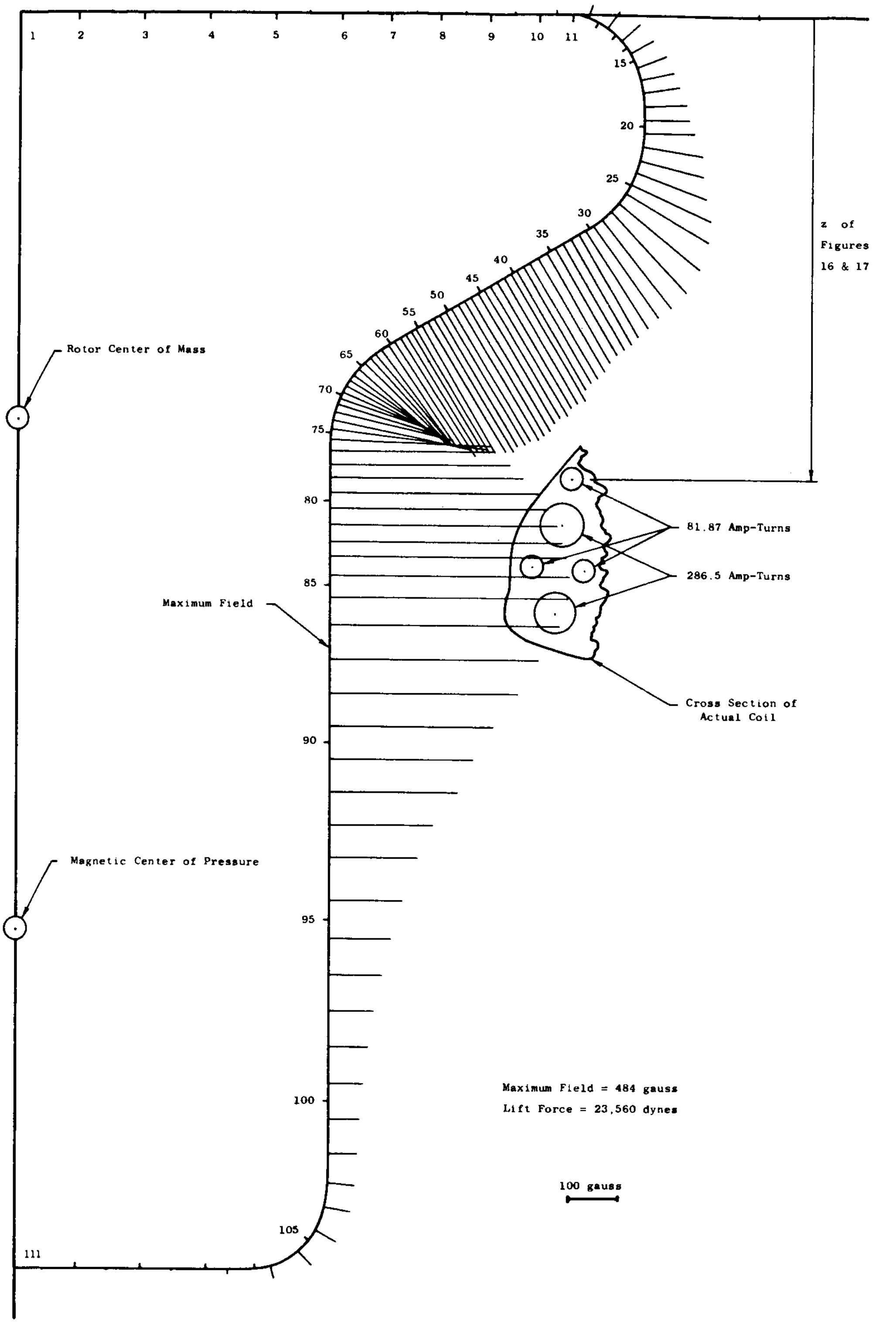

FIG. 15. MAGNETIC FIELD DISTRIBUTION: TANGENTIAL STRENGTH PLOTTED IN THE NORMAL DIRECTION

TABLE 2A

COMPARISON OF CALCULATED LIFT FORCES BY HARDING'S AND PRESENT METHODS

Geometry of Fig. 14A; Constant Coil Strength

z(cm)	Horizontal Force (dynes/cm)		
	Harding	50 pts	100 pts
1.135	5350.	5200.	5270.
1.435	584.	551.	564.
1.635	-312.	-323.	-322.

TABLE 2B

Geometry of Fig. 14B; Constant Coil Strength

z(cm)	Horizontal Force/Unit Offset (dynes/cm)		
	Harding	50 pts	100 pts
.4823	116050.	105487.	107156.
1.0234	26878.	26184.	26490.
.635	69700.	67194.	68088.
.4292	135120.	131749.	133998.
-.1816	3453260.	3326130.	3484060.

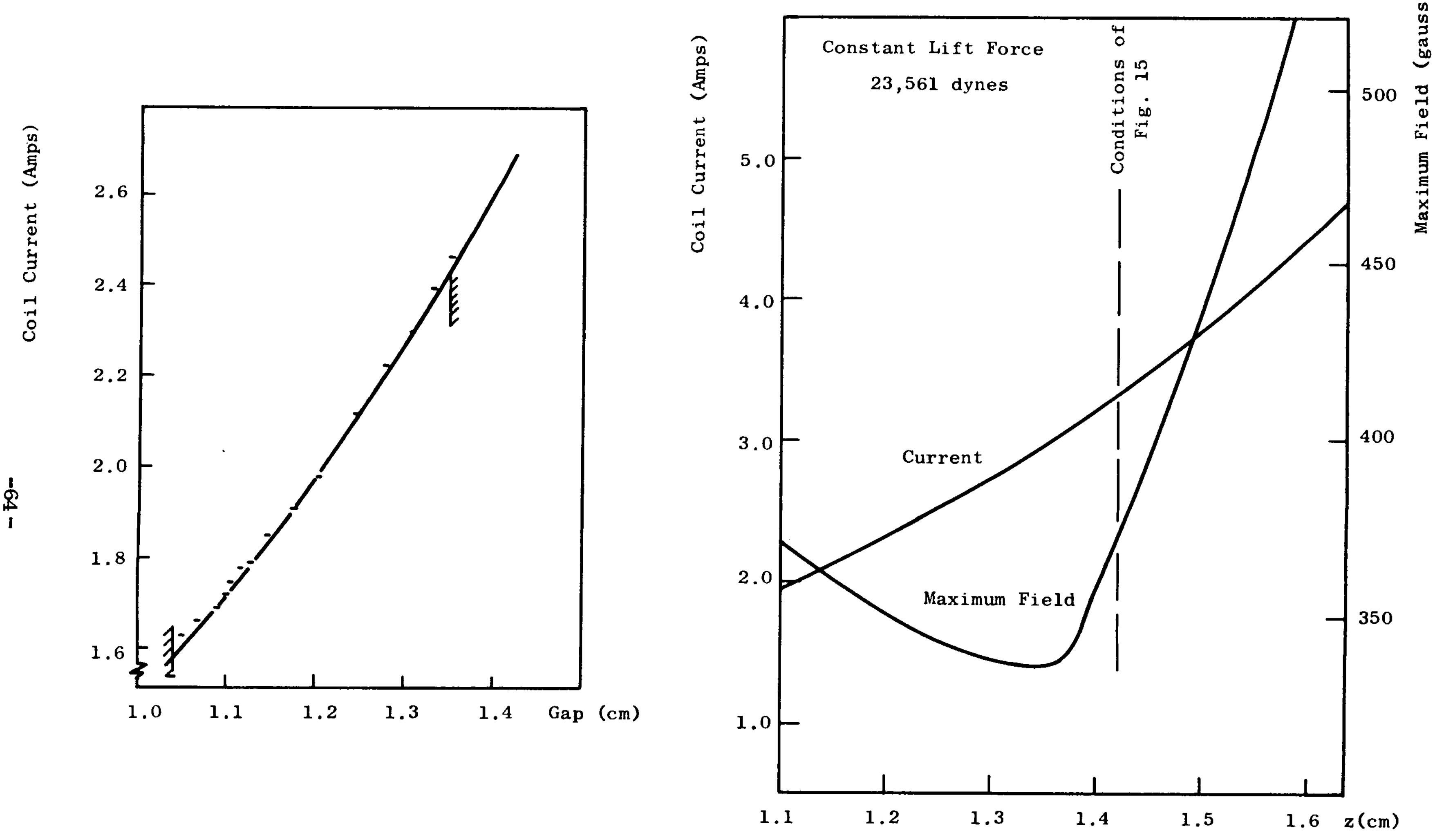

16A

16B

FIG. 16. CURRENT AND MAXIMUM FIELD VS. HEIGHT

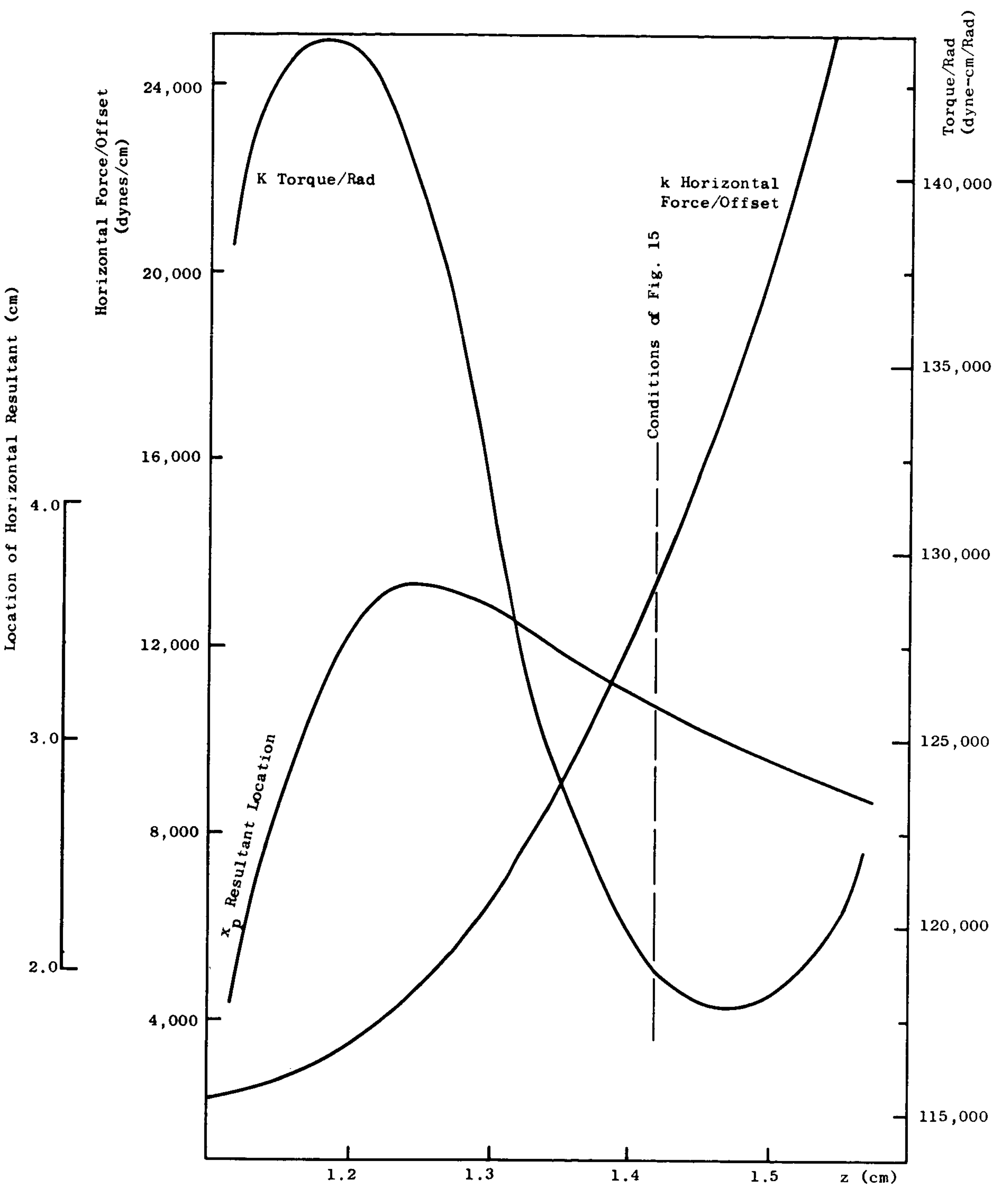

FIG. 17. RESTORING FORCES VS. HEIGHT

The currents in each of the coils is adjusted such that the net upward force is 23.561 kilodynes, the weight of the rotor. Each of the coils does, however, maintain that proportion of the current indicated in Fig. 15 so that Fig. 17 effectively shows the variation of the quantities with increasing current. Note that the restoring constant k varies over a wide range from 3000 to 30,000 dyne/cm in the interval of interest. This indicates the effect that when the body is supported with larger currents at higher elevations it becomes considerably stiffer laterally. For a coil of slightly larger diameter the body is actually laterally unstable for the lower elevations. This property was used in the spin-up procedure (see Chapter VII, Section E). The resultant or magnetic center of pressure location varies within about one centimeter of its value of Fig. 15. Note that it is always below the center of mass.

The results of the TILT program may also be checked using a sphere. First, the most obvious fact is that rotation of the body about its center should result in no torque. This has been the case for all coil-sphere configurations calculated. Second, when the sphere is rotated through a small angle about an axis far away it should experience the same horizontal force as when it is simply translated. In this respect the OFFSET and TILT programs agree. One point should be mentioned: The program calculates the horizontal force in the body axis system (x direction of Fig. 13). Thus the axial force on the sphere, which is still along the original vertical (ζ direction), contributes to the apparent horizontal force.

Rotating the body of interest about the effective center of pressure causes a restoring moment of magnitude 120,400. dyne-cm/radian and a horizontal force proportional to the weight and rotation. The variation of this restoring moment between 117,000 and 142,000 dyne-cm/rad is plotted in Fig. 17. Note that, unlike k, it varies only 20 percent over the range of interest.

One possible reason for the differences between the JPL and present results might be mentioned. Harding generated the field of the coil using Bartberger's tabulation [Ref. 28] whereas here it was evaluated directly from the elliptic integrals of Eq.(34), using the algorithm shown in Appendix B. There is a small discrepancy between the two methods and this author feels the second is slightly more accurate.

V. EQUATIONS OF MOTION

A. EQUATIONS

Having calculated the forces and torques on the magnetically-supported body we are in a position to predict its motion. To this end this chapter will present the equations of motion for the spinning body and proceed to solve them in the linearized case. The result will be a prediction of the frequencies and modes of oscillation which then can be compared to the experimentally observed behavior.

The basic equations of motion we wish to write for the rigid rotor are

$$\vec{M} = \dot{\vec{H}}$$

$$\vec{F} = m\dot{\vec{v}} ,$$

where $\vec{M}$ and $\vec{F}$ are, respectively, the resultant moment (about its mass center) and force acting on the body, $\vec{H}$ is its angular momentum (about its mass center) and $\vec{v}$ is the translational velocity of the mass center.

To determine $\dot{\vec{H}}$, consider a coordinate system X,Y,Z whose origin is at the center of mass of the rotor and the direction of whose axes is fixed in inertial space (Fig. 18A). Let a rotation about X through φ go to a new system X, y, z_1, and let a rotation through θ about y go to x,y,z. This last system shall be a symmetry axis system which does not rotate with the body; i.e., z lies along the body axis of symmetry, but the coordinate system fixed in the body, x',y',z', is reached by another rotation through ψ about z.

The angular velocity of the x,y,z system is

$$\vec{\omega}^C = \hat{X}\,\dot{\varphi} + \hat{y}\,\dot{\theta}$$

$$= \hat{x}(\cos\,\theta)\dot{\varphi} + \hat{y}\,\dot{\theta} + \hat{z}(\sin\,\theta)\dot{\varphi} .$$

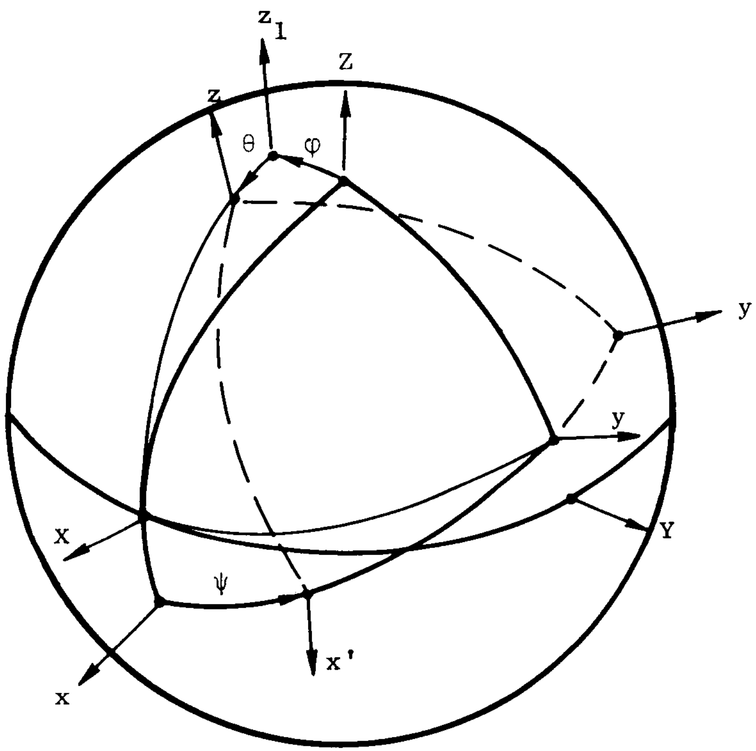

18A

Euler Angles

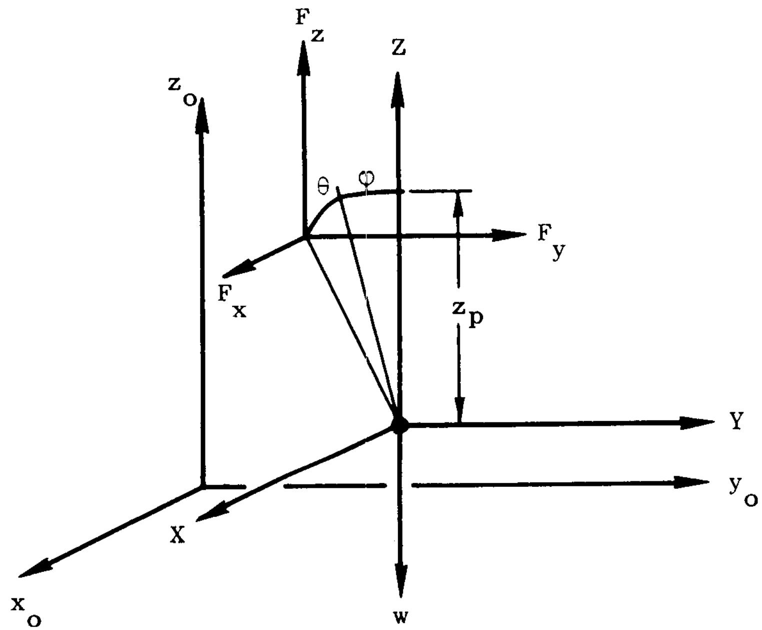

18B

Body Forces

FIG. 18. COORDINATE SYSTEMS

The angular velocity of the body is

$$\vec{\omega}^{B} = \vec{\omega}^{C} + \hat{z}\,\dot{\psi} .$$

Assume that the moments of inertia about x' and y' are equal so that $I_x = I_y = I$, and the x,y,z axes are always principal. Then

$$\vec{H} = \bar{\bar{I}}\,\vec{\omega}^{B} = \hat{x}\; I(\cos\,\theta)\dot{\varphi} + \hat{y}\; I\;\dot{\theta} + \hat{z}\; J[(\sin\,\theta)\dot{\varphi} + \dot{\psi}] ,$$

where I and J are the transverse and polar moments of inertia respectively. It is now possible to find the time derivative of $\vec{H}$ in the inertial system.

$$\dot{\vec{H}} = \overset{\circ}{\vec{H}} + \vec{\omega}^{C} \times \vec{H}$$

$$= \hat{x}[I(\cos\,\theta\;\ddot{\varphi} - \dot{\theta}\;\dot{\varphi}\;\sin\,\theta) + J\;\dot{\theta}(\dot{\psi} + \sin\,\theta\;\dot{\varphi})]$$

$$+ \hat{y}[I(\ddot{\theta} + J\;\dot{\varphi}\;\cos\,\theta\;(\dot{\psi} + \dot{\varphi}\;\sin\,\theta)]$$

$$+ \hat{z}\; J(\ddot{\psi} + \ddot{\varphi}\;\sin\,\theta + \dot{\theta}\;\dot{\varphi}\;\cos\,\theta). \tag{36}$$

To study translational motion consider a fixed reference frame x_o,y_o,z_o whose axes are parallel to X,Y,Z and whose origin is fixed in the apparatus at the nominal location of the rotor's center of mass. The location of the mass center is then given by coordinates x_o,y_o,z_o.

To study forces and torques, let the effective magnetic center of pressure be located at $x,y,z = 0,0,z_p$. For small displacements the forces acting on the body are the weight w at the center of mass, the lift force F_z and the two horizontal forces at the center of pressure (Fig. 18B).

$$F_x = - k(x_o + \theta\, z_p)$$

$$F_y = - k(y_o - \varphi\, z_p)$$

$$F_z = w - k_1 z_o .$$

Thus the translational equations of motion are

$$m\, \ddot{x}_o = - k(x_o + \theta\, z_p)$$

$$m\, \ddot{y}_o = - k(y_o - \varphi\, z_p)$$

$$m\, \ddot{z}_o = - k_1\, z_o .$$

The torque acting about the center of mass is (to first order in the coordinates)

$$\begin{aligned} M_X &= - (K + F_z\, z_p)\varphi - F_y\, z_p \\ &= - (K + w\, z_p)\varphi + k(y_o - \varphi\, z_p)z_p \\ M_Y &= - (K + w\, z_p)\theta - k(x_o + \theta\, z_p)z_p \\ M_Z &= 0 . \end{aligned} \tag{37}$$

To first order in the displacements, $\vec{M}$ in the X,Y,Z system is identical to $\vec{M}$ in the x,y,z system since the off-diagonal terms in the transformation between the two systems are all first or higher powers of the coordinates. Since the derivation of the forces and torques neglected products of the coordinates this should also be done in Eq. (36) to be consistent:

$$\dot{\vec{H}} = \hat{x}[I(\ddot{\varphi} - \dot{\theta}\,\dot{\varphi}\,\theta) + J\,\dot{\theta}(\dot{\psi} + \theta\,\dot{\varphi})]$$

$$+ \hat{y}[I(\ddot{\theta} - J\,\dot{\varphi}(\dot{\psi} + \dot{\varphi}\,\theta)] \tag{38}$$

$$+ \hat{z}\,J(\ddot{\psi} + \ddot{\varphi}\,\theta + \dot{\theta}\,\dot{\varphi}).$$

Note that $\dot{\psi} + \theta\dot{\varphi}$ is the component of angular velocity along the axis of symmetry and, by the last of Eqs. (37), is constant. Let $\dot{\psi} + \theta\dot{\varphi} = n$. For sinusoidal motions the terms $\dot{\theta}\dot{\varphi}\theta$ and $\dot{\varphi}^2\theta$ may be neglected compared to $\ddot{\varphi}$ and $\ddot{\theta}$ because they are third order in the magnitude of the rotations. We then have the linearized equations of motion

$$\begin{aligned} I\ddot{\varphi} + J\,n\,\dot{\theta} &= -\,(K + w\,z_p + k\,z_p^2)\varphi + k\,z_p\,y_o \\ I\ddot{\theta} - J\,n\,\dot{\varphi} &= -\,(K + w\,z_p + k\,z_p^2)\theta - k\,z_p\,x_o \\ m\,\ddot{x}_o &= -\,k(x_o + \theta\,z_p) \\ m\,\ddot{y}_o &= -\,k(y_o - \varphi\,z_p)\ , \end{aligned} \tag{39}$$

and a fifth decoupled equation

$$m\,\ddot{z}_o = -\,k_1\,z_o\ .$$

B. SOLUTION

The solution of these linearized equations may be obtained quite generally by taking Laplace transforms and solving for the roots of the resulting characteristic equation. The fifth equation merely states that the body is free to bounce up and down without affecting any of the other motions (to first order). The other four indicate a coupling between motions in the x_o, y_o plane and rotations about axes parallel to that plane.

1. Non-Spinning

The non-spinning ($n = 0$) case will be investigated first. Note that for $n = 0$ the φ, y_o equations are uncoupled from the θ, x_o equations. In both sets the characteristic equation is

$$(s^2 + \omega_L^2)(s^2 + \omega_T^2) - \beta^4 = 0$$

where

$$\omega_L^2 = k/m; \quad \omega_T^2 = (K + w\, z_p + k\, z_p^2)/I; \quad \beta^4 = z_p^2\, k^2/Im .$$

The criterion for the solutions of this equation to be stable is that β^4 must lie in the interval

$$4\, \omega_L^2\, \omega_T^2 > 4\, \beta^4 > -(\omega_L^2 - \omega_T^2)^2 .$$

Since β^4 is positive definite

$$\omega_L^2\, \omega_T^2 > \beta^4 ,$$

which implies that

$$K + w\, z_p > 0 ,$$

for static stability. This could have been introduced intuitively since it merely states that any diverging moment due to the weight (z_p negative) must be offset by the magnetic restoring torque.

The non-spinning characteristic equation can be written

$$(s^2 + \sigma_1^2)(s^2 + \sigma_2^2) = 0 ,$$

where σ_1 and σ_2 are the roots. It is interesting to note that these roots always bracket those for $\beta = 0$ -- i.e., σ_2^2 is greater than both ω_L^2 and ω_T^2, and σ_1^2 is less than both ω_L^2 and ω_T^2 -- for all values of β^4 in the stable region.

2. Spinning

The equations of motion of the spinning body after Laplace transforming are

$$\begin{bmatrix} (s^2 + \omega_T^2) & + \alpha s & 0 & - kz_p/I \\ - \alpha s & (s^2 + \omega_T^2) & + kz_p/I & 0 \\ 0 & z_p\omega_L^2 & +(s^2 + \omega_L^2) & 0 \\ - z_p\omega_L^2 & 0 & 0 & +(s^2 + \omega_L^2) \end{bmatrix} \begin{Bmatrix} \Phi \\ \Theta \\ X \\ Y \end{Bmatrix} = 0 \qquad (40)$$

where $\alpha = Jn/I$.

The ratio of the linear to angular motion in one plane can be formed

$$\frac{X}{\Theta} = - \frac{z_p\omega_L^2}{s^2 + \omega_L^2} = - \frac{Y}{\Phi} .$$

Thus at a particular natural frequency the angular and linear displacements are either in phase or 180^o out of phase and proportional. This means that for a pure mode at natural frequency ω_n the body in a plane appears to be rocking about some axis a distance

$$\left[- z_p\omega_L^2/(s^2 + \omega_L^2)\right]_{s^2 = -\omega_n^2}$$

above the center of mass.

The relation between motion in the two planes is given by

$$\frac{Y}{\Theta} = \frac{I}{\alpha s\ k\ z_p} \left[(s^2 + \omega_T^2)^2 + \alpha^2 s^2 - \beta^4 \frac{s^2 + \omega_T^2}{s^2 + \omega_L^2}\right]$$

$$= \frac{I}{\alpha s\ k\ z_p} \left[\frac{s^2 + \omega_T^2}{s^2 + \omega_L^2} (s^2 + \sigma_1^2)(s^2 + \sigma_2^2) - \alpha^2 s^2\right],$$

where σ_1 and σ_2 are again the roots to the non-spinning equation. Note that the magnitude of the coupling between the planes increases with the speed and that furthermore Y is 90° out of phase with Θ. Therefore in a particular mode the oscillation can be thought of as an elliptical motion of some point in the body about the nominal axis of symmetry.

If the point of interest is the intersection of the symmetry axis and the top plane (origin in Fig. 15), then Lissijous patterns of this point may be plotted for the various modes of operation. This has been done in Fig. 19 for two distinct spin speeds and the support situation of Fig. 15. Figure 19A shows the four modes at $n = 2.0$ cps and Fig. 19B shows them at $n = 8.0$ cps. The high eccentricity of the ellipses indicates a rather weak coupling between the planes at these speeds.

The characteristics themselves are found by setting the determinant in Eq. (40) equal to zero.

$$(s^2 + \sigma_1^2)^2 (s^2 + \sigma_2^2)^2 + \alpha^2 s^2 (s^2 + \omega_L^2)^2 = 0 ,$$

a fourth-order equation in s^2. The values of m, I, J and the center of mass location can be measured and the values of k, K and the center of pressure location can be obtained from Fig. 17. For the rotor of Fig. 15 typical frequencies and the x locations of the rotation axes are: at $n = 0$, $f_1 = f_2 = 3.569$ cps, $x_1 = x_2 = -1.681$ cm, $f_3 = f_4 = 8.713$ cps, $x_3 = x_4 = 2.116$ cm; at $n = 2.0$ cps, $f_1 = 3.405$ cps, $x_1 = -1.469$ cm, $f_2 = 3.722$ cps, $x_2 = -1.921$ cm, $f_3 = 8.224$ cps, $x_3 = 2.297$ cm, $f_4 = 9.279$ cps, $x_4 = 1.964$ cm.

The dynamic stability at various spin speeds can be inferred from plot of the locus of roots of the characteristic equation with n as the gain, Fig. 20 . Such a plot implies that all speeds are stable if ω_L lies in the interval $\sigma_1 < \omega_L < \sigma_2$, but it has been shown above that σ_1 and σ_2 always bracket ω_L if $K + wz_p > 0$. Therefore the only condition for dynamic stability in this case is that the body must be statically stable.

Plots of calculated values of the four natural frequencies are shown vs. spin speed, in Fig. 35.

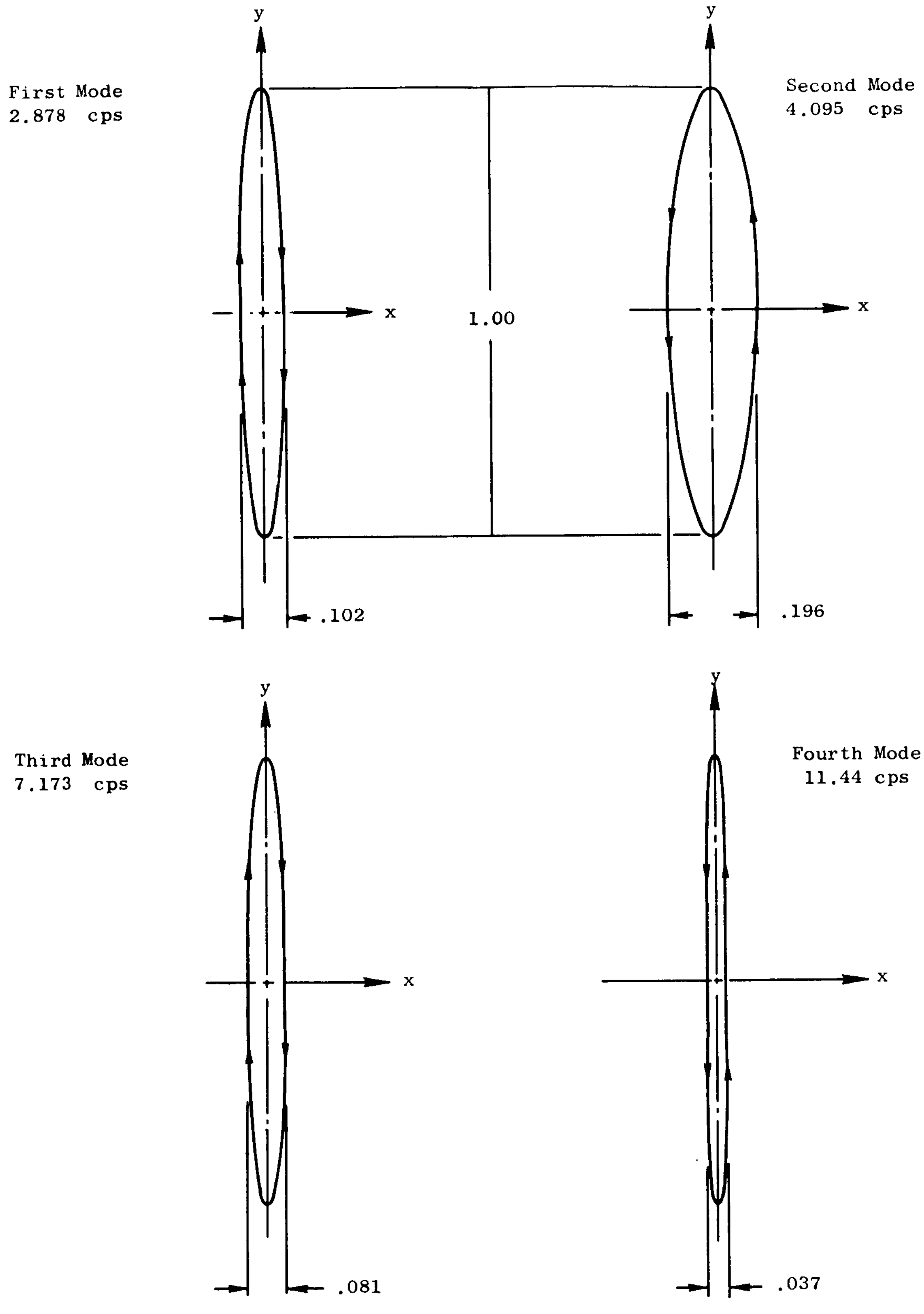

FIG. 19A. LISSIJOUS PATTERNS OF ROTOR TOP: n = 2 cps

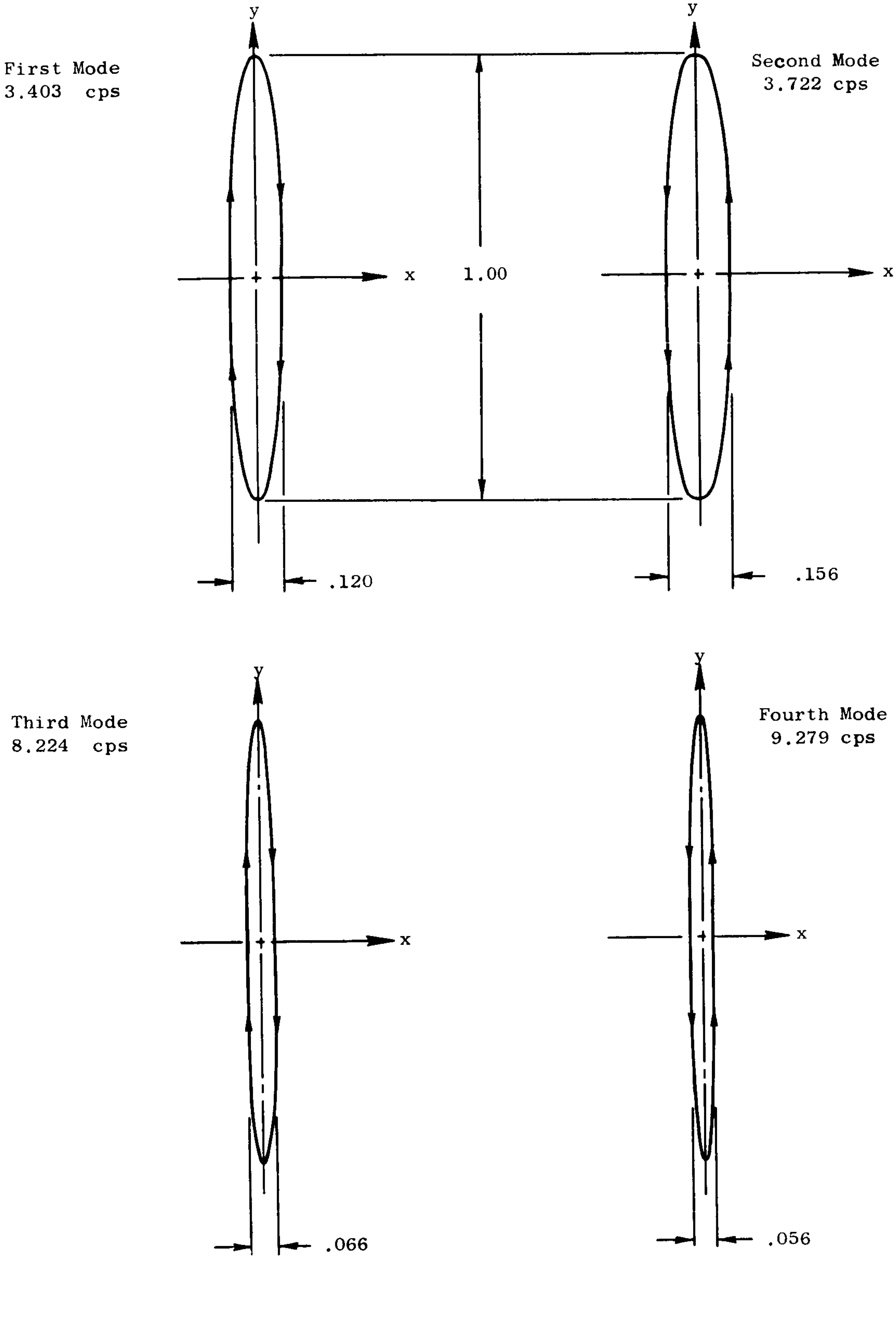

FIG. 19B. LISSIJOUS PATTERNS OF ROTOR TOP: n = 8 cps

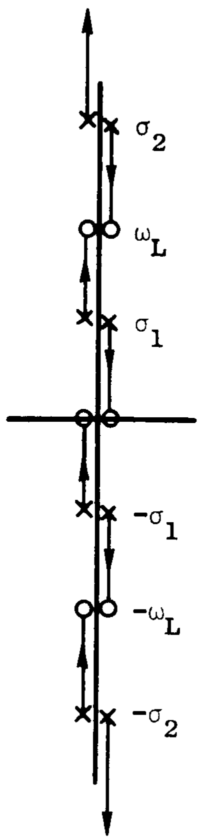

$$(s^2 + \sigma_1^2)^2 (s^2 + \sigma_2^2)^2 + \alpha^2 s^2 (s^2 + \omega_L^2)^2 = 0$$

FIG. 20. ROOT LOCUS DIAGRAM OF SPINNING CHARACTERISTIC EQUATION

VI. INSTRUMENTATION OF POSITION

A. SPECIFICATIONS

The great advantage of superconductive magnetic support is the minimization of frictional forces. If one wishes to monitor the position of a body without losing the benefits of this sort of support, the instrumentation should not add any additional friction. Furthermore, if one is interested in the effect of the magnetic forces alone, then the non-frictional forces introduced by the instrumentation should be very small compared to those of interest. The body of Fig. 15 has a mass of approximately 20 grams so that net instrumentation forces should be less than about 20 dynes if .1 percent deviations are to be tolerated. It might be noted that the relativity experiment requires stray forces on the sphere to be several orders of magnitude less than this in order to be successful. Requirements for the cylinder, however, are not as stringent.

A second consideration is sensitivity. The experiment on which this project is based requires that angles less than one tenth second of arc be measured. If this is to be done by measuring the relative displacement of the ends of a body two centimeters long, the difference must be measured to 10^{-6} cm, a small fraction of the wavelength of light. For the purposes of this preliminary experiment, the sensitivity requirements might well be relaxed to something in the order of 10^{-3} cm. Nevertheless, it would be desirable to use a technique capable of the more precise measurements. Inherently associated with the problem of sensitivity are the related problems of repeatability and calibration.

Another problem to be considered is interference. In this experiment dynamic motions are to be studied, so that the body must be free to move. Furthermore the effective spring constants of Fig. 17 indicate that the support is so soft that only moderate disturbances may cause excursions up to a millimeter. Thus the necessary pickoffs must not be located so nearby that they severely confine the motion to be studied.

B. THE CAPACITANCE BRIDGE

The requirements quoted above suggest three types of remote position measuring methods: optical, inductance, (e.g., a Shaevitz differential transformer) and capacitance. The last was chosen in this case because it met the specifications and some critical components were easily available. Reference 29 gives a general discussion of a capacitance bridge with application to remote measurement of translation.

The principle of operation and circuit diagram for measurement of the body of interest are shown in Fig. 21A. An AC signal is induced on the body of interest through capacitor plate A. If the gaps at B and C are equal then their capacitances are equal (assuming identical geometry) and equal displacement currents flow across the gaps giving no signal at the center-tapped transformer. When the body moves to the right the gap at C decreases and the capacitance increases; whereas the capacitance at B decreases. Thus more current flows across C, unbalancing the bridge and giving a signal at the output. If the body moves in the other direction the mechanism for the signal is the same, but the phase of the output is now 90° on the other side of the input. Thus by monitoring the phase it is possible to detect the direction as well as the magnitude of the motion. If measurement of rotation is desired then the scheme of Fig. 21B can be used. Note that in both cases the body is capacitively isolated so that no contact forces are present.

The sensitivity of this arrangement is enhanced by the fact that it operates about a null, i.e., there is no output when the body is capacitively centered. The sensitivity close to null is given by

$$\frac{dv}{dx} = -2 \frac{K L\omega^2 \epsilon A/d^2}{(1 + \omega^2 L\epsilon Z/d)^2} V ,$$

where K is the turns ratio of the transformer; L is the inductance of half the transformer; ω is the frequency of the signal; A is the area of the capacitor plates (assuming both are equal); d is the distance between the body and one plate at null; and V is the potential

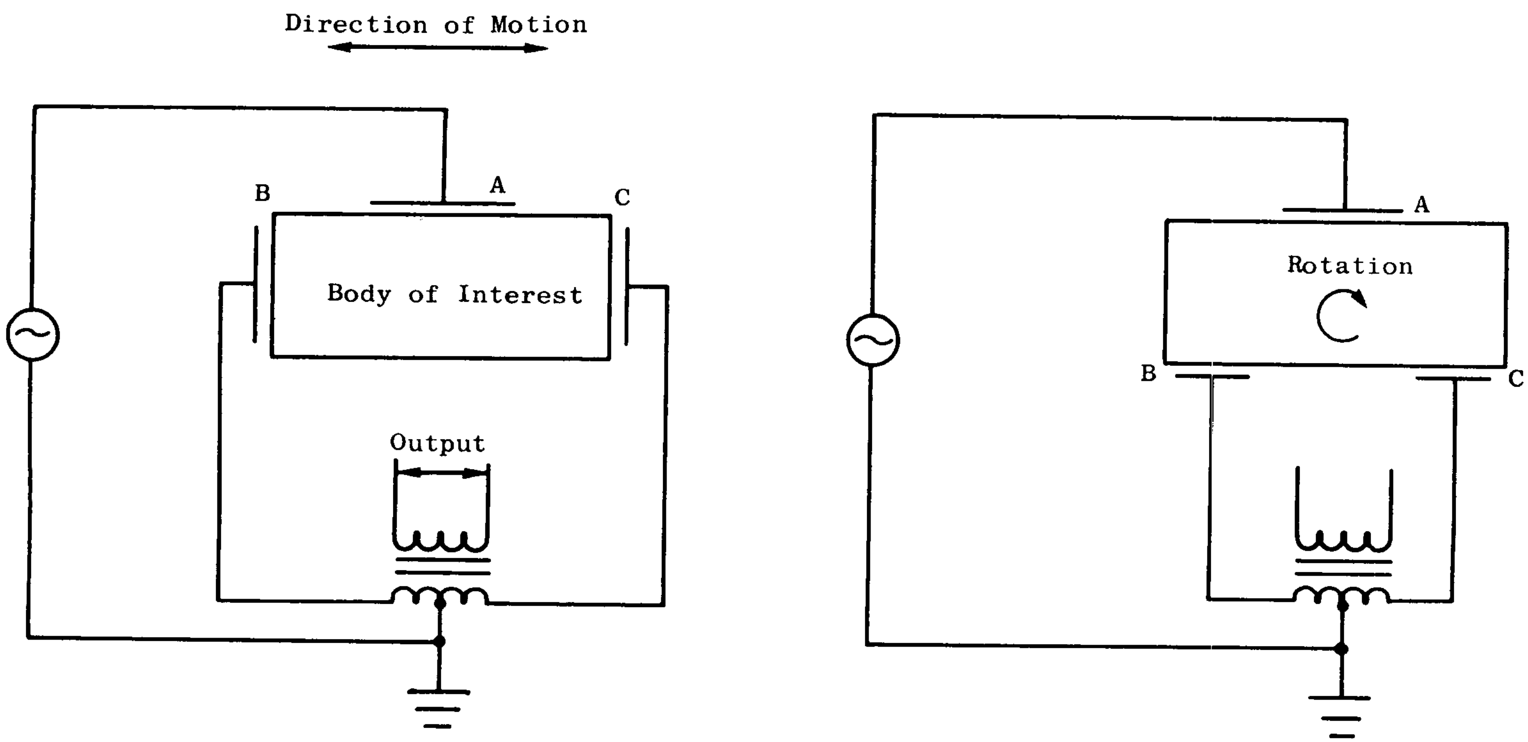

21A

Translation

21B

Rotation

FIG. 21. CAPACITANCE BRIDGE

of the body with respect to the center tap. Picking nominal values one may estimate the sensitivity: Let $K = 1$, $L = 50$ henrys, $\omega = 5$ kc, $\epsilon = \epsilon_o$, $A = 1\ cm^2$, $d = 1$ mm, $V = 10$ volts. This gives approximately 880 mv/mm. Thus, if one is able to measure changes of 10 mv the required sensitivity is achieved. Furthermore the nominal gap, d, is a measure of the interference and in this case is not restrictively small.

The force between one capacitor plate and the body is given by

$$\vec{F} = \oiint \frac{D^2}{2\epsilon} \, d\vec{S} \ .$$

For the values above, $F = 4.4 \times 10^{-3}$ dynes which is less than one millionth the weight. Even though this force is quite small, it need not be tolerated for the electric forces on each end tend to cancel one another and the net force is proportional to x/d, the deviation from null. The input capacitor plate (A in Fig. 21) also exerts an electric force, but this can be minimized by making it annular or in some other symmetrical shape.

The value of the capacitances are in the order of picofards so that currents are in the order of microamps or less. Thus only low-power power supplies are needed to operate the system, and the surface currents flowing from one capacitor plate to another are not so high that they might exceed the critical current of the superconductor.

An advantage inherent to this system is its electrical and mechanical simplicity. The capacitor plates need only be conducting planes on some insulator and can therefore be plated, painted, evaporated, etc. onto any regular or irregular shape. Once fixed into place they can be made dimensionally stable by using a rigid support. Electrically the system is also quite simple; it involves no active elements and has only one critical component, the transformer. Shielding is necessary to reduce the 60 cycle noise and this in turn introduces some stray capacitance, but changes in the stray capacitance don't effect the calibration. At the point that the capacitances are equal, the signal may not be zero because there is also a resistance bridge in parallel with the plates. This, however, can be biased out. The output signal can be recorded after being demodulated by a phase sensitive detector (e.g., Varo Model 1802, an all passive unit).

A possible scheme for instrumenting the body of Fig. 15 is as follows: The input capacitor is an annular ring facing the sloping lifting surface as shown in Fig. 22. The output plates for vertical motion are disks above and below the rotor. The lower disk will not be affected by horizontal translation and tilting if the difference between the rotor and disk diameters is large compared to the disk-rotor gap.

Horizontal motion of point A in Fig. 22 is detected by a pair of plates on either side of the rotor as shown. These are segments of a concentric cylinder whose diameter is slightly larger than that of the rotor. A similar pair of plates detects motion into the paper as shown in the section view. None of these plates will be influenced by vertical translation if the distance between the cylinder base and lower plate edge is large compared to the plate-rotor gap. Rotations about point A will not be detected because they will cause identical capacitance changes at the two plates.

Finally, rotations about a horizontal axis into the paper are detected by the pair of plates at the top made from segments of a ring. These plates are not affected by horizontal translation if their diameter is sufficiently smaller than that of the top edge.

Calibration of this arrangement can be accomplished by holding the rotor in a jig which is designed to perform the desired displacements. The vertical location of point A can be found by rotating about various axes until no signal at the output is obtained. Chapter VIII, Section A discusses the method actually used for vertical calibration.

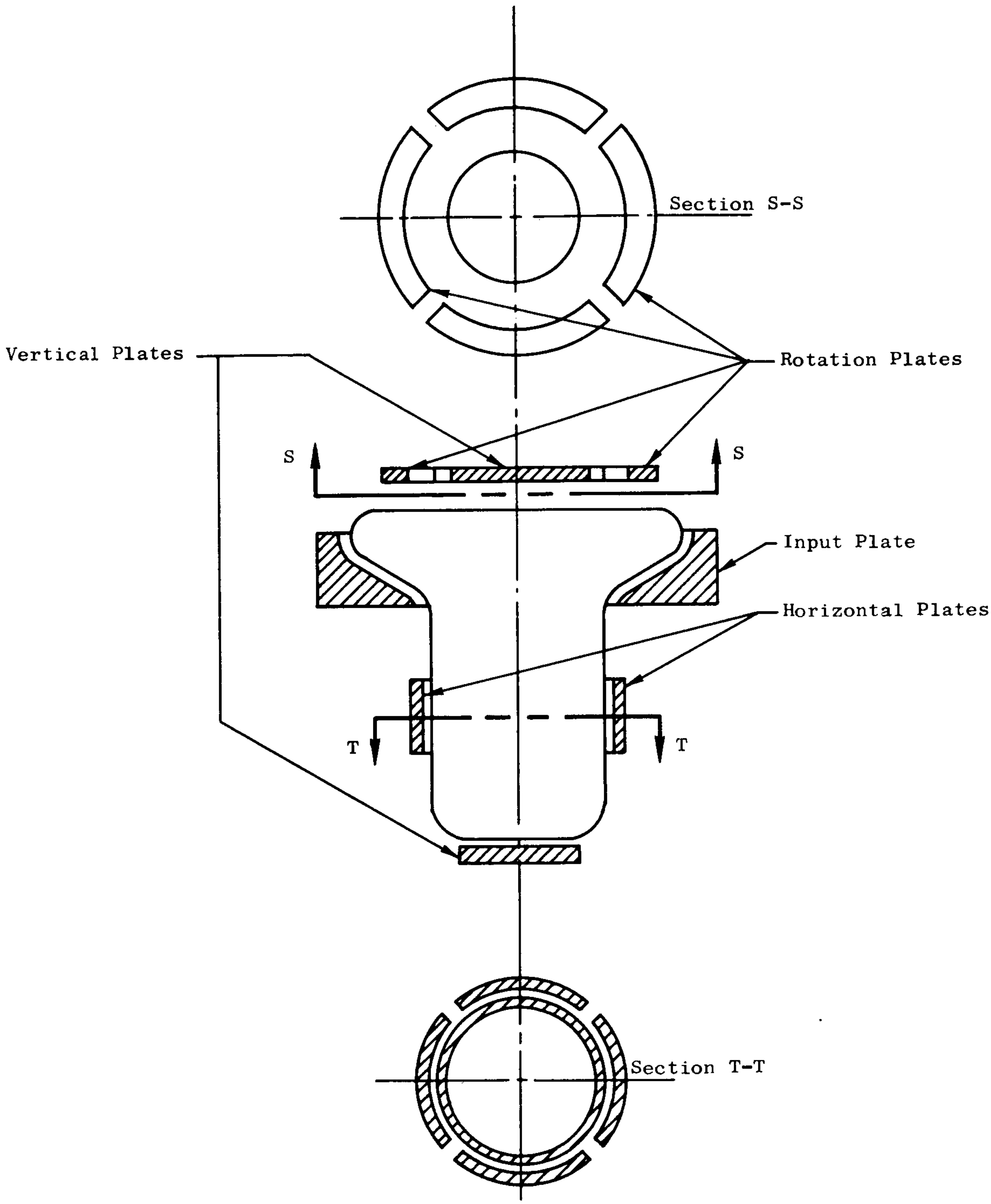

FIG. 22. POSSIBLE CAPACITOR ARRANGEMENT

VII. EXPERIMENTAL APPARATUS AND TECHNIQUES

A. GENERAL

The basic problem of studying a magnetically supported, superconducting body can be divided into several specific problem areas. The first is to obtain a low temperature environment for actually performing the experiment. The second is to design and construct a rotor on whose surface there is a superconductor having sufficiently high critical field. The third task is to provide a properly shaped magnetic field for supporting the rotor. Fourth is to spin the levitated rotor to the speed desired. Associated with this is the problem of encountering resonance or unstable spin speeds. Fifth is to provide low friction surroundings in which the body may operate. Finally there is the problem of reading out and recording the motions of the spinning body.

The first problem in experimentally verifying the theoretical results that have been presented so far is to achieve the low temperatures necessary for superconductivity. For the engineer unfamiliar with low temperature operations this seems like a very difficult task, but the solution is really quite straightforward. The portion of the apparatus containing the items to be superconducting is immersed in liquid helium, a commercially available product. The atmospheric boiling point of helium is $4.2^{\circ}K$ and the temperature can be readily lowered to about $2^{\circ}K$ by reducing the vapor pressure over the bath. The container of liquid helium is itself within one of liquid nitrogen. Figure 23 shows diagramatically the general arrangement of the experimental apparatus, and a photo of the working system is shown in Fig. 24.

The actual experiment is carried out within the glass cryostat blown from 51 mm Pyrex tubing of overall length 36 inches. A photo of the unpainted cryostat is shown in Fig. 25, and the various details are discussed in subsequent subsections.

The rotor is hollow and is made of 6061 aluminum; Fig. 26 shows machine drawings of its two parts. The cap is shrunk into the recess and then machined off and polished to form a continuous surface. The demarcation between the two pieces cannot be seen under a microscope,

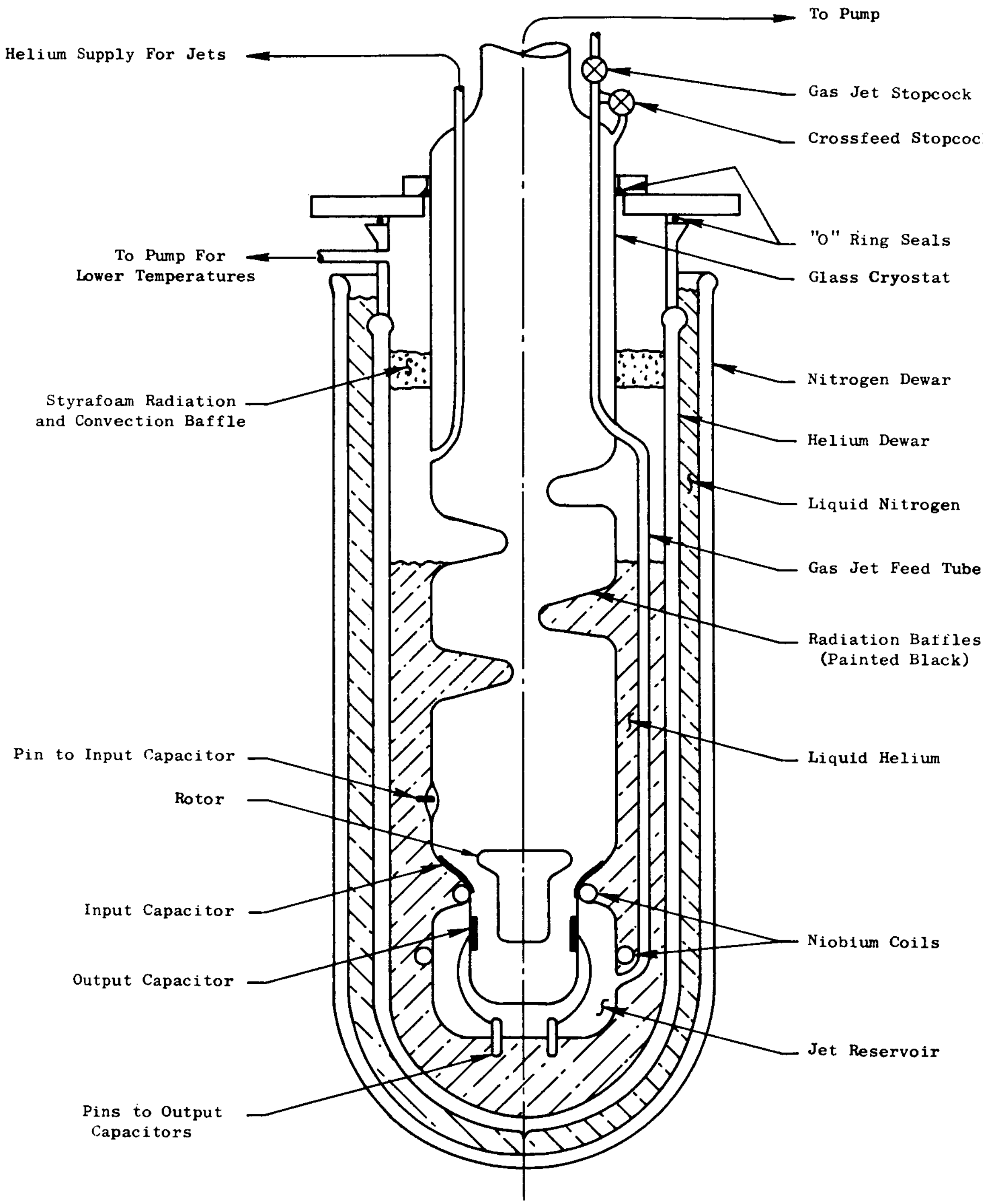

FIG. 23. EXPERIMENTAL APPARATUS

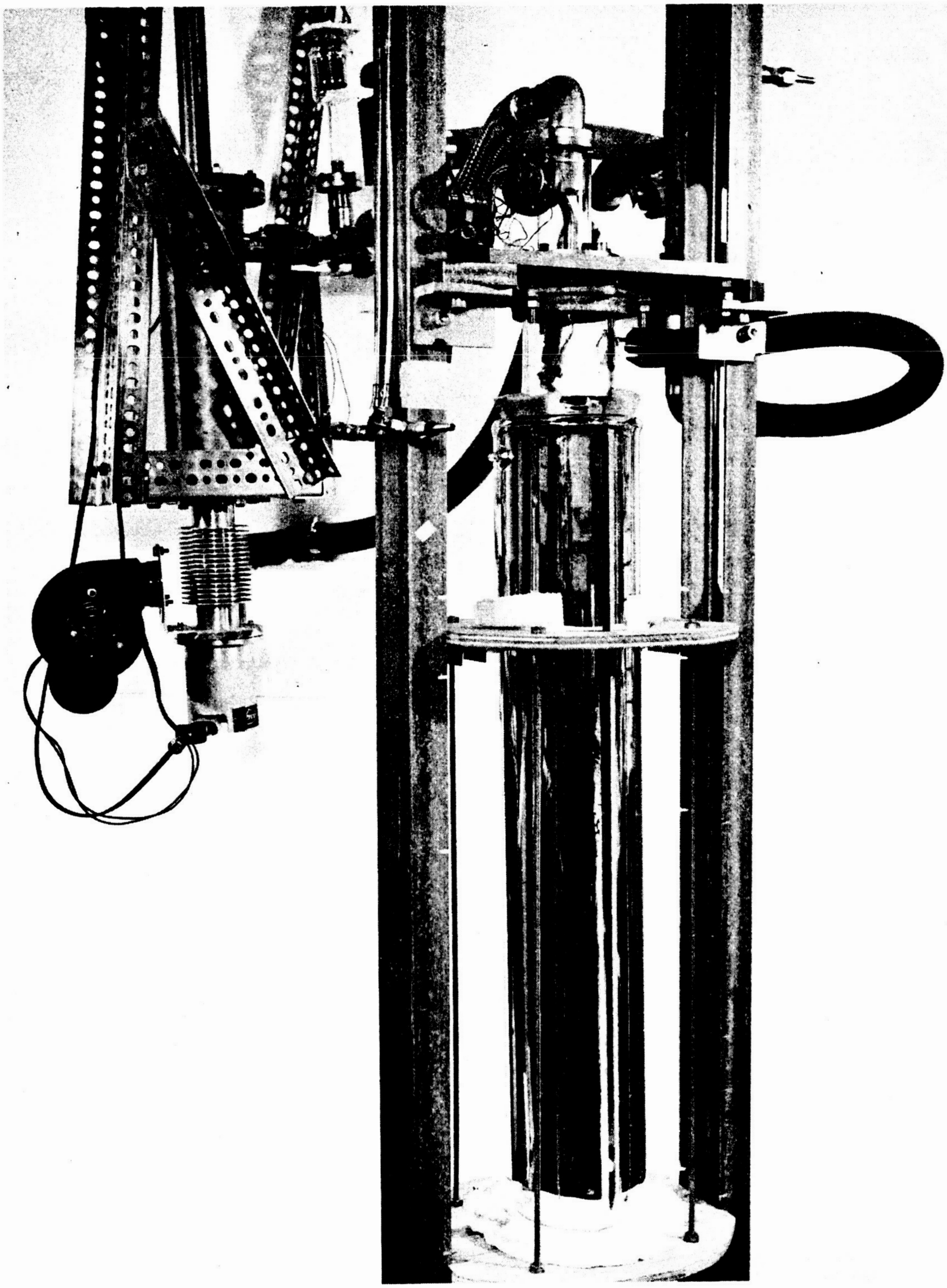

FIG. 24. PHOTOGRAPH OF WORKING APPARATUS

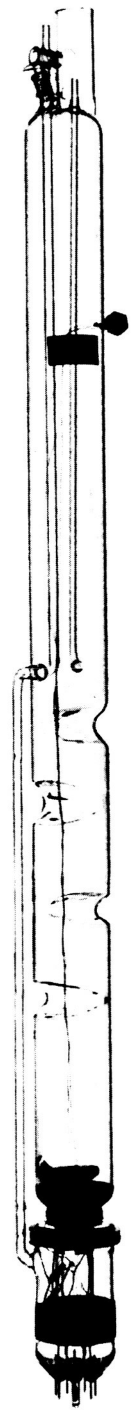

FIG. 25. PHOTOGRAPH OF CRYOSTAT

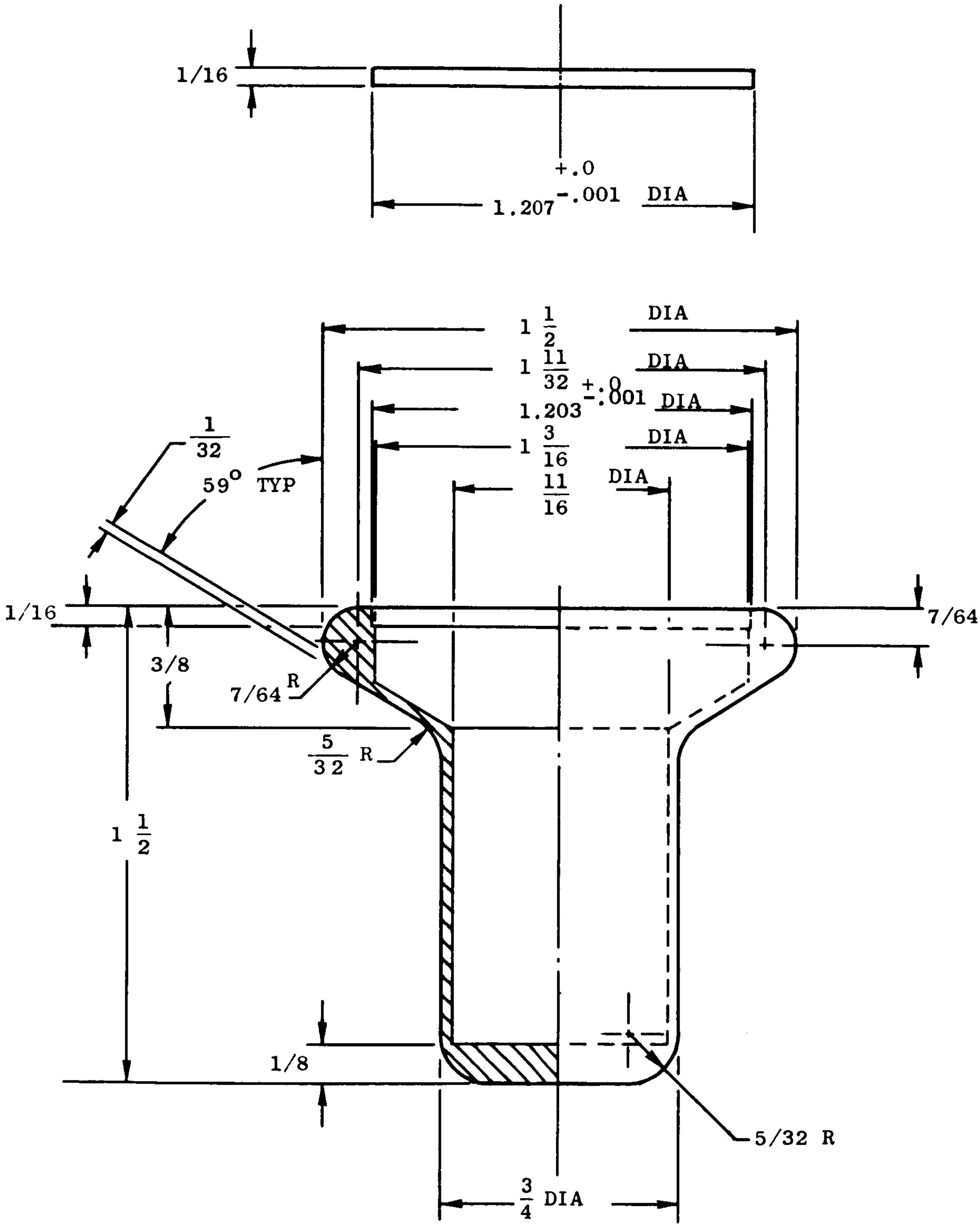

FIG. 26. MACHINE DRAWING OF ROTOR

indicating that the two have actually flowed into one another. The polished rotor was chemically cleaned, zinc coated by immersion, dipped in copper strike, and lead plated in a bath of $Pb(BF_4)_2$ (lead-fluoborate) as discussed in Ref. 30 to a thickness of .003-.005 inches. The surface was sprayed with Krylon Crystal Clear to minimize oxidation. The finished weight was 23.561 grams. The location of the center of mass was determined by balancing the body on a knife edge with the axis horizontal and the distance from the knife edge to the plane of the rotor top was measured with an optical comparitor as $\bar{x} = 1.236 \pm .015$ cm. The transverse and polar moments of inertia were determined by comparing the period in a torsion pendulum to that of a known standard and to that of the empty pendulum. The transverse moment was $I = 60.55 \pm .17$ gr-cm^2 and the polar moment was $J = 41.475 \pm .030$ gr-cm^2. No attempt was made to mass balance the completed rotor.

B. FIELD GENERATION

The magnetic field for lifting the rotor is produced by a coil wound directly on the recess of the glass cryostat (Figs. 23, 25). The coil consists of 200 turns of .007" diameter double silk wrapped niobium wire. An outline of the cross section determined by optical comparitor tracings before and after winding is shown in Fig. 15. The coil is able to remain superconducting while carrying ten amperes. When the desired current has been established it is trapped in a superconducting loop by the circuit of Fig. 27 using the following procedure: With the heater switch B open, the switch A is closed. Since the resistance of the short and coil are the same (zero), the distribution of current is determined by the inductance and most of the current flows in the short. The switch B is then closed heating the short and making it locally normal; current flows into the coil because it still has zero resistance. The heater is turned off and the short allowed to cool. Now there is a certain amount of flux trapped inside a superconducting loop so that when switch A is opened a persistent current will flow to maintain the flux constant. During actual experiments a

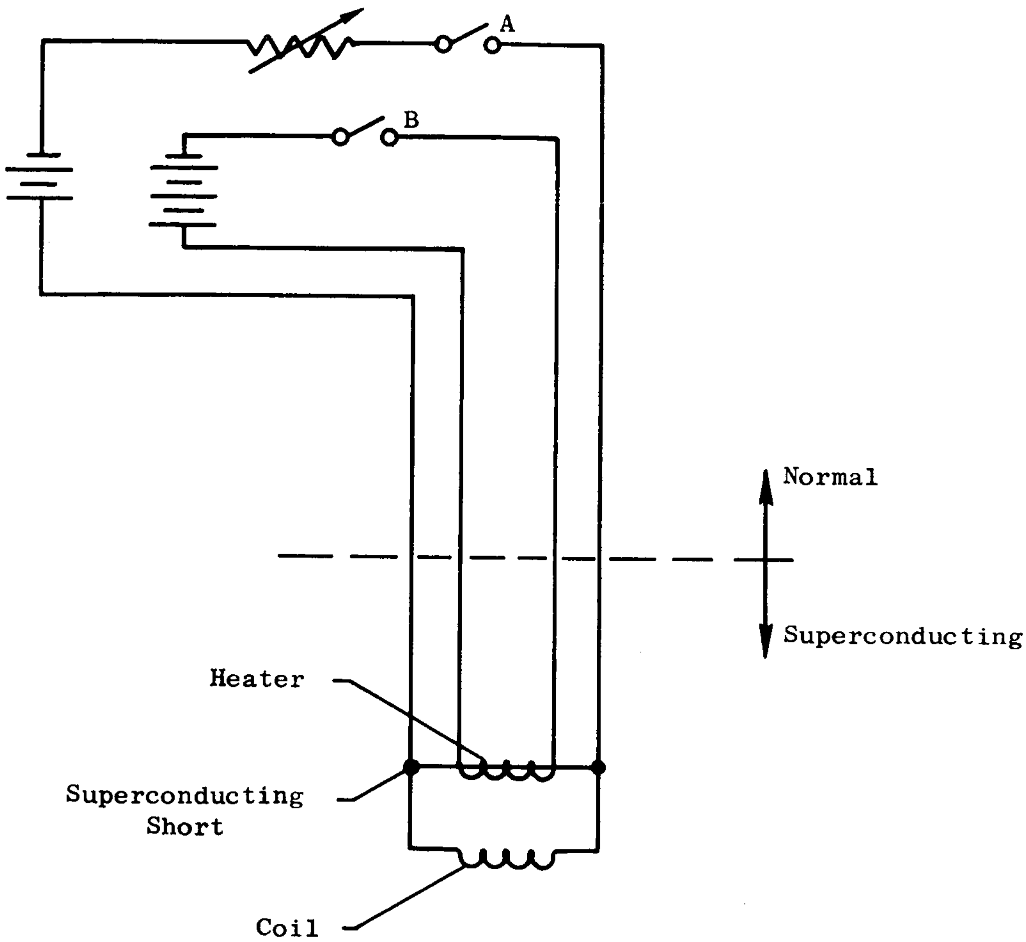

FIG. 27. FLUX TRAPPING CIRCUIT

magnetometer probe was located at the outside of the nitrogen dewar so that the operation of the flux trapping circuit could be observed. The heater is made by wrapping .003" diameter nichrome wire around the niobium and then potting everything inside two concentric stainless tubes which are soldered at their ends. This thermal insulation minimizes the heat input to the bath. Approximately 100 milliwatts activates the heater in about one second and it takes 2-3 seconds to cool.

C. SPIN-UP SYSTEM

The system used to spin the magnetically supported rotor is similar in principle to the one used at JPL to operate their gyro: it consists of gas jets impinging on the periphery of the body.

The diagram of Fig. 23 shows the system. Helium gas is fed down a long tube to the jet reservoir in the double walled lower section of the glass cryostat (below the top coil). The inner wall has .020" diameter holes, impact ground, at such an angle that their axes are tangential to the circumference of the body. When the vacuum pump is applied to the main chamber of the cryostat the gas is drawn from the reservoir through the jet holes striking the rotor tangentially and spinning it with an acceleration of .4-.8 cps/minute indicating a torque in the order of 2 dyne-cm.

One problem is that the gas impinging on the rotor must be no warmer than about $5^{o}K$ or the surface may become normal. This limits the volume flow of gas and the torque on the body, for the slow movement through the large diameter sections is relied upon for cooling the incoming gas. Attempts to increase the flow to provide more torque have consistently resulted in the rotor falling down. If necessary, higher flows and torques could be achieved by installing a helium temperature heat exchanger (e.g., a coil of copper tubing), but the present levels have proved adequate.

Early experiments used helium gas from an external cylinder to feed the jets, but this proved to be too impure as evidenced by great amounts of condensate in the jet reservoir. Since very pure helium could be drawn from the boiling bath, another tube was run down to collect it and was connected at the top through a rubber hose and metering valve to the gas jet feed (Fig. 23).

D. LOW FRICTION ENVIRONMENT

After the body has been spun to the desired speed it is necessary to remove the surrounding gas to minimize the friction. To do this the jet stop cock of Fig. 23 is closed and the vacuum pump allowed to pump out the chamber. Since the jet reservoir would have to be pumped through its small holes and therefore take a very long time, a cross feed stopcock was located at the top so that the pump may work on both sides of the jets simultaneously. The pressure as measured between the top of the cryostat and the pump (about two feet away) reaches about 5×10^{-5} torr in about five minutes.

Unfortunately the removal of gas and reduction of friction introduces a problem of heat transfer. Light falling on the rotor when measuring speed with a strobe, or just looking at it, tends to heat the rotor and causes it to become normal. When sufficient gas is present the heat is carried off by conduction to the surrounding walls; but removal of the gas eliminates this heat transfer mechanism.

To minimize the thermal radiation falling on the rotor, four radiation baffles are built into the cryostat (Fig. 25). Furthermore, the exterior of the glass is painted flat black from the coil to the top baffle so that the rotor can only be seen from the bottom. The strobe light is filtered with a band pass filter of about 10 $m\mu$ in the green to cut down unnecessary radiation. Even with these precautions the body will stay up for only about 30 minutes at 10^{-5} torr. Some heating may be due to hot pump oil migrating into the system and condensing on the rotor, although most of it should be stopped by the helium-cooled baffles.

E. SECOND COIL AND RESONANCE PROBLEMS

During early experiments it was found that when the rotor spin speed reached the first natural oscillation frequency small imbalances would cause lateral oscillations to grow until the rotor hit the sides of the surrounding glass. It seemed that no manner of operation of the jets or support could get it through this speed.

After an extensive computer study it was found that addition of a 2.7 cm radius coil 1.5 cm below the first (Fig. 23) helped solve the problem in the following way: If the body was first levitated using only the main (upper) coil it was found, theoretically and experimentally, to have a certain first natural frequency and critical speed. If now the second coil was turned on and the current in the first lowered such that the current in both were equal but the force on the body unchanged, then the body was observed to have a first natural frequency as much as 40 percent below that of a single coil. Thus the first critical speed was considerably lower in the two-coil case than in the one coil.

It was then possible to spin the body in the following manner: With one coil on, the body was spun to its maximum possible speed just below the critical. The currents in both coils were then suddenly altered to the configuration described above so that the body was spinning above the critical speed for this situation. It then could be spun on up.

During the transition from one- to two-coil support it was necessary to provide some damping of the lateral oscillations. When the body moves from side to side it changes the magnetic field in its vicinity so that if a lossy medium were present there would be eddy current dissipation which would remove kinetic energy from the oscillating body. Harding [Refs. 31, 32] has made some calculations on using a spherical lossy shield to damp the motions of a sphere and his analysis can be extended to a cylinder. Making some very rough approximations it was found that damping could be accomplished by installing a surrounding cylinder of 1/16" thick copper. A photo of the cryostat with the damper in place is shown in Fig. 28.

FIG. 28. PHOTOGRAPH OF CRYOSTAT WITH DAMPER

Presumably this trick of changing support can be applied at every critical speed encountered as long as it is a resonance problem and not one of inherent instability.

F. CAPACITIVE PICKOFF

An instrumentation arrangement like that discussed in Chapter VI was incorporated into the glass cryostat for monitoring motions in two horizontal directions. The carrier signal is fed capacitively to the rotor through an annular plate on the sloping glass surface above the top coil. The two capacitor pairs are made from plates approximately one centimeter square on the outside of the inner tube at the bottom of the cryostat (Figs. 23, 29).

The plates themselves are made from Du Pont Silver Preparation, Electronic Grade, No. 7713. This is a suspension of finely powdered silver and glass in an organic binder which is painted directly on a glass surface and fired. During the firing the binder evaporates and the powdered glass fuses to the glass beneath leaving a layer of conducting silver fused to the top. For the input capacitor plate, electrical connection to the exterior is made by painting a strip from the capacitor plate to the back of a tungsten pin sealed into the glass. At the output plates, four tungsten ribbons with platinum spots welded on the ends press against the silvered surface. At the other end they are spot welded to the pins of a standard NRC vacuum gauge base sealed to the bottom of the cryostat.

This arrangement actually measures the motion of some point in the rotor whose elevation is approximately at the center of the plates. Thus if the rotor oscillates about an axis which does not pass through this point (Chapter V), the plates will detect its motion.

The 5 kc signal is provided by an Hewlett-Packard Model 400B audio oscillator at 150 volts RMS. The transformers and amplifier-demodulators were built by Autonetics and supplied by Messrs. Joe Boltinghouse and Doyle Wilcox of that company. The transformers are mounted near the top of the cryostat where their temperature will not fall below $0^{o}C$.

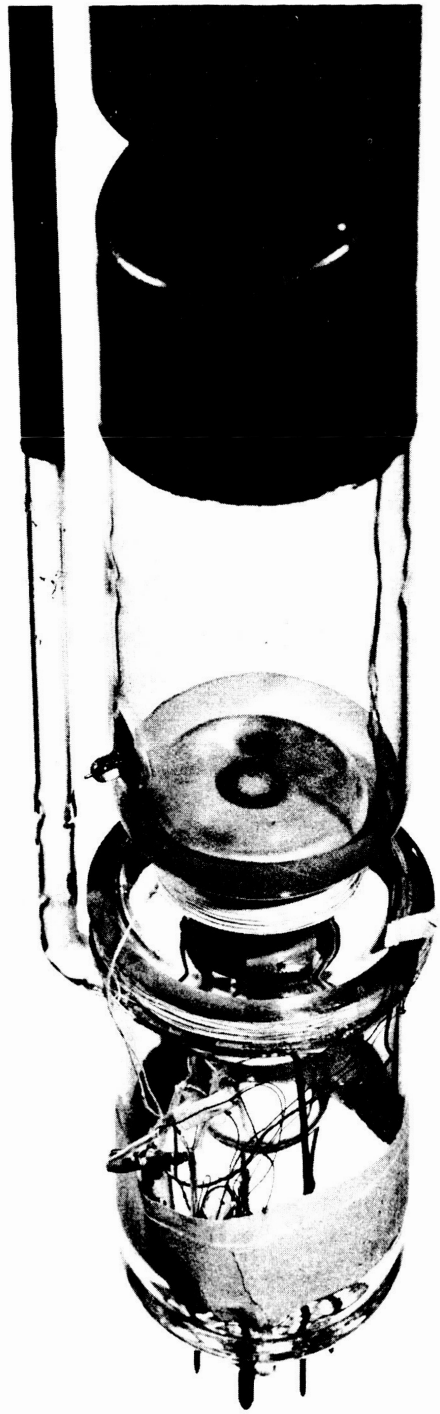

FIG. 29. PHOTOGRAPH OF CRYOSTAT SHOWING CAPACITOR PLATES

It was found that reducing their temperature much below this level resulted in a marked change in the magnetic properties of the core and a consequent loss in performance. The output is amplified, demodulated and fed to a Sanborn pen recorder as shown in Fig. 30.

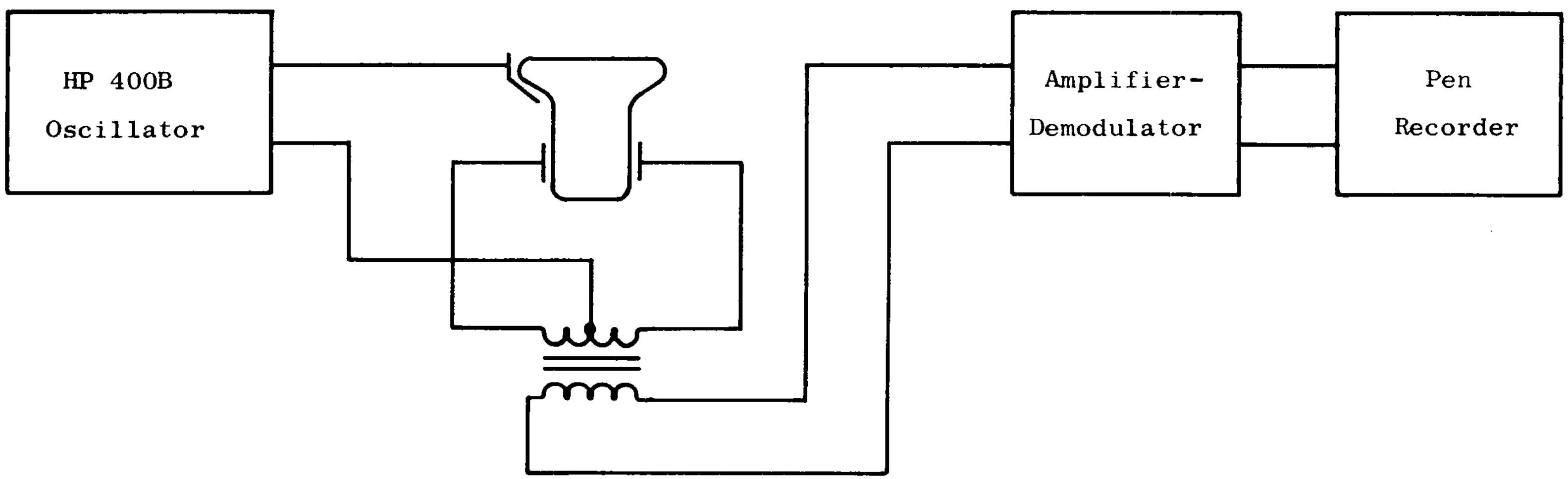

FIG. 30. POSITION MEASUREMENT BLOCK DIAGRAM

VIII. EXPERIMENTAL RESULTS

A. CURRENT VERSUS HEIGHT MEASUREMENTS

As discussed in Chapter IV the body should stand at a certain elevation dependent on the current in the levitation coils. To check this a separate apparatus was constructed using capacitor plates above and below the rotor. Calibration was accomplished by lifting the body with a string attached to a micrometer and noting the capacitive output. The experiment was carried out in liquid helium so the buoyancy force (about 3000 dynes) had to be subtracted for the calculations. The results are shown in Fig. 16A.

B. SPIN DOWN TESTS

Before the capacitor plates were installed a number of spin down tests were made. The rotor was spun to 13.6 cps (where another critical speed occurred) using the method outlined in Chapter VII, Section E. The jets were shut off, the cavity pumped out, and the body allowed to spin down. The speed was measured with a Strobotac. Because of the heat transfer problems mentioned in Chapter VII, Section D, the pressure was only reduced to 10^{-3} torr.

Figure 31 is a semilog plot of speed versus time at two pressures. The mean free path at 80μ is approximately .002 cm which means the body is in continuum flow. (Since the viscosity is independent of pressure the drag should be the same throughout the continuum flow regime.) The spin down time constant (time for speed to decrease by 1/e) is 120 minutes. At 1μ the mean free path is approximately 2 mm which is about the width of the gap between the body and the wall; thus the body is in the transition between continuum and free molecular flow. The spin down time constant is 126 minutes which shows the trend toward lower drag as the free molecular regime is entered.

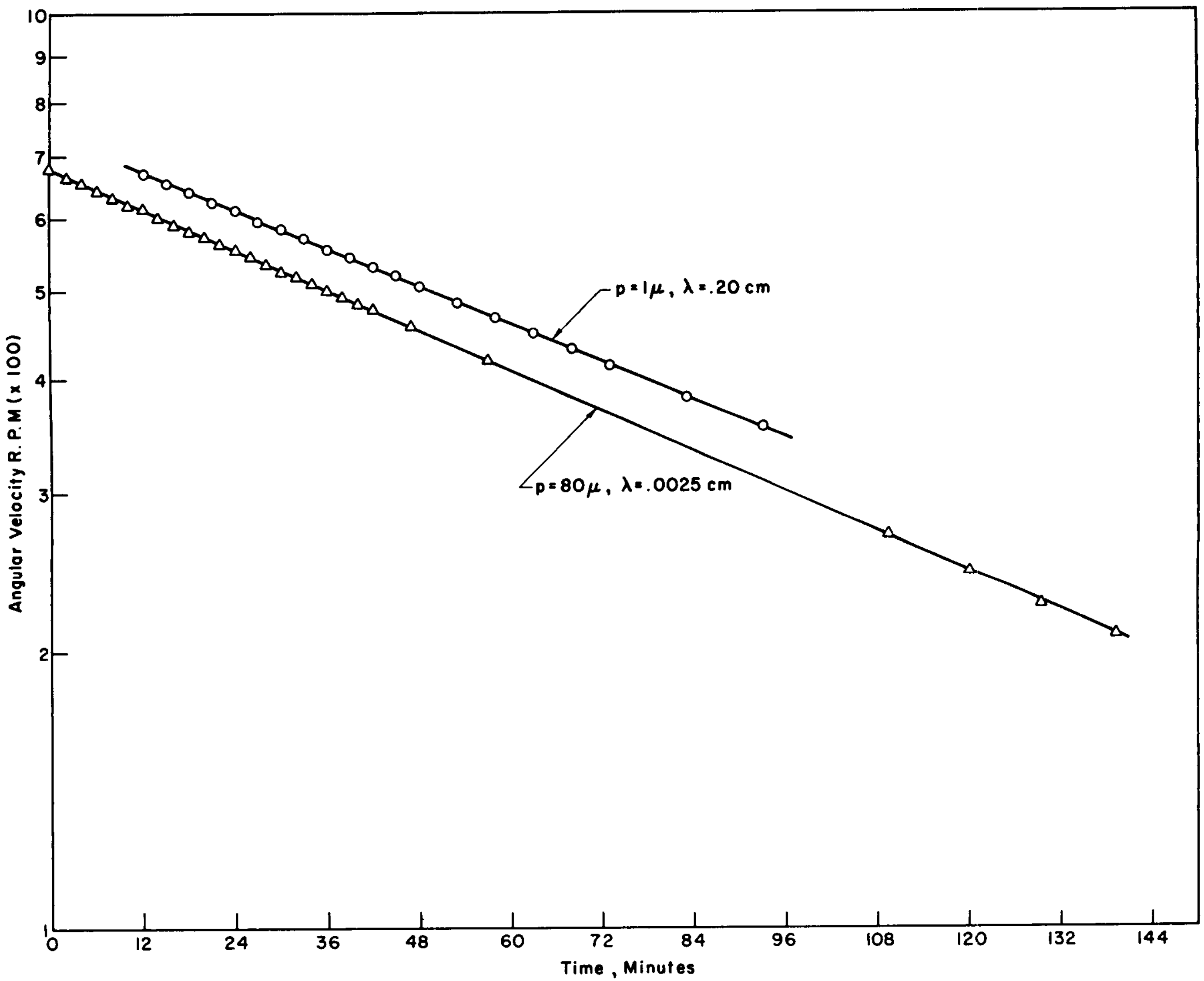

FIG. 31. ROTOR SPIN SPEED VS. TIME

When the capacitor plates were installed the rotor was replated because at one point on its surface the lead was chipped off from handling. Apparently the new plate was somewhat non-uniform, for the body would no longer turn about its axis of symmetry as noted by the capacitive pickoff. Consequently as the body spun it changed the magnetic field around it so that the copper damper along with the residual gas removed energy from the spin.

Because of the non-symmetry of the spin axis it was possible to read the speed from the traces on the pen recording. A plot of speed versus time with the mechanical pump operating is shown in Fig. 32. The right side of the curve seems to be leveling out indicating that the gas friction is going into the free molecular flow regime, as it should around the low pressure limit of the fore pump. The exponential time constant is approximately 40 minutes.

C. VIBRATION FREQUENCIES

After installation of the capacitor plates it was possible to record lateral motion of a point in the rotor. A typical plot of motions versus time is given in Fig. 33A. Note that two distinct frequencies are present: The low-frequency component is that due to the rotation about a non-body axis as discussed in Chapter V, Section B, and the high-frequency component is motion at one of the natural frequencies, induced by tapping the structure. The components of the low-frequency motion in the two planes are, of course, 90° out of phase.

At some particular spin speeds a unique means of observing natural frequencies presented itself. A multiple of the spin speed would beat with one of the natural frequencies, and this beating was very apparent on the trace (Fig. 33B). Measurement of the beat frequency δ gave the difference $(n\Omega - \omega)$ where Ω is the spin speed and ω is the natural frequency of interest. The spin speed was obtained by measuring it at various points near the beat and fairing in a curve to determine it right at the beat.

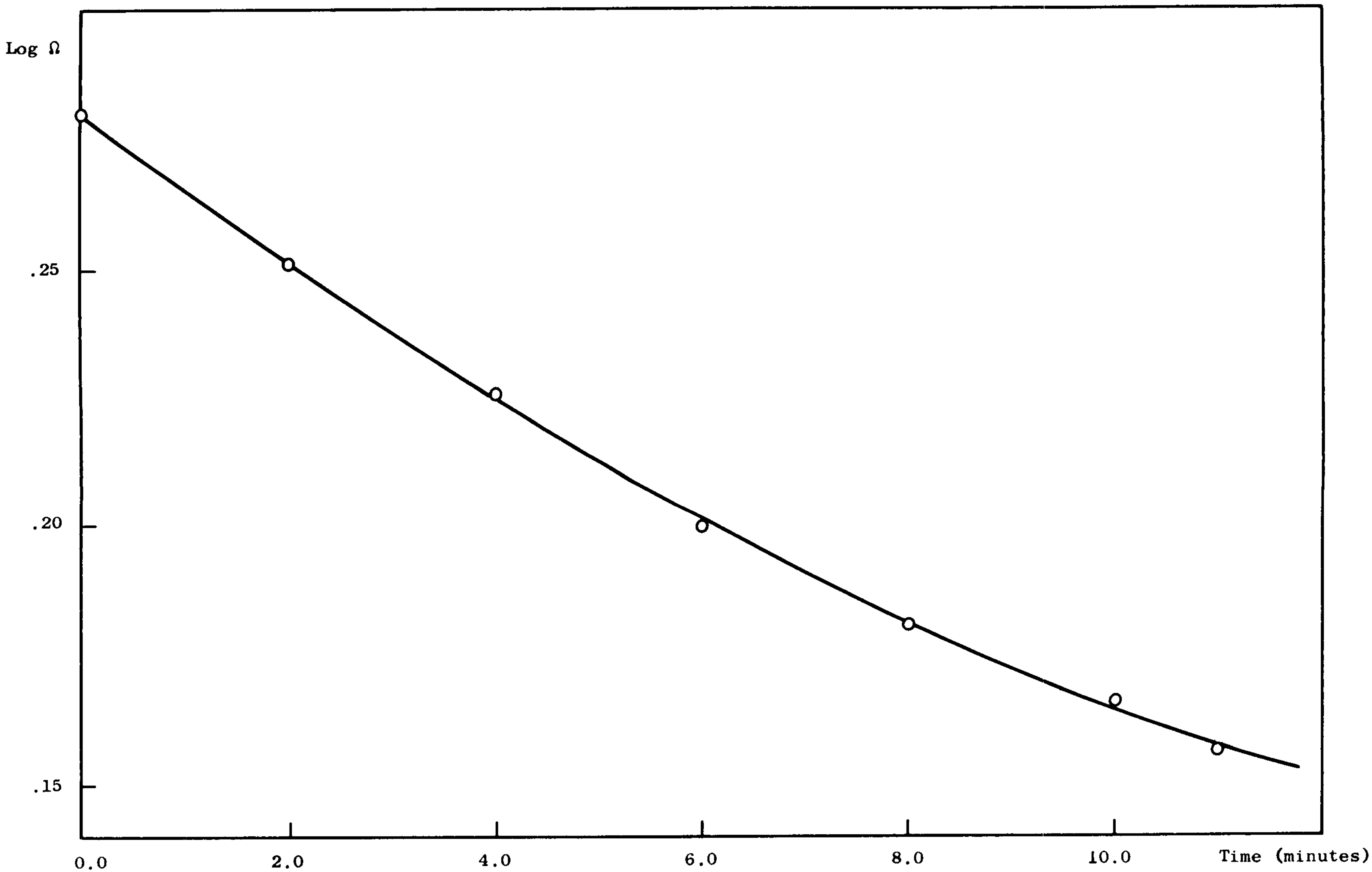

FIG. 32. ROTOR SPIN SPEED VS. TIME WITH PUMP RUNNING

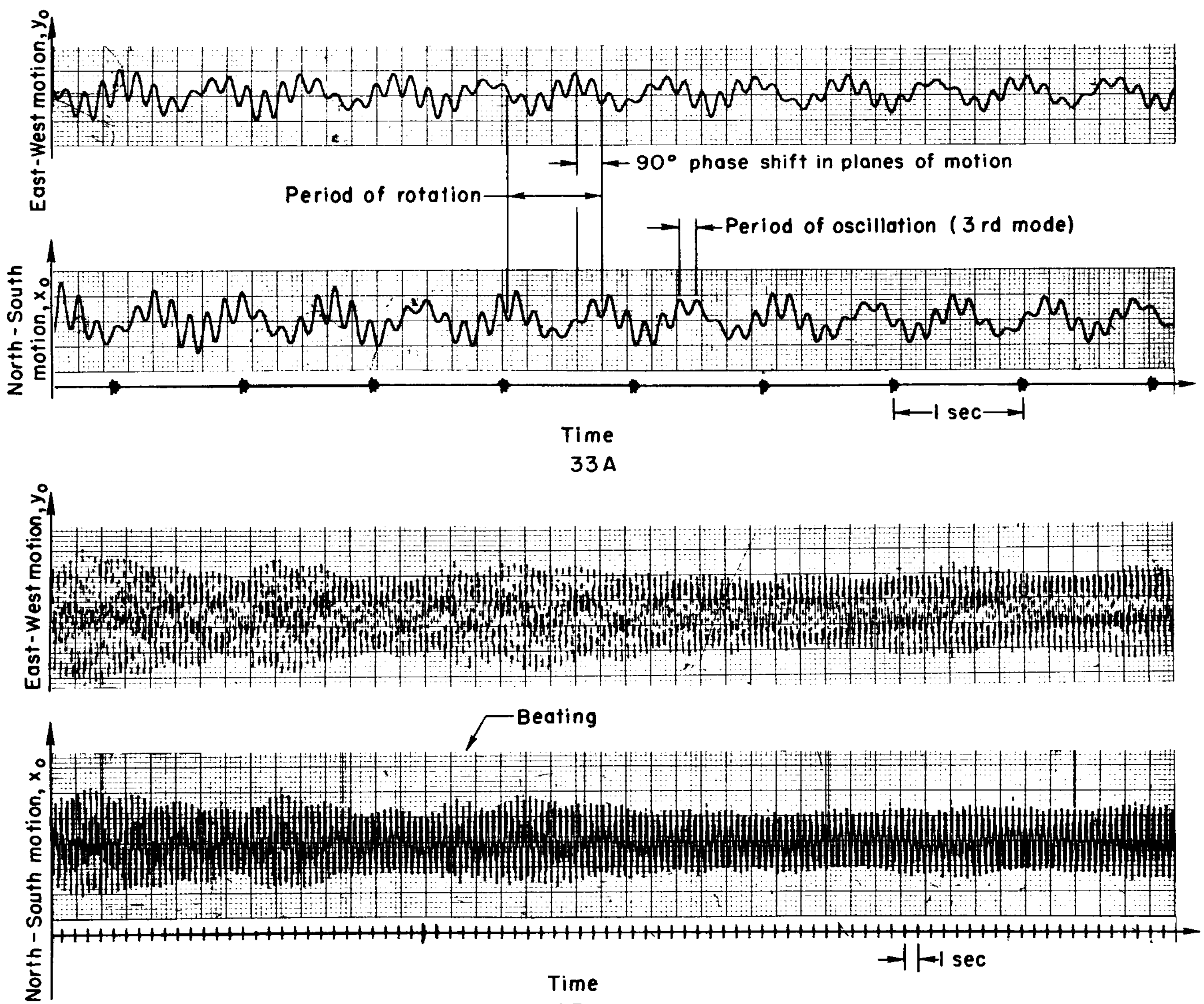

FIG. 33. PLOT OF MOTIONS IN TWO HORIZONTAL DIRECTIONS AT HIGH AND LOW CHART SPEEDS

Natural frequencies were calculated and measured for two distinct support currents. The calculated and experimental values are shown in Figs. 34 and 35 for 3.14 and 4.10 amp currents respectively. Note that the frequencies measured seem to correspond quite closely to the third mode. The lines $n = f$, $3n = f$, and $4n = f$, where n and f are the spin and oscillation speeds respectively, have been drawn on the frequency plots. The points at which the lines $3n = f$ and $4n = f$ intersect the theoretical frequency versus speed curves are points of expected harmonic resonance, i.e., where the beating of Fig. 33B should occur. Beating in the third mode did occur near these points; no fourth mode beating, however, could be recognized.

Measurement of the first and second mode frequencies (which are quite close over the whole range of speeds) was hampered by the fact that the copper shield was designed for maximum damping just at these frequencies. Some frequency data in this mode was obtained, but it could not be averaged over a large number of cycles and is therefore somewhat less accurate than that for the higher mode. The best check of the fundamental frequency comes from the maximum speed measurement where n equals f and excitation of the natural mode by the spin speed caused the rotor to hit the surrounding wall.

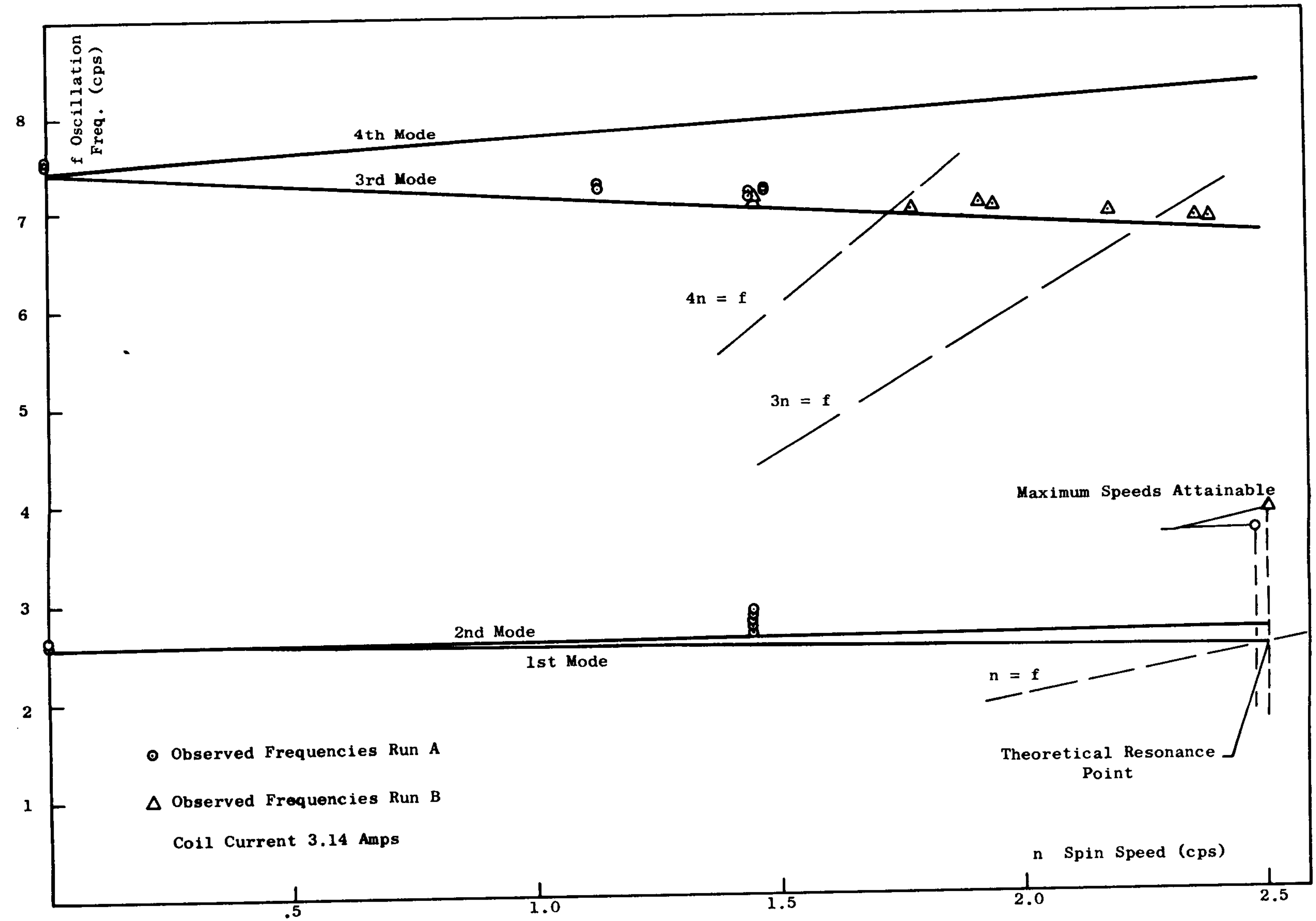

FIG. 34. THEORETICAL AND OBSERVED FREQUENCIES VS. SPEED

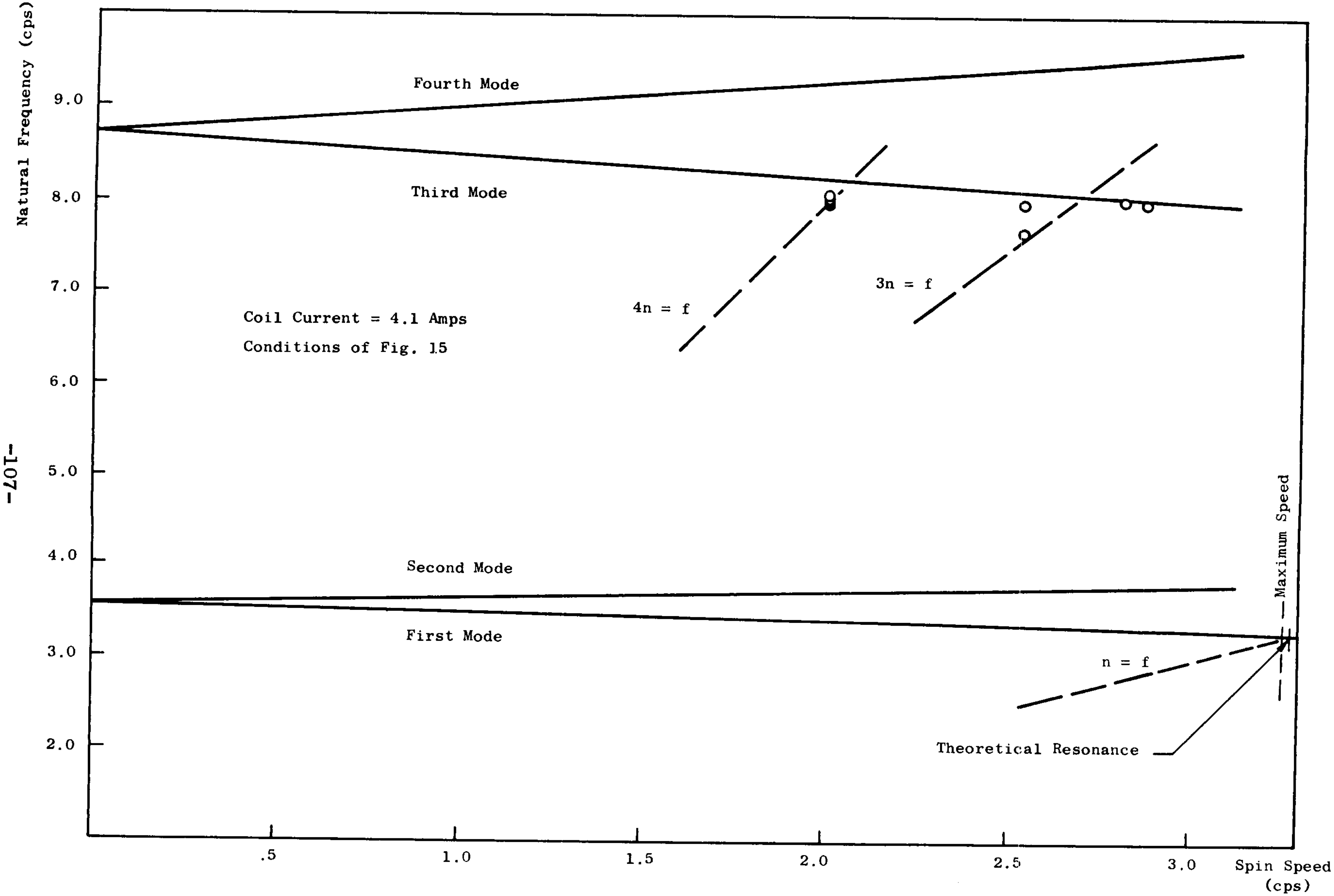

FIG. 35. THEORETICAL AND OBSERVED FREQUENCIES VS. SPEED

IX. CONCLUSIONS AND SUGGESTIONS FOR FURTHER STUDY

A. CONCLUSIONS

The frequency data presented in Chapter VIII seems definitely to confirm the magnetic force calculations of the previous chapters. Thus, there has been developed here a reliable model for a magnetically-supported, superconducting, spinning body.

Unfortunately some limitations have been encountered which preclude more extensive measurements. Most discouraging are the rather low spin speeds which have been achieved due to rotor imbalances and uncertain superconducting properties of the lead. The first difficulty can most likely be overcome by the scheme outlined in Chapter VII, Section E; the second is discussed below.

The instrumentation of the spinning rotor has been rather incomplete in that only two of the five interesting degrees of freedom have been adequately monitored. This has been sufficient to measure frequencies but insufficient to really see the coupled rotation-translation discussed in Chapter V, Section B. The complete instrumentation setup shown in Fig. 22 would adequately measure the desired motions but would be difficult to install in the present cryostat. One of the major problems associated with installation of additional instrumentation is that it would inhibit the flow of gas from around the rotor during the evacuation phase of the operation and possibly cause excessive pump down times.

Despite these limitations, this thesis presents quantitative tools for designing magnetically-supported, axially symmetric superconducting bodies to be operated in nominally axially symmetric fields. A design procedure using these tools is as follows: Select a body and field generator shape as determined by the geometrical constraints of the particular problem. Using the methods presented, calculate the fields, forces, characteristics, and stability regimes. Modify the currents, field generator or body shape to produce the desired dynamic behavior.

The small deviations between the experimental and theoretical values in the present study are probably due to the computer slightly misrepresenting the field of the undisturbed coil, and to numerical errors associated with manipulating the large influence-coefficient matrices.

B. FURTHER STUDY

Several possible extensions and modifications of the work to date suggest themselves. In the field calculation programs there are inherent inaccuracies in working with large matrices. The matrix inversion program of Appendix A should be replaced by one using iterative improvement, and the matrix multiplications should be carried out in double precision arithmetic. Furthermore, all the programs can be speeded up by various modifications. The subroutine COILFD in Appendix B calculates the field of a plane circular loop. This should be replaced by one which calculates the actual field of the generator of interest, e.g., a coil of square cross section. Furthermore, simply by modifying COILFD the effect of any axially-symmetric field can be calculated.

The tools are now available for optimization of the body-coil system. Using the present methods of calculation, it should be possible to write computer programs which will change the various parameters to converge on a design meeting the selected criterion of optimality.

The field calculations might be checked by direct experiment by attaching measuring devices (e.g., magneto-resistive bismuth probes) directly to the surface of the body of interest. Also, static measurements of the restoring forces could be made as in [Ref. 7].

As mentioned above the superconductive properties of the lead plating are somewhat in doubt. Experiments could be performed which test such items as flux trapping and critical field of a plated specimen. Magnetization tests on lead plated samples could easily be run using an oppositely wound coil system like that discussed in Refs. 10

and 11. Little information is readily available on the superconducting properties of "thick" films prepared by various processes; this sort of test would help considerably. Some work along this line has been performed using a lead plated superconducting microwave cavity [Ref. 33].

Some of the items cited in Chapter I, Section B may now be pursued with the quantitative tools given here. In Ref. 5, for example, Buchhold qualitatively suggests some designs for magnetic bearings. In a separate inertial guidance application, Cannon [Ref. 34], in an analysis of a pair of reaction wheels storing momentum in opposite directions, suggests a means for transferring momentum from one wheel to the other with a minimum of energy loss. If all parts of his arrangement were magnetically supported, the problem of bearing friction would be minimized.

Finally, these results can be applied to the development of the Mössbauer readout method introduced in Chapter II. A body to carry the Mössbauer absorber can be designed and built using the procedure outlined above and the parameters necessary for controlling its behavior are available from this analysis. The design and demonstration of a system for controlling precisely the position and orientation of the spinning cylinder, by means of capacitive pickoff and feedback to the magnetic support coils, still represents a significant challenge.

APPENDIX A. INFLUENCE COEFFICIENT PROGRAM AND SUBROUTINES

```
C ICISA INFLUENCE COEFFICIENT INTEGRATION,SYMMETRIC,ASSYMMETRIC
C      EXPANDED INTEGRATION PROCEDURE AS PER DOUGLAS REPORT ES 26988
       DIMENSION X(111),Y(111),GRAN1(65),GRAN2(65)
       DIMENSION VT(110,110),VNI(110,110)
       COMMON VNI,GRAN1,GRAN2
     1 FORMAT (6F12.5)
     2 FORMAT (16H X INFLUENCE AT 2F6.3,23H DUE TO ELEMENT NUMBER I3,E18.
      C6)
     3 FORMAT (16H Y INFLUENCE AT 2F6.3,23H DUE TO ELEMENT NUMBER I3,E18.
      C6)
     4 FORMAT (24H THE MATRIX IS SINGULAR I2)
     5 FORMAT (I4)
     6 FORMAT (72H0PROBLEM COMPLETED,MATRICES WRITTEN ON TAPE 12 AS VNIS
      C,VTS,VNIA,VTA FOR I3,15H DESCRIBING PTS)
     7 FORMAT (37H0MATRIX HAS BEEN SUCCESFULLY INVERTED)
    11 READ INPUT TAPE 5,5,NUM
C      NUM IS THE NUMBER OF DESCRIBING PTS, IT MUST BE ODD AND LESS T 102
C      BOUNDARY CONDITIONS ARE MET BETWEEN EACH OF THESE POINTS
       NUP=NUM-1
       READ INPUT TAPE 5,1,(X(I),I=1,NUM)
       READ INPUT TAPE 5,1,(Y(I),I=1,NUM)
       LOFST=1
C      LOFST IS PROBLEM CONTROL,LOFST=1 FOR SYMMETRIC,LOFST=2 FOR ASSYMMETRIC
    52  DO 17 I=1,NUP
        DELTS=SQRTF((X(I+1)-X(I))**2.+(Y(I+1)-Y(I))**2.)
       SINB=(Y(I+1)-Y(I))/DELTS
       COSB=(X(I+1)-X(I))/DELTS
       XMDPT=(X(I+1)+X(I))/2.
       YMDPT=(Y(I+1)+Y(I))/2.
C      THESE ARE THE PTS AT WHICH WE ARE FINDING THE INFLUENCE
       DO 17 J=1,NUP
        AREA1=0.0
        AREA2=0.0
       DELTS=SQRTF((X(J+1)-X(J))**2.+(Y(J+1)-Y(J))**2.)
        IF(I-J) 9,19,9
     9 D1=SQRTF((XMDPT-X(J))**2.+(YMDPT-Y(J))**2.)
       D2=SQRTF((XMDPT-X(J+1))**2.+(YMDPT-Y(J+1))**2.)
       IF(D2-D1) 12, 12,10
    10 D2=D1
    12 CONTINUE
C      D2 IS THE SHORTEST DISTANCE TO INTEGRATING ELEMENT
       INTRV=8.*DELTS/D2
       IF(INTRV) 13, 13,14
    13 INTRV=1
    14 IF(32-INTRV) 15, 15,18
    15 INTRV=32
    18 INTRV=2*INTRV
       TRV=INTRV
C      INTRV=NUMBER OF INTEGRATING PTS, IT IS EVEN ,BETWEEN 2 AND 64
       H=DELTS/TRV
       NTRV=INTRV+1
       DO 16 N=1,NTRV
       EN=N-1
       XI=X(J)+EN*(X(J+1)-X(J))/TRV
       ETA=Y(J)+EN*(Y(J+1)-Y(J))/TRV
       CALL        INTEGR (XMDPT,YMDPT,XI,ETA,LOFST,N,GRAN1(N),GRAN2(N))
    16    CONTINUE
       CALL SIMP(GRAN1,H,INTRV,AREA1)
       CALL SIMP(GRAN2,H,INTRV,AREA2)
```

```
      GO TO (43,44),LOFST
   44 AREA1=2.*AREA1
      AREA2=2.*AREA2
      GO TO 26
   43 AREA1=(-4.)*AREA1
       AREA2=(-2.)*AREA2
         GO TO 26
   19 SPRIM=.08
      IF(DELTS-2.*SPRIM*YMDPT) 22, 22,23
   22 SPRIM=.5*DELTS/YMDPT
      GO TO 37
C     THE INTEGRAL IS REPRESENTED BY THE SERIES ONLY
   23 INTRV=8.-16.*SPRIM*YMDPT/DELTS
      IF(INTRV) 24, 24,25
   24 INTRV=1
   25 INTRV=2*INTRV
C     INTRV IS THE NUMBER OF SUBELEMENTS BEFORE THE SINGULAR SUB ELEMENT
      TRV=INTRV
      H=(.5*DELTS-SPRIM*YMDPT)/TRV
      NTRV=2*INTRV+2
C     MAXIMUM NTRV IS 34 WHICH DOESNT EXCEED DIMENSION OF GRANS
      DO 31N=1,NTRV
      EN=N-1
      IF(N-(INTRV+1))27,27,28
   27 XI=X(I)+ EN *H *COSB
      ETA=Y(I)+ EN *H *SINB
      GO TO 20
   28 XI=X(I+1)+((EN-1.)/TRV-2.)*COSB*H*TRV
      ETA=Y(I+1)+((EN-1.)/TRV-2.)*SINB*H*TRV
   20 CALL       INTEGR (XMDPT,YMDPT,XI,ETA,LOFST,N,GRAN1(N),GRAN2(N))
   29 IF(N-(INTRV+1))31,30,31
   30 CALL SIMP(GRAN1,H,INTRV,AREA1)
      CALL SIMP(GRAN2,H,INTRV,AREA2)
   31 CONTINUE
      NTRV=INTRV+1
      DO 36 L=1,NTRV
      LL=L+INTRV+1
      GRAN1(L)=GRAN1(LL)
   36 GRAN2(L)=GRAN2(LL)
C     WE HAVE SHIFTED THE GRANS SO WE MAY NOW INTEGRATE BY SIMP
      CALL SIMP(GRAN1,H,INTRV,AREA11)
      CALL SIMP(GRAN2,H,INTRV,AREA22)
       AREA1=AREA1+AREA11
       AREA2=AREA2+AREA22
C     ADDS THE TWO INTEGRALS
      GO TO (45,46),LOFST
   46 AREA1=2.*AREA1
      AREA2=2.*AREA2
      GO TO 37
   45 AREA1=(-4.)*AREA1
       AREA2=(-2.)*AREA2
   37 GOR=LOGF(.125*SPRIM)
      GO TO (47,48),LOFST
   48 XII=2.*SINB*COSB*SPRIM*(1.-SPRIM*SPRIM*(9.-2.*SINB*SINB+6.*GOR)/
     C 48.)
      YII=2.*SPRIM*(2.+SINB*SINB+GOR+SPRIM*SPRIM*(9.-43.*SINB*SINB+6.*
     C SINB**4.+(27.-24.*SINB*SINB)*GOR)/144.)
      GO TO 49
   47 XII=SINB*COSB*(2.*SPRIM+(13./72.+(GOR+SINB*SINB)/12.)*SPRIM**3.)
      YII=2.*SPRIM*(SINB*SINB+GOR)-SPRIM**3.*(3.+3.*(GOR-SINB*SINB)-2.*
     CSINB**4.)/24.
```

```
   49  AREA1=XII+AREA1
       AREA2=YII+AREA2
C      ADDS IN SERIES
C      NOTE THAT X(I,I)=0 IF BETA=0 AND I IS WELL OFF THE AXIS
   26 CONTINUE
      VT(I,J)=COSB*AREA1+SINB*AREA2
      VNI(I,J)=COSB*AREA2-SINB*AREA1
      IF(I-J)17,32,17
   32 VNI(I,J)=VNI(I,J)-6.28318
   17 CONTINUE
      CALL INVERT (VNI,NUP,M1)
      IF (M1) 53,53,34
   34 WRITE OUTPUT TAPE 6,4,M1
      GO TO 35
   53 WRITE OUTPUT TAPE 6,7
   35 CONTINUE
      WRITE TAPE 12,((VNI(I,J),J=1,NUP),I=1,NUP)
      WRITE TAPE 12,((VT (I,J),J=1,NUP),I=1,NUP)
      GO TO (50,51),LOFST
   50 LOFST=2
      GO TO 52
   51 END FILE 12
      CALL RWD
      WRITE OUTPUT TAPE 6,6,NUP
      GO TO 11
      END

C INV SUBROUTINE TO INVERT A MATRIX                                      HINT0001
      SUBROUTINE INVERT(A,IMAX,ISING)                                    HINT0002
      DIMENSION A(110,110),GRAN1(65),GRAN2(65),IN(110),TEMP(110)
      COMMON A  ,GRAN1,GRAN2
      ISING=0                                                            HINT0004
      N=IMAX                                                             HINT0005
      IMAXO=N-1                                                          HINT0006
      I1=1                                                               HINT0007
    1 I3=I1                                                              HINT0008
      IN(I1)=0                                                           HINT0009
      SUM=ABSF(A(I1,I1))                                                 HINT0010
      DO3I=I1,N                                                          HINT0011
      IF(SUM-ABSF(A(I,I1)))2,3,3                                         HINT0012
    2 I3=I                                                               HINT0013
      IN(I1)=I                                                           HINT0014
      SUM=ABSF(A(I,I1))                                                  HINT0015
    3 CONTINUE                                                           HINT0016
      IF(I3-I1)4,6,4                                                     HINT0017
    4 DO5J=1,N                                                           HINT0018
      SUM=A(I1,J)                                                        HINT0019
      A(I1,J)=A(I3,J)                                                    HINT0020
    5 A(I3,J)=SUM                                                        HINT0021
    6 I3=I1+1                                                            HINT0022
      IF(A(I1,I1))97,99,97                                               HINT0023
   97 DO7I=I3,N                                                          HINT0024
    7 A(I,I1)=A(I,I1)/A(I1,I1)                                           HINT0025
      J2=I1-1                                                            HINT0026
      IF(J2)8,11,8                                                       HINT0027
    8 DO9J=I3,N                                                          HINT0028
      DO9I=1,J2                                                          HINT0029
    9 A(I1,J)=A(I1,J)-A(I1,I)*A(I,J)                                     HINT0030
   11 J2=I1                                                             HINT0031
      I1=I1+1                                                            HINT0032
      DO12I=I1,N                                                         HINT0033
```

```
      DO12J=1,J2                                                      HINT0034
   12 A(I,I1)=A(I,I1)-A(I,J)*A(J,I1)                                  HINT0035
      IF(I1-N)1,14,1                                                  HINT0036
   14 DO600JP=1,N                                                     HINT0037
      J=N+1-JP                                                        HINT0038
      A(J,J)=1.0/A(J,J)                                               HINT0039
      IF(J-1)603,700,603                                              HINT0040
  603 DO600IP=2,J                                                     HINT0041
      I=J+1-IP                                                        HINT0042
      IPO=I+1                                                         HINT0043
      SUM=0.                                                          HINT0044
      DO602L=IPO,J                                                    HINT0045
  602 SUM=SUM-A(I,L)*A(L,J)                                           HINT0046
  600 A(I,J)=SUM/A(I,I)                                               HINT0047
  700 DO151J=1,IMAXO                                                  HINT0048
      JPO=J+1                                                         HINT0049
      DO151I=JPO,N                                                    HINT0050
      SUM=0.                                                          HINT0051
      IMO=I-1                                                         HINT0052
      DO154L=J,IMO                                                    HINT0053
      IF(L-J)152,153,152                                              HINT0054
  152 SUM=SUM-A(I,L)*A(L,J)                                           HINT0055
      GO TO154                                                        HINT0056
  153 SUM=SUM-A(I,L)                                                  HINT0057
  154 CONTINUE                                                        HINT0058
  151 A(I,J)=SUM                                                      HINT0059
      DO901I=1,N                                                      HINT0060
      DO900J=1,N                                                      HINT0061
      TEMP(J)=0.0                                                     HINT0062
      DO899K=I,N                                                      HINT0063
      IF(K-J)899,897,898                                              HINT0064
  898 TEMP(J)=TEMP(J)+A(I,K)*A(K,J)                                   HINT0065
      GO TO899                                                        HINT0066
  897 TEMP(J)=TEMP(J)+A(I,K)                                          HINT0067
  899 CONTINUE                                                        HINT0068
  900 CONTINUE                                                        HINT0069
      DO901J=1,N                                                      HINT0070
  901 A(I,J)=TEMP(J)                                                  HINT0071
      DO500I=2,N                                                      HINT0072
      M=N+1-I                                                         HINT0073
      IF(IN(M))502,500,502                                            HINT0074
  502 ISS=IN(M)                                                       HINT0075
      DO503L=1,N                                                      HINT0076
      SUM=A(L,ISS)                                                    HINT0077
      A(L,ISS)=A(L,M)                                                 HINT0078
  503 A(L,M)=SUM                                                      HINT0079
  500 CONTINUE                                                        HINT0080
      GO TO 805                                                       HINT0081
   99 ISING=1                                                         HINT0082
  805 RETURN                                                          HINT0083
      END                                                             8953  8

CRWD  SUBROUTINE TO REWIND AND UNLOAD TAPE 12
*     FAP
       ENTRY   RWD
   RWD RUN     1174
       TRA     1,4
       END

CSSRDB INTEGRATION BY SIMPSONS RULE GIVEN INTEGRAND,INTERVALYNUM+ER
      SUBROUTINE SIMP(A,H,N,AREA)
```

```
      DIMENSION A(65)  .
      AREA=H*(A(1)+A(N+1))/3.
      J=N-1
      IF(J-1)8,8,9
    8 AREA=H*(A(1)+4.*A(2)+A(3))/3.
      GO TO 12
    9 DO 10 I=3,J,2
   10  AREA=AREA+2.*H*A(I)/3.
       DO 11 I=2,N,2
   11  AREA=AREA+4.*H*A(I)/3.
   12 RETURN
      END

C INTE SUBROUTINE TO EVALUATE INTEGRANS
      SUBROUTINE INTEGR (XMDPT,YMDPT,XI,ETA,LOFST,N,RAN1,RAN2)
      DIMENSION A(110,110),GRAN1(65),GRAN2(65)
      COMMON A   ,GRAN1,GRAN2
   20 DELT=XMDPT-XI
      HOLD1=(YMDPT+ETA)**2.+DELT*DELT
      HOLD2=(YMDPT-ETA)**2.+DELT*DELT
      ARG2=4.*ETA*YMDPT/HOLD1
      HOLD1=SQRTF(HOLD1)
C     CALCULATION OF ELLIPTIC INTEGRALS.
C     METHOD USED IS THAT OF ALGOITHMS 55 + 56 (COMMUNICATIONS OF THE ACM,
C     APR 61). ALGORITHM 165 (COM OF THE ACM,APR 63) STATE THE ABOVE IS GOOD TO
C     SIX PLACESAND GIVES A SLIGHTLY MORE ACCURATE PROCEDURE. CERTIFICATION IS
C     IN THE SAME ISSUE WITH A CORRECTION OF ONE OF THE CONSTANTS.
         T=1.-ARG2
      ELL1=(((.032024666*T+.054544409)*T+.097932891)*T+1.3862944)-
     X(((.010944912*T+.060118519)*T+.12475074)*T+.5)*LOGF(T)
      ELL2=(((.040905094*T+.085099193)*T+.44479204)*T+1.)-
     X    (((.01382999*T+.08150224)*T+.24969795)*T)*LOGF(T)
      GO TO (40,41),LOFST
   41 HOLD4=DELT*DELT+ETA*ETA
      HOLD5=HOLD4-2.*ETA*ETA
      HOLD3=HOLD4+YMDPT*YMDPT
       RAN1    =DELT*(ELL1-HOLD3*ELL2/HOLD2)/(YMDPT*HOLD1)
       RAN2    =(-HOLD4*ELL1+ELL2* (HOLD4*HOLD4+YMDPT*YMDPT*HOLD5)/
     CHOLD2)/(YMDPT*YMDPT*HOLD1)
      GO TO 42
   40  RAN1    =ETA*DELT       *ELL2/(HOLD2*HOLD1)
       RAN2    =(ETA/(YMDPT*HOLD1))*(ELL1+ELL2*(YMDPT*YMDPT-ETA*ETA-
     C  DELT*DELT)/HOLD2)
   42 RETURN
      END
```

APPENDIX B. AXIALLY SYMMETRIC PROGRAM AND SUBROUTINES

```
C RDB  FIELD CALCULATION ON THE SURFACE OF A CYLINDRICALLY SYMETRIC BODY
C     AXIAL SYMMETRIC BODY USING  SUBROUTINE FOR  FIELD COMPONENTS
C     BOUNDARY CONDITIONS ARE MET BETWEEN EACH DESCRIBING POINT.
      DIMENSION  X(111),Y(111),VT(110,110),VNI(110,110)
      DIMENSION VNO(110),VTO(110),Q(110),B(110)
   11 FORMAT (4F10.4,I4)
   12 FORMAT (24H FIELD BY TABLE AND SUB 4F14.5)
   13 FORMAT (28H MAXIMUM FIELD OCCURS AT PT I4,18H WITH COORDS X,Y= 2F1
     X0.4,14H ITS VALUE IS F14.5)
   14 FORMAT (26H0COIL COORDS IN CM,XC,YC= 2F10.4,22H CURRENT IN AMP-TUR
     XNS F10.4)
   15 FORMAT (I4)
   16 FORMAT (20H NORMAL FIELD AT PT I4,F14.5)
   17 FORMAT (5F14.6)
   18 FORMAT (24H CENTRAL FIELD IN GAUSS F14.5)
   19 FORMAT (6O12)
   20 FORMAT (6F12.5)
   21 FORMAT (3F12.5,I2,I4)
   22 FORMAT(22H FIELD IN GAUSS AT PT I4,F14.5)
   23 FORMAT (36H NET MAGNETIC LIFT FORCE IN GRAMS   F14.5)
      READ IMPUT TAPE 5,15,NUM
      NUP=NUM-1
      READ INPUT TAPE 5,20,(X(I),I=1,NUM)
      READ INPUT TAPE 5,20,(Y(I),I=1,NUM)
      READ INPUT TAPE 5,11,FVMAX,FVMIN,FACT,CMIN,ITL
   10 READ TAPE 12,((VNI(I,J),J=1,NUP),I=1,NUP)
      READ TAPE 12,((VT (I,J),J=1,NUP),I=1,NUP)
   26 READ INPUT TAPE 5,21,YC,XC,AMP,LO,KOILN
C     YC=COIL RADIUS IN CM, XC=X COIL COORD IN CM,AMP=CURRENT IN AMP-TURNS
C     LO=OUTPUT CONTROL,LO=1 GIVES FIELD DISTRUBUTION,LO=2 GIVES FORCE ONLY
C     KOILN=COIL CONTROL,0=ONE COIL ONLY,1=FIRST COIL OF A SERIES
C         2=INTERMEDIATE COIL OF A SERIES,3=LAST COIL OF A SERIES
   31 AMP=AMP/10.
      WRITE OUTPUT TAPE 6,14,XC,YC,AMP
      IF (KOILN-1) 32,32,34
   32 DO 33 K=1,NUP
   33 B(K)=0.0
   34 CONTINUE
      BO=6.28318*AMP/YC
      IF (LO-1) 38,37,38
   37 WRITE OUTPUT TAPE 6,18,BO
   38 CONTINUE
      DO 56 K=1,NUP
      XMDPT=(X(K+1)+X(K))/2.
      YMDPT=(Y(K+1)+Y(K))/2.
      HOLD1=SQRTF((X(K+1)-X(K))**2.+(Y(K+1)-Y(K))**2.)
      COSB=(X(K+1)-X(K))/HOLD1
      SINB=(Y(K+1)-Y(K))/HOLD1
      ZS=(XC-XMDPT)/YC
      RHOS=YMDPT/YC
      CALL COILFD(RHOS,ZS,BRHO,BZ)
      BRHO=BRHO*BO
      BZ=BZ*BO
      VNO(K)=BRHO*COSB+BZ*SINB
      VTO(K)=BRHO*SINB-BZ*COSB
   56 CONTINUE
      DO 60 J=1,NUP
      Q(J)=0.0
      DO 60 K=1,NUP
   60 Q(J)=Q(J)-VNI(J,K)*VNO(K)
      DO 65 K=1,NUP
```

```
62    B(K)=VTO(K)+B(K)
      DO 64 J=1,NUP
64    B(K)=B(K)+Q(J)*VT(K,J)
65 CONTINUE
   KOILN=KOILN+1
   GO TO (72,26,26,72),KOILN
72 CONTINUE
   FV=0.0
   DO 66 N=1,NUP
   AV=3.14159*(Y(N)*Y(N)-Y(N+1)*Y(N+1))
   P=.125*B(N)**2./3.14159
   FV=P*AV+FV
   GO TO (76,66),LO
76 WRITE OUTPUT TAPE 6,22,N,B(N)
66 CONTINUE
   FV=FV/981.
   WRITE OUTPUT TAPE 6,23,FV
73 CONTINUE
   BMAX=B(1)*B(1)
   NMAX=2
   DO 70 K=2,NUP
    BMIN=B(K)*B(K)
    IF (BMIN-BMAX) 70,70,69
69  BMAX=BMIN
   NMAX=K
70 CONTINUE
   XNMAX=(X(NMAX+1)+X(NMAX))/2.
   YNMAX=(Y(NMAX+1)+Y(NMAX))/2.
   BMAX=SQRTF(BMAX)
   WRITE OUTPUT TAPE 6,13,NMAX,XNMAX,YNMAX,BMAX
C     DERIVE IS ONLY CALLED IF KOILN=0 OR 3, IE LAST OR ONLY COIL
C     ITL=DERIVE CONTROL,SEE SUBROUTINE
   BC=450.
   CCRIT=AMP*SQRTF(FVMAX/FV)
74 CALL DERIVE (XC,YC,AMP,FV,BMAX,BC,ITL,FVMIN,FVMAX,CMIN,FACT,CCRIT)
79 GO TO 26
81 END

C CFD CALCULATES THE RADIAL AND AXIAL COMPONENTS OF THE MAGNETIC FIELD
C     DUE TO A PLANE CIRCULAR LOOP USING SMYTHES FORMULAS 7.10(6) AND (7)
C     R AND Z ARE THE FIELD PT COORDS NORMALIZED BY THE COIL RADIUS
C     BR AND BZ ARE THE FIELD COMPONENTS NORMALIZED BY THE CENTRAL FIELD
C     STRENGTH = MU I/ 2 A WHERE A IS THE COIL RADIUS
      SUBROUTINE COILFD(R,Z,BR,BZ)
      HOLD1=(1.+R)**2.+Z*Z
      HOLD2=(1.-R)**2.+Z*Z
      T=HOLD2/HOLD1
C     CALCULATION OF ELLIPTIC INTEGRALS.
C     METHOD USED IS THAT OF ALGOITHMS 55 + 56 (COMMUNICATIONS OF THE ACM,
C     APR 61). ALGORITHM 165 (COM OF THE ACM,APR 63) STATE THE ABOVE IS GOOD TO
C     SIX PLACESAND GIVES A SLIGHTLY MORE ACCURATE PROCEDURE. CERTIFICATION IS
C     IN THE SAME ISSUE WITH A CORRECTION OF ONE OF THE CONSTANTS.
C     FIELD COMPONENTS USING THIS AND  ALGORITHM 165 DIFFER ONLY 1 DIGIT
C     IN THE SIXTH PLACE FOR R=0 TO 2,Z=.3. THESE COMPONENTS DIFFER FROM
C     THOSE TABULATED BY BLEWETT (J OF APPLIED PHYS,NOV 47,VOL18,P 968.
C     ABOUT SIX DIGITS IN THE FIFTH PLACE. BLEWETT INTERPOLATES DWIGHTS TABLES
C     FOR K AND E AND THEREFORE IS PROBABLY NOT AS ACCURATE AS THIS.
      ELL1=(((.032024666*T+.054544409)*T+.097932891)*T+1.3862944)-
     X(((.010944912*T+.060118519)*T+.12475074)*T+.5)*LOGF(T)
      ELL2=(((.040905094*T+.085099193)*T+.44479204)*T+1.)-
     X     (((.01382999*T+.08150224)*T+.24969795)*T)*LOGF(T)
      BR=Z*(-ELL1+((1.+R*R+Z*Z)/HOLD2)*ELL2)/(R*SQRTF(HOLD1)*3.1415926)
        BZ=(ELL1+((1.-R*R-Z*Z)/HOLD2)*ELL2)/(3.1415926*SQRTF(HOLD1))
```

```
      RETURN
      END

CDERIVIF CONTROL STATEMENT ITL=4,THIS SUBROUTINE RETURNS TO THE AXIAL SYDERIVE01
C     MMETRIC PROGRAM. IF ITL=3 THE CURRENT AND FIELD CORRESPONDING TO  DERIVE02
C     ANY GIVEN LIFT FORCE(FACT) ARE CALCULATED. IF ITL=1 OR 2 THE SUB- DERIVE03
C     ROUTINE COMPUTES INCREMENTS OF THE COIL CURRENT(CRMT) AND GIVES A DERIVE04
C     SET OF 5 VALUES FOR THE COIL CURRENT(CCRIT),FIELD STRENGTH(BCRITI)DERIVE05
C     AND LIFTING FORCE(FVI). IF ITL=1 THE CRITICAL FIELD(BC) IS THE CRIDERIVE06
C     TERIA FOR INCREMENTING THE CURRENTS, IF ITL=2 THE MAX AND MIN LIFTDERIVE07
C     FORCE(FVMAX, FVMIN) ARE THE CRITERIA.                             DERIVE08
      SUBROUTINE DERIVE(XC,YC,AMP,FV,BMAX,BC,ITL,FVMIN,FVMAX,CMIN,FACT,C
     XCRIT)
    1 FORMAT(79H0      FOR EACH OF THE FOLLOWING CURRENTS THE COIL COORDIDERIVE10
     XNATES  IN CM ARE XC,YC= 2F10.4)                                   DERIVE11
    2 FORMAT(10X24H CURRENT IN ABAMP TURNS F10.4,23H DER LIFT FORCE IN GDERIVE12
     XMS F14.5,24H DERIVED FIELD IN GAUSS F14.5)
    3 FORMAT(10X21H LIFT FORCE IN GRAMS F10.5,16H FIELD IN GAUSS F10.5, DERIVE14
     X25H CURRENT IN AB-AMP TURNS F10.4)                                DERIVE15
      WRITE OUTPUT TAPE 6,1,XC,YC                                       DERIVE16
      GO TO(10,20,30,40),ITL                                            DERIVE17
   10 CCRIT =BC*AMP/BMAX                                                DERIVE18
      ICRMT =(CCRIT - CMIN)/5.                                          DERIVE19
      CRMT =ICRMT                                                       DERIVE20
   15 FVI =(CCRIT/AMP)**2.*FV                                           DERIVE21
      BCRITI =CCRIT*BMAX/AMP                                            DERIVE22
   16 WRITE OUTPUT TAPE 6,2,CCRIT,FVI,BCRITI                            DERIVE23
      IF(CCRIT-CMIN)30,30,17
   17 CCRIT=CCRIT-CRMT
      GO TO 15                                                          DERIVE26
   20 CMIN =SQRTF(FVMIN/FV)*AMP                                         DERIVE28
      ICRMT =(CCRIT - CMIN)/5.                                          DERIVE29
      IF (ICRMT)25,24,25
   24 ICRMT=1
   25 CONTINUE
      CRMT =ICRMT                                                       DERIVE30
      ICCRIT = CCRIT
      CCRIT = ICCRIT
      GO TO 15                                                          DERIVE31
   30 CACT =SQRTF(FACT/FV)*AMP                                          DERIVE32
      BACT =CACT*BMAX/AMP                                               DERIVE33
      WRITE OUTPUT TAPE 6,3,FACT,BACT,CACT                              DERIVE34
   40 RETURN                                                            DERIVE35
      END                                                               DERIVE36
```

APPENDIX C. OFFSET AXES PROGRAM AND SUBROUTINES

```
C A-SYM FIELD CALCULATION ON THE SURFACE OF A CYLINDRICALLY SYMMETRIC BODY
C     AXES OF COILS OFFSET FROM BODY AXIS A DISTANCE EPSLN
C     BOUNDARY CONDITIONS ARE MET BETWEEN EACH DESCRIBING PT
      DIMENSION X(111),Y(111),VT(110,110),VNI(110,110)
      DIMENSION VNO(110),VTO(110),Q(110),B(110),BASYM(110)
   11 FORMAT (40H LATERAL RESTORING FORCE IN DYNES AT PT I4,F12.7)
   12 FORMAT (42H LINE OF ACTION OF HORIZONTAL FORCE IS X= F8.3)
   13 FORMAT (28H MAXIMUM FIELD OCCURS AT PT I4,18H WITH COORDS X,Y= 2F1
     C0.4,14H ITS VALUE IS F14.5)
   14 FORMAT (26H0COIL COORDS IN CM,XC,YC= 2F10.4,22H CURRENT IN AMP-TUR
     XNS F10.4)
   15 FORMAT (I4)
   16 FORMAT (50H INCREASE IN MAXIMUM FIELD PER MM OFFSET IN GAUSS F14.5
     C )
   17 FORMAT (36H ASSYMETRIC SURFACE SOURCE STRENGTH E14.6)
   18 FORMAT (24H CENTRAL FIELD IN GAUSS F14.5)
   20 FORMAT (6F12.5)
   21 FORMAT (3F12.5,I2,I4,F8.3)
   22 FORMAT(22H FIELD IN GAUSS AT PT I4,F14.5)
   23 FORMAT (21H RESTORING FORCE PER F8.4,20H CM OFFSET IN GRAMS F14.5,
     C32H RESTORING CONSTANT IN DYNES/CM F14.5)
      READ INPUT TAPE 5,15,NUM
      NUP=NUM-1
      LOFST=1
C     LOFST=PROBLEM CONTROL,LOFST=1 FOR SYMETRIC,LOFST=2 FOR ASSYMMETRIC
      READ INPUT TAPE 5,20,(X(I),I=1,NUM)
      READ INPUT TAPE 5,20,(Y(I),I=1,NUM)
   26 READ INPUT TAPE 5,21,YC,XC,AMP,LO,KOILN,EPSLN
C     YC=COIL RADIUS IN CM, XC=X COIL COORD IN CM,AMP=CURRENT IN AMP-TURNS
C     LO=OUTPUT CONTROL,LO=1 GIVES FIELD DISTRUBUTION,LO=2 GIVES FORCE ONLY
C     LO=1 ALSO GIVES SIDE FORCE DISTRIBUTION.
C     KOILN=COIL CONTROL,0=ONE COIL ONLY,1=FIRST COIL OF A SERIES
C         2=INTERMEDIATE COIL OF A SERIES,3=LAST COIL OF A SERIES
C     EPSLN=COIL AXIS-BODY AXIS SPACING IN CM,IF ZER OR BLANK, ONE
C     MILLIMETER IS ASSUMED.
      IF(EPSLN) 31,30,31
   30 EPSLN=.1
   31 AMP=AMP/10.
      WRITE OUTPUT TAPE 6,14,XC,YC,AMP
   10 READ TAPE 12,((VNI(I,J),J=1,NUP),I=1,NUP)
      READ TAPE 12,((VT (I,J),J=1,NUP),I=1,NUP)
      GO TO (29,28),LOFST
   28 REWIND 12
   29 CONTINUE
      IF (KOILN-1)33,33,34
   33 GO TO (35,34),LOFST
   35 DO 34 K=1,NUP
      B(K)=0.0
      BASYM(K)=0.0
   34 CONTINUE
      BO=6.28318*AMP/YC
      IF (LO-1) 38,37,38
   37 WRITE OUTPUT TAPE 6,18,BO
   38 CONTINUE
      DO 56 K=1,NUP
      XMDPT=(X(K+1)+X(K))/2.
      YMDPT=(Y(K+1)+Y(K))/2.
      HOLD1=SQRTF((X(K+1)-X(K))**2.+(Y(K+1)-Y(K))**2.)
      COSB=(X(K+1)-X(K))/HOLD1
      SINB=(Y(K+1)-Y(K))/HOLD1
      ZS=(XC-XMDPT)/YC
```

```
      RHOS=YMDPT/YC
      GO TO (39,40),LOFST
   39 CALL COILFD(RHOS,ZS,BRHO,BZ)
      BRHO=BRHO*BO
      BZ=BZ*BO
      VNO(K)=BRHO*COSB+BZ*SINB
      VTO(K)=BRHO*SINB-BZ*COSB
      GO TO 56
   40 CALL FLDDER(RHOS,ZS,DBRDR,DBZDR)
      DBRDR=DBRDR*BO/YC
      DBZDR=DBZDR*BO/YC
      VNO(K)=DBRDR*COSB+DBZDR*SINB
      VTO(K)=DBRDR*SINB-DBZDR*COSB
   56 CONTINUE
      DO 60 J=1,NUP
      Q(J)=0.0
      DO 60 K=1,NUP
   60 Q(J)=Q(J)-VNI(J,K)*VNO(K)
C     CALCULATES THE SURFACE SOURCE STRENGTH
      GO TO (61,41),LOFST
   41 DO 45 K=1,NUP
      BASYM(K)=VTO(K)+BASYM(K)
      DO 44 J=1,NUP
   44 BASYM(K)=BASYM(K)+Q(J)*VT(K,J)
   45 CONTINUE
      GO TO 65
   61 DO 65 K=1,NUP
   62   B(K)=VTO(K)+B(K)
        DO 64 J=1,NUP
   64   B(K)=B(K)+Q(J)*VT(K,J)
   65 CONTINUE
      GO TO (46,48),LOFST
   46 LOFST=2
      GO TO 10
   48 LOFST=1
      IF (KOILN) 72,72,71
   71 IF (KOILN-3) 26,72,72
   72 CONTINUE
C     LAST OR ONLY COIL,CALCULATE FORCE AND BMAX,BS
      FH=0.0
      T=0.0
      DO 66 N=1,NUP
      FH1=EPSLN*(Y(N+1)+Y(N))*(X(N+1)-X(N))*B(N)*BASYM(N)*.125
      FH=FH+FH1
      T=FH1*(X(N+1)+X(N))*.5+T
      T=T-EPSLN*(Y(N+1)+Y(N))*(Y(N+1)+Y(N))*(Y(N)-Y(N+1))*B(N)*
     1   BASYM(N)/16.
      B(N)=B(N)+EPSLN*BASYM(N)
      IF (LO-1) 66,67,66
   67 WRITE OUTPUT TAPE 6,22,N,B(N)
      WRITE OUTPUT TAPE 6,17,Q(N)
      WRITE OUTPUT TAPE 6,11,N,FH1
   66 CONTINUE
      T=T/FH
C     T=SIGMA(FH1*X)/SIGMA FH1
      CONST=FH/EPSLN
      FH=FH/981.
      WRITE OUTPUT TAPE 6,23,EPSLN,FH,CONST
      WRITE OUTPUT TAPE 6,12,T
   73 CONTINUE
      BMAX=B(1)*B(1)
      NMAX=2
      DO 70 K=2,NUP
```

```
      BMIN=B(K)*B(K)
      IF (BMIN-BMAX) 70,70,69
   69 BMAX=BMIN
      NMAX=K
   70 CONTINUE
      XNMAX=(X(NMAX+1)+X(NMAX))/2.
      YNMAX=(Y(NMAX+1)+Y(NMAX))/2.
      BMAX=SQRTF(BMAX)
      WRITE OUTPUT TAPE 6,13,NMAX,XNMAX,YNMAX,BMAX
      BASY=.01*BASYM(NMAX)/EPSLN
      WRITE OUTPUT TAPE 6,16,BASY
   79 GO TO 26
   81 END

C FDD CALCULATES THE DERIVATIVES OF THE FIELD COMPONENTS WITH RESPECT TOFDD   01
C     R. R AND Z ARE THE RADIAL AND AXIAL COORDINANTS NORMALIZED BY THE FDD   02
C     COIL RADIUS. THE DERIVATIVES ARE NORMALIZED BY BO/A WHFRE BO IS   FDD   03
C     THE CENTRAL FIELD AND A IS THE COIL RADIUS.                       FDD   04
      SUBROUTINE FLDDER(R,Z,DBRDR,DBZDR)                                FDD   00
      CALL COILFD(R,Z,BR,BZ)                                            FDD   05
      HOLD1=(1.+R)*(1.+R)+Z*Z                                           FDD   07
      HOLD2=(1.-R)*(1.-R)+Z*Z                                           FDD   08
      T=HOLD2/HOLD1                                                     FDD   09
      ELL2=(((.040905094*T+.085099193)*T+.44479204)*T+1.)-              FDD   10
     X(((.01382999*T+.08150224)*T+.24969795)*T)*LOGF(T)                 FDD   11
      HOLD3=R*R-1.+Z*Z                                                  FDD   12
      DBZDR=-BZ*(1.+R)/HOLD1
      HOLD2=HOLD1*HOLD2                                                 FDD   14
      DBRDR=-BR*((1./R)+R*HOLD3/HOLD2)                                  FDD   15
      HOLD3=1.-R*R+Z*Z                                                  FDD   16
      DBZDR=DBZDR+BR*(1.-R)*HOLD3/(Z*HOLD2)                             FDD   17
      E=6.*Z*HOLD3*ELL2*SQRTF(HOLD1)/(3.14159*HOLD2*HOLD2)              FDD   18
      DBRDR=DBRDR+E                                                     FDD   19
C     END OF DERIVATIVE OF BR                                           FDD   20
      E=HOLD1-R*(3.*R+1.)                                               FDD   21
      E=E*HOLD3/HOLD2-1.                                                FDD   22
      E=2.*ELL2*E*SQRTF(HOLD1)/(3.14159*R*HOLD2)
      DBZDP=DBZDR+E                                                     FDD   24
C     END OF DERIVATIVE OF BZ                                           FDD   25
      RETURN                                                            FDD   26
      END                                                               FDD   27
```

```
C TILT FIELD CALCULATION ON THE SURFACE OF A CYLINDRICALLY SYMMETRIC BODY
C     BODY TILTED THROUGH AN ANGLE DELTA
C     BOUNDARY CONDITIONS ARE MET BETWEEN EACH DESCRIBING PT
      DIMENSION X(111),Y(111),VT(110,110),VNI(110,110)
      DIMENSION VNO(110),VTO(110),Q(110),B(110),BASYM(110)
   11 FORMAT (40H LATERAL RESTORING FORCE IN DYNES AT PT I4,F12.7)
   12 FORMAT (28H RESTORING MOMENT CONSTANT, F14.5,35H DYNE-CM/RADIAN FO
     XR TILTS ABOUT X= F8.3)
   13 FORMAT (28H MAXIMUM FIELD OCCURS AT PT I4,18H WITH COORDS X,Y= 2F1
     C0.4,14H ITS VALUE IS F14.5)
   14 FORMAT (26H0COIL COORDS IN CM,XC,YC= 2F10.4,22H CURRENT IN AMP-TUR
     XNS F10.4)
   15 FORMAT (I4)
   16 FORMAT (56H INCREASE IN MAXIUM FIELD PER 1/50 RADIAN TILT IN GAUSS
     X F14.5)
   17 FORMAT (36H ASSYMETRIC SURFACE SOURCE STRENGTH E14.6)
   18 FORMAT (24H CENTRAL FIELD IN GAUSS F14.5)
   20 FORMAT (6F12.5)
   21 FORMAT (3F12.5,I2,I4,2F8.3)
   22 FORMAT(22H FIELD IN GAUSS AT PT I4,F14.5)
   23 FORMAT (28H NET LATERAL FORCE IN GRAMS F14.5,20H FOR INCLINATION O
     1F F9.4,8H RADIANS)
      REWIND 12
      READ INPUT TAPE 5,15,NUM
      NUP=NUM-1
      LOFST=1
C     LOFST=PROBLEM CONTROL,LOFST=1 FOR SYMETRIC,LOFST=2 FOR ASSYMMETRIC
      READ INPUT TAPE 5,20,(X(I),I=1,NUM)
      READ INPUT TAPE 5,20,(Y(I),I=1,NUM)
   26 READ INPUT TAPE 5,21,YC,XC,AMP,LO,KOILN,DELTA,XT
C     YC=COIL RADIUS IN CM, XC=X COIL COORD IN CM,AMP=CURRENT IN AMP-TURNS
C     LO=OUTPUT CONTROL,LO=1 GIVES FIELD DISTRUBUTION,LO=2 GIVES FORCE ONLY
C     LO=1 ALSO GIVES SIDE FORCE DISTRIBUTION.
C     KOILN=COIL CONTROL,0=ONE COIL ONLY,1=FIRST COIL OF A SERIES
C         2=INTERMEDIATE COIL OF A SERIES,3=LAST COIL OF A SERIES
C     DELTA = TILT ANGLE IN RADIANS,IF ZERO OR BLANK,.02 IS ASSUMED
C     XT=X LOCATION OF TILT AXIS (YT=0)
      IF(DELTA) 31,30,31
   30 DELTA=.02
   31 AMP=AMP/10.
      WRITE OUTPUT TAPE 6,14,XC,YC,AMP
   10 READ TAPE 12,((VNI(I,J),J=1,NUP),I=1,NUP)
      READ TAPE 12,((VT (I,J),J=1,NUP),I=1,NUP)
      GO TO (29,28),LOFST
   28 REWIND 12
   29 CONTINUE
      IF (KOILN-1) 33,33,34
   33 GO TO (35,34),LOFST
   35 DO 34 K=1,NUP
        B(K)=0.0
        BASYM(K)=0.0
   34 CONTINUE
      BO=6.28318*AMP/YC
      IF (LO-1) 38,37,38
   37 WRITE OUTPUT TAPE 6,18,BO
   38 CONTINUE
      DO 56 K=1,NUP
      XMDPT=(X(K+1)+X(K))/2.
      YMDPT=(Y(K+1)+Y(K))/2.
      HOLD1=SQRTF((X(K+1)-X(K))**2.+(Y(K+1)-Y(K))**2.)
      COSB=(X(K+1)-X(K))/HOLD1
```

```
      SINB=(Y(K+1)-Y(K))/HOLD1
      ZS=()C-XMDPT)/YC
      RHOS=YMDPT/YC
      CALL COILFD(RHOS,ZS,BRHO,BZ)
      BRHO=BRHO*BO
      BZ=BZ*BO
      GO TO (39,40),LOFST
   39 CONTINUE
      VNO(K)=BRHO*COSB+BZ*SINB
      VTO(K)=BRHO*SINB-BZ*COSB
      GO TO 56
   40 CALL BDERIV(RHOS,ZS,DBRDR,DBZDR,DBRDZ,DBZDZ)
      DBRDR=DBRDR*BO/YC
      DBZDR=DBZDR*BO/YC
      DBRDZ=DBRDZ*BO/YC
      DBZDZ=DBZDZ*BO/YC
      HOLD1=BZ+(XMDPT-XT)*DBRDR+YMDPT*DBRDZ
      HOLD2=-BRHO+(XMDPT-XT)*DBZDR+YMDPT*DBZDZ
      VNO(K)=HOLD1*COSB+HOLD2*SINB
      VTO(K)=HOLD1*SINB-HOLD2*COSB
   56 CONTINUE
      DO 60 J=1,NUP
      Q(J)=0.0
      DO 60 K=1,NUP
   60 Q(J)=Q(J)-VNI(J,K)*VNO(K)
C     CALCULATES THE SURFACE SOURCE STRENGTH
      GO TO (61,41),LOFST
   41 DO 45 K=1,NUP
      BASYM(K)=VTO(K)+BASYM(K)
      DO 44 J=1,NUP
   44 BASYM(K)=BASYM(K)+Q(J)*VT(K,J)
   45 CONTINUE
      GO TO 48
   61 DO 65 K=1,NUP
   62   B(K)=VTO(K)+B(K)
        DO 64 J=1,NUP
   64   B(K)=B(K)+Q(J)*VT(K,J)
   65 CONTINUE
   46 LOFST=2
      GO TO 10
   48 LOFST=1
      IF (KOILN) 72,72,71
   71 IF (KCILN-3) 26,72,72
   72 CONTINUE
C     LAST OR ONLY COIL,CALCULATE FORCE AND BMAX,BS
      FH=0.0
      T=0.0
      DO 66 N=1,NUP
      FH1=DELTA*(Y(N+1)+Y(N))*(X(N+1)-X(N))*B(N)*BASYM(N)*.125
      FH=FH+FH1
      T=(XT+XT-X(N)-X(N+1))*FH1*.5+DELTA*(Y(N+1)+Y(N))*(Y(N+1)+Y(N))*
     1  (Y(N)-Y(N+1))*B(N)*BASYM(N)/16.+T
       B(N)=B(N)+DELTA*BASYM(N)
      IF (LO-1) 66,67,66
   67 WRITE OUTPUT TAPE 6,22,N,B(N)
      WRITE OUTPUT TAPE 6,17,Q(N)
      WRITE OUTPUT TAPE 6,11,N,FH1
   66 CONTINUE
      FH=FH/981.
      T=-T/DELTA
C     T= TORQUE PER RADIAN
      WRITE OUTPUT TAPE 6,23,FH,DELTA
      WRITE OUTPUT TAPE 6,12,T,XT
```

```
   73 CONTINUE
      BMAX=B(1)*B(1)
      NMAX=2
      DO 70 K=2,NUP
       BMIN=B(K)*B(K)
       IF (BMIN-BMAX) 70,70,69
   69  BMAX=BMIN
      NMAX=K
   70 CONTINUE
      XNMAX=(X(NMAX+1)+X(NMAX))/2.
      YNMAX=(Y(NMAX+1)+Y(NMAX))/2.
      BMAX=SQRTF(BMAX)
      WRITE OUTPUT TAPE 6,13,NMAX,XNMAX,YNMAX,BMAX
        BASY=.02*BASYM(NMAX)/DELTA
      WRITE OUTPUT TAPE 6,16,BASY
   79 GO TO 26
   81 END
C BDR CALCULATES THE DERIVATIVES OF THE FIELD COMPONENTS WITH RESPECT TO
C     R. R AND Z ARE THE RADIAL AND AXIAL COORDINANTS NORMALIZED BY THE
C     COIL RADIUS. THE DERIVATIVES ARE NORMALIZED BY BO/A WHERE BO IS
C     THE CENTRAL FIELD AND A IS THE COIL RADIUS.
C     ALSO CALCULATES DERIVATIVES WITH RESPECT TO Z.
      SUBROUTINE BDERIV (R,Z,DBRDR,DBZDR,DBRDZ,DBZDZ)
      CALL COILFD(R,Z,BR,BZ)
      HOLD1=(1.+R)*(1.+R)+Z*Z
      HOLD2=(1.-R)*(1.-R)+Z*Z
      T=HOLD2/HOLD1
      ELL2=(((.040905094*T+.085099193)*T+.44479204)*T+1.)-
     X(((.01382999*T+.08150224)*T+.24969795)*T)*LOGF(T)
      HOLD3=R*R-1.+Z*Z
      DBZDR=-BZ*(1.+R)/HOLD1
      HOLD2=HOLD1*HOLD2
      DBRDR=-BR*((1./R)+R*HOLD3/HOLD2)
      HOLD3=1.-R*R+Z*Z
      DBZDR=DBZDR+BR*(1.-R)*HOLD3/(Z*HOLD2)
      E=6.*Z*HOLD3*ELL2*SQRTF(HOLD1)/(3.14159*HOLD2*HOLD2)
      DBRDR=DBRDR+E
C     END OF DERIVATIVE OF BR
      E=HOLD1-R*(3.*R+1.)
      E=E*HOLD3/HOLD2-1.
      E=2.*ELL2*E*SQRTF(HOLD1)/(3.14159*R*HOLD2)
      DBZDR=DBZDR+E
C     END OF DERIVATIVE OF BZ
      DBRDZ=DBZDR
C     END OF  Z DERIVATIVE OF BR
      DBZDZ=-(DBRDR+BR/R)
C     END OF Z DERIVATIVE OF BZ
      RETURN
      END
```

REFERENCES

1. E. A. Lynton, Superconductivity, London, Methuen and Co. Ltd., 1962.

2. F. London, Superfluids: Macroscopic Theory of Superconductivity, Vol. I, New York, Dover, 1961.

3. I. Simon, "Forces Acting on Superconductors in Magnetic Fields," J. of Applied Physics, Vol. 24, No. 1, Jan 1953.

4. W. H. Culver and M. H. Davis, "An Application of Superconductivity to Inertial Navigation," RAND, R-363, 19 Apr 1960; also RAND, RM-1852, Classified Secret, 7 Jan 1957.

5. T. A. Buchhold, "Applications of Superconductivity," Scientific American, Vol. 202, No. 3, Mar 1960.

6. T. A. Buchhold, "The Magnetic Forces on Superconductors and Their Applications for Magnetic Bearings," Cryogenics, Vol. 1, No. 4, Jun 1961.

7. J. T. Harding, and R. H. Tuffias, "The Cryogenic Gyro," JPL Technical Release No. 34-100, 1 Aug 1960.

8. JPL Research Summary No. 36-5, Vol. 1, Guidance and Control Research, "Cryogenic Gyro," pp. 20-28, 15 Oct 1960.

9. J.T. Harding and R. H. Tuffias, "AC Losses in Superconductors," JPL Technical Report No. 345-4, Feb 1963.

10. JPL Research Summary No. 36-14, Guidance and Control Research, "Measurements of AC Losses in Superconductors," pp. 22-26, 1 May 1962.

11. JPL Space Programs Summary No. 37-16, Guidance and Control Research, "Alternating Magnetic Field Losses in Superconductors," pp. 105-108, 31 Aug 1962.

12. T. A. Buchhold and P. J. Molenda, "Surface Electrical Losses of Superconductors in Low Frequency Fields," Cryogenics, Vol. 2, No. 6, Dec 1962.

13. L. I. Schiff, "Possible New Experimental Test of General Relativity," Phys. Rev. Lett., Vol. 4, pp. 215-217, 1 Mar 1960, submitted 8 Feb 1960.

14. L. I. Schiff, "A Report on the NASA Conference on Experimental Tests of Theories of Relativity," Physics Today, Vol. 14, No. 11, Nov 1961.

15. R. H. Cannon, Jr., "Requirements and Design for a Special Gyro for Measuring General Relativity Effects," presented at the International Union of Theoretical and Applied Mechanics, 1962, Celerina, Switzerland; also in H. Ziegler, Ed., Gyrodynamics, Symposium Celerina, Aug 20-23, 1962, Springer Verlag, Berlin.

16. W. M. Fairbank and M. Bol, "Check of General Relativity Using a Superconducting Gyroscope," presented at ARS National Meeting on Guidance, Control and Navigation, Stanford University, Aug 1961.

17. R. H. Cannon, Jr., "Performance of Hydrofoil Systems," Ph.D. Thesis, MIT, 1950.

18. JPL Space Programs Summary No. 37-16, Guidance and Control Research, "Investigation of Niobium Films for Superconductivity," p. 108, 31 Aug 1962.

19. W. B. Nowak, W. P. Munro, and D. F. Kaufman, "Spherical Rotors for Cryogenic Gyroscopes," Report 4980, Nuclear Metals, Inc., Concord, Mass., 15 Mar 1962.

20. W. B. Nowak, and A. R. Lumbert, "Coated Spheres for Cryogenic Gyroscopes," Report 4986, Nuclear Metals, Inc., Concord, Mass., 21 Jun 1962.

21. O. D. Kellogg, Foundations of Potential Theory, New York, Dover, 1953.

22. A. M. O. Smith and J. Pierce, "Exact Solution of the Neumann Problem: Calculation of Non-Circulatory Plane and Axially Symmetric Flows about or within Arbitrary Bodies," Douglas Aircraft Co. Report No. ES 26988, 25 Apr 1958; also Proceedings of the Third US National Congress of Applied Mechanics, New York, ASME, pp. 807-811, 1958.

23. I. Lotz, "Calculation of Potential Flow Past Airship Bodies in Yaw," NACA TM 675, July 1932.

24. J. L. Hess, "Calculation of Potential Flow about Bodies of Revolution having Axes Perpendicular to the Free Stream Direction," Douglas Aircraft Co. Report No. ES 29813, 16 May 1960; also J. of the Aerospace Sciences, Vol. 29, No. 6, Jun 1962, pp. 726-740.

25. W. R. Smythe, Static and Dynamic Electricity, New York, McGraw-Hill Book Co., Inc., 1950, Second Edition.

26. J. T. Harding, "Force and Torque on a Superconducting Ellipsoid in an Axially Symmetric Magnetic Field," JPL Technical Release No. 32-242, 6 Feb 1961.

27. JPL Research Summary No. 36-8, Guidance and Control Research, "Restoring Forces on Spherical Gyro Rotor," pp. 11-12, 1 May 1961.

28. Bartberger, "The Magnetic Field of a Plane Circular Loop," J. of Appl. Phys., Vol. 21, pp. 1108-1114, Nov 1950.

29. P. Weiby, "The Capacitance Bridge," Instruments and Control Systems, Vol. 34, No. 8, pp. 112-115, Aug 1962.

30. A. H. DuRose and William Blum, "Lead," in F. A. Lowenheim, Ed., Modern Electroplating, 2nd Ed., New York, John Wiley and Sons, Inc., 1963, pp. 242-259.

31. J. T. Harding, "Eddy Current Damping of a Magnetically Supported Superconducting Sphere by a Resistive Shield," JPL Technical Release No. 34-250, 3 March 1961.

32. JPL Research Summary No. 36-8, Guidance and Control Research, "Damping of a Cryogenic Gyro," pp. 12-13, 1 May 1961.

33. W. M. Fairbank, J. M. Pierce, and P. B. Wilson, "High Power Superconductive Cavities for Accelerators," in Proceedings of the VIII International Conference on Low Temperature Physics, London, 1962, pp. 179-181.

34. R. H. Cannon, Jr., "Some Basic Response Relations for Reaction-Wheel Attitude Control," presented at the Joint Automatic Control Conference, Boulder, Colorado, 28-30 Jun 1961; also ARS J., Vol. 32, No. 1, Jan 1962.